IMPACT OF WATERSHED MANAGEMENT ON VEGETATION COVER AND SOIL MOISTURE USING REMOTE SENSING, IN MAGERA AND WUTAME MICRO WATERSHED, OMO GIBE BASIN

M.Sc. THESIS
BY
AKLILU ASSEFA TILAHUN

FEBRUARY, 2020
ADDIS ABABA, ETHIOPIA

IMPACT OF WATERSHED MANAGEMENT ON VEGETATION COVER AND SOIL MOISTURE USING REMOTE SENSING, IN MAGERA AND WUTAME MICRO WATERSHED, OMO GIBE BASIN

By
Aklilu Assefa Tilahun

A thesis submitted to the Africa center of excellence for water management, school of post graduate studies, Addis Ababa University in partial fulfillment of the requirements for the degree of Master of Science in water management specialization of hydrology and water resources

Adviser:

Alemseged Tamiru Haile (PhD)

FEBRUARY, 2020
ADDIS ABABA

Declaration Page

I, Aklilu Assefa Tilahun, declare that the thesis entitled **"Impact of Watershed Management on Vegetation Cover and Soil Moisture Using Remote Sensing, In Magera and Wutame Micro Watershed, Omo Gibe Basin"** is my own original work and it has not been presented and will not be presented by me to any other university for the similar or any other degree award

Signature…… ……

Acknowledgements

My greatest thanks go to the Almighty God; I don't have sufficient words to praise you. Your grace was enough for me.

I am tremendously grateful thanks to my supervisor Dr. Alemseged Tamiru Haile for his earnest guidance, critical comments and timely suggestions. His support and advice makes me motivated and energetic all the way through this study.

I would like to express my sincere and heartfelt gratitude to the IWMI and REACH –WSRS project for financial support in my research work and for providing instrument such as Portable sensor and GPS.

I would like also to thank Mr. Dawit Bunduro who is with me throughout the data collection period in the study area and showed me every parts of the watershed that is targeted by SLM.

I would like also to send my special thanks to Mr. Barana Bassa who is hydrological data collector for me in the watershed. He is very hard worker.

Finally, I am grateful to Arbamich University Irrigation Engineering Department for providing instrument like Auger and soil moisture can for soil sampling and Civil Enginerring Department for giving the opportunity to acces the Geotechnical Laboratory for soil lab analysis.

ABSTRACT

Despite the importance of watershed management as an approach to curve land degradation, to date, there has been little research on their impact on hydrological variables. This study evaluated the potential of remote sensing in quantifying and detecting vegetation cover, land cover and soil moisture dynamics as caused by the watershed management in a micro watershed in Ethiopia. To address these, multi-temporal data of Landsat imageries were used to retrieve NDVI for detecting vegetation cover change and to produce the LULC map for assessing the land cover changes from 2010 to 2019 which incompass the period before and after the watershed intervention. Mann-Kendal trend test was used to examine long trends in the monthly NDVI area of vegetation cover. In addition, multiple change-point analyses were carried out using Pettitt's, Buishand's and SNHT tests to detect the change point (year), if any, and to find its possible relation with watershed intervention. Long-term station based monthly rainfall data from 2010 was used to check the possible influences of rainfall in the increased the vegetation density. The accuracy of maps was also assessed using the error matrix.

Furthermore, a remote sensing-based soil moisture index (SMI) model and ground measurement from 40 sampling scheme was used for soil moisture estimation and validation. The model is validated using adj-R^2, root mean squared error (RMSE), the absolute average difference (AAD), and the precision model. The threshold NDVI classification analysis revealed three vegetation cover classes, including no plants or bare land, weak plants or shrub and grassland and healthy plants or forests which were designated in increasing order of vegetation densities. Significant increasing and decreasing trends in vegetation cover classes have been detected from the Mann-Kendal test. The area coverage of healthy plants dramatically increased from 1.5% to 33%; in contrast, the area under bare land decreased drastically from 40.9% to 0.6% post-intervention. The year 2015 was detected as a change point (year) for continues conversion of three vegetation cover classes. The weak and decreasing correlation was shown in between monthly NDVI area and rainfall, which further verified the increment in vegetation cover is not only from the rainfall influences. The fundamental LULC changes in the watershed were, increased in both the forest land and agricultural land area and decreased in bare, shrub and grassland areas. According to SMI data, the value near 0 showed low vegetation cover and little soil moisture, whereas the value near to 1 showed high vegetation cover and high moisture content. The SMI model accurately estimated the ground soil moisture based on its high R^2 (0.768) and low RMSE (0.033cm^3/cm^3). Because of the vegetation cover increased after intervention, the watereshed also experienced an increase in soil moisture over the study period. The study shows that the watershed management intervention has an overall positive impact on the wateshed. Based on the findings of this research, remote sensing approaches have the potential to evaluate watershed intervention and also have to quantify and detect the vegetation cover, land-use changes and soil moisture changes.

***Key words**: Land degradation, watershed management, Landsat, NDVI, SMI, LULC, soil moisture.*

Table of Contents

Abbreviations and Acronyms

AAD	Absolute Average Difference
EC	Ethiopian Calendar
GCP	Ground Control Point
GIS	Geographic Information System
GPS	Global Position System
HA	Hectare
ILWIS	Integrated Land and Water Information System
IWMI	International Water management Institute
LC	Land Cover
LST	Land Surface Temperature
LU	Land Use
MAPE	Mean Absolute Percentage Error
MI	Moisture Index
NDVI	Normalized Difference Vegetation Index
NDWI	Normalized Difference Water Index
NIR	near Infrared
NMA	National Metrological Agency
OLI	Operational Land Imager
PCC	Post Classification Comparison
RMSE	Root Mean Square Error
RS	Remote Sensing
SLM	Sustainable Land Management
SLMP	Sustainable Land Management Program
SMC	Soil Moisture Content
SMI	Soil Moisture Index
SNHT	Standard Normal Homogeneity Test
SNNPR	Southern Nation Nationality and Peoples Region
SWIR	Short Wave Infrared
TIRS	Thermal Infrared Sensor
ToA	Top of Atmospheric Reflectance

List of Figures

List of Tables

1. INTRODUCTION

1.1 Background

Land degradation is a severe and complex global environmental problem. Out of the world's 8.7 billion ha of agricultural land, pasture, forest and woodland, around 2 billion ha (22.5%) have been degraded since 1950 (Scherr and Yadav, 1996; Mekonen *et al*., 2011), and 5-10 million ha (0.36–0.71% of global arable land) are lost every year to severe degradation (Buckwell, 2009, Mekonen *et al*., 2011). Reportedly, if such a trend continues, 1.4 - 2.8% of the total agricultural, pasture and forest land will be lost by 2030 (Scherr and Yadav, 1996; Mekonen *et al*., 2011). The issue of watershed degradation has been one of the main constraints for agricultural productivity in Ethiopia. The degradation in the form of soil erosion and nutrient depletion often results from the anthropogenic influences and natural interaction, such as rugged topography, erratic rainfall and unsustainable land management practices, both in areas of grazing lands and crop lands. The economy of the country has been under stress, due to the land degradation, which in turn constraint the provision of goods and service from rainfed agricultural watersheds in Ethiopia (Adimassu and Langan, 2016). Watershed degradation can decrease land productivity and also increase social problems (Darghouth *et al*., 2008).

To counter these, several governmental and non-governmental organizations have launched an integrated watershed management program to curve some of these severe problems (Yoganand and Tesfa, 2006). Watershed management practices (e.g., changes in land use, vegetation cover, etc.) are implemented with the objectives of rehabilitation of degraded lands, protection of soil and water systems, meet rising food fiber demands while sustaining ecosystem service (Alemayehu *et al*., 2009). In Ethiopia, watershed development planning had started in the 1980s for large watersheds (MoRAD, 2005). Watershed management aims to improve the standard of living of the population residing within the watersheds by decreasing the population pressure and increasing land productivities so that sustainable livelihoods and land-use practices can be secured for the community (McCormick *et al*., 2003).

Among the regions, Boloso Bombe woreda in Omo-Gibe Basin is targeted by the intensive Sustainable Land Management Program (SLMP) since 2013/14. It was a 5 years resource management and development project with four broad objectives such as soil and water

conservation, income generation, land administration and capacity building development. Sustainable Land Management (SLM) was initially targeted over seven mini watersheds in Magera micro watershed: Buna mini watershed in Udula Matala kebele of 544.02ha, Buna mini watershed in Matala Walana kebele of 417.9ha, Gandisa mini watershed in Farawocha kebele of 659.4ha, Choche mini watershed Zaba kebele of 606.2ha, Zabato mini watershed in Gido Matala kebele of 855.5ha and Magera of 196ha. Magera and Wutame watershed was known for its low ground and surface water availability, scarce vegetation cover, little soil moisture, and degraded land. Consequently, the productivity of the land and land production decreased to the extent of disabling the farming community to cover their daily food. To address these serious and urgent problems, many watershed management measures are underway in this micro watershed. Some of the physical and biological soil and water conservation works that have been introduced are hillside terraces, deep trenches, Fanajuu, stone-faced soil bunds, stone bounds, road maintenance/construction, runoff water harvesting practices and community ponds ($5000m^3$). Further, SLM has also been implemented over more mini watersheds in 2014/15 (e.g., Yanda micro watershed in Dalga Hejere kebele of 1096.9ha, and Yanda micro watershed in Hejere kebele of 371.9ha, Babi Buna of 237ha, Ajora Buna of 249ha, Tolmela of 102ha, Kashaleya of 329ha, Madoye of 176ha, Hagaza of 147ha, and Mechancho of 352ha).

Among these soil and water conservation works, 80% have been done through SLMP by the Government and 20% have been done with citizen participation ((Boloso Bombe Woreda SLMP report, unpublished). Substantial national resources have been investing in promoting these SLMP activities (Beshah, 2003; Admassu et al., 2014; Haregeweyn et al., 2017). Hence, SLM has to invest in these watersheds about 0.15-0.2 million dollars each year to promote the works according to the Boloso Bombe Woreda SLMP report. It is worthwhile to note here there is no proper quantification of the impact of these SLMPs on the watershed characteristics/ productivity, yet. This research is, therefore, intended to evaluate the impact of SLM intervention in Magera and Wutame micro watershed.

1.2 Problem Statement

The Earth's surface has witnessed severe land degradation, over the past many decades. This land degradations had resulted in many problems like periodic low soil moisture, poorly distributed rainfall, soil erosion, drought, floods, vegetation degradation, excess runoff

(Conacher, 2004; Mekonen and Tesfahunegn, 2011; Haregeweyn et al., 2012). Management of watershed is needed to alleviate these problems for improving soil conservation, water resource management and maintaining a sustainable ecological status (Zribi et al., 2011). Watershed management practices like soil bunds and terrace have a direct positive impact on soil moisture by reducing soil loss, runoff and maintaining infiltration rate a high level (Mekonen and Tesfahunegn, 2011). According to Bosshart, (1997), soil and water conservation structures like soil bunds have a potential of reducing the soil loss and eroding capacity of overland flow and increasing soil moisture. Despite the growing importance of watershed management as an approach to curb land degradation, there has been little research on their impact, till date.

Evidently, investigations are needed to ensure the pros and cons of these new measures, so as to facilitate improved conservation measures. Evaluation is difficult, however, due to the social and technical complexity of watershed management (Kerr and Chung, 2002). Sufficient availability of data is also another the major threat, to evaluate these watershed projects.

Impact studies have demonstrated that investment in watershed management in developing world do pay off in economic terms (Holden et al., 2005; Nyssen et al., 2010, Haregeweyn et al., 2012). However, such impact studies do not typically include detail hydrological components, though watershed management is a major determinant of hydrological process (Rohde and Hilhorst 2001; Nyssen et al., 2010, Haregeweyn et al., 2012). Quantitative impact studies may include thorough model simulations with ground truth, comparison between nearby similar twinned watersheds, statistical comparisons of several homogenous small watersheds, monitoring over several years before and after watershed management etc.(Twery and Hornbeck, 2001; Serrano Muela et al., 2005; Shipitalo et al., 2006; Lacombe et al., 2008; Nyssen et al., 2010). General tendencies indicate positive impacts from watershed management practices.

However, despite the result show positive achievement, collecting of such data's are labor-intensive, cost-prohibitive, impractical in the inhospitable terrain, cannot be carried out on daily basis (Dwivedi et al.,2001; Younis and Iqbal, 2015) and also using of such data for evaluating the impact of interventions shows deficient in describing Spatio-temporal characteristic of the watershed (Dwivedi et al.,2001).

A noble approach which is remote sensing overcomes this limitation and it is effective in evaluating the impact of watershed intervention on hydrological behavior such as on Spatio-temporal variability of vegetation cover (Hishe et al. 2017), on LULC dynamics (Thakkar et al.,

2017a), soil moisture (Alemayehu et al., 2009), on soil erosion (Mekuriaw, 2017) and also remote sensing data is easily accessible, gives daily or weekly data and freely available. The coupling of remote sensing data with GIS is a recent technology and helps to quantify the impact of watershed management interventions. Many studies have also demonstrated the capability of remote sensing and GIS in the impact assessment of watershed management interventions (Shanwad et al., 2008; Haregeweyn, .2012; Kumar et al., 2014; Thakkar, 2017b).

An evaluation of the impact is hence essential to differentiate between the positive and negative, to replicate only the positive (Kumar *et al*., 2014). Most of the previous studies are conducted on evaluating the impacts of watershed management on biophysical and socio-economic activities (Hurni., 2015; Nigussie.,2017; Teressa and Guteta, 2018). In addition, a few studies had analyzed the impact of watershed management on hydrological variables such as runoff, sediment yield, streamflow, and groundwater. (Huang and Zhang, 2004; Dou et al., 2008; Tadele and Dananto, 2018). However, less attention has given to quantify the impact of watershed management on fluxes and state variables such as vegetation cover and soil moisture that will provide a measure of the direct impact of these activities at a macro level. Hence, in this study, the impact of SLMP on land cover dynamics, vegetation cover and soil moisture is assessed for Magera and Wutame micro-watershed.

1.3 General Objective

The main objective of this research is to evaluate the impact of SLM intervention on vegetation cover, land cover dynamics and moisture distribution in Magera and Wutame micro-watershed.

To achieve the main research objective, the following specific objectives are identified:

- To quantify the changes in the area of vegetation cover using Normalized Difference Vegetation Index (NDVI).
- To evaluate the exact change point (year) if any, and to find its possible relation with SMLM intervention.
- To detect actual changes in land cover and soil moisture in the watershed as caused by SLM interventions.
- To analyze the Spatio-temporal soil moisture content in the watershed.

- To evaluate the accuracy of remote sensing-based on land cover mapping and soil moisture mapping.

1.4 Research Questions

The following research questions are raised to address the specific objective.

- Is it possible to quantify the area of vegetation cover accurately in a micro watershed using the Normalized Difference Vegetation Index (NDVI)?
- Is it possible to know the exact change point (year) in the NDVI time series as caused by intervention? What is the relationship between vegetation cover and SLM intervention?
- Has the soil moisture content increased or decreased after watershed management?
- Among the different land use/cover types, which land use/cover is increased by the direct impact of SLM intervention and which is decreased? Does SLM intervention can cause any changes in soil moisture distribution?
- Does remote sensing have a potential of accurately mapping the land cover and soil moisture in the micro watershed

1.5 Significance of the study

The primary findings of this study will contribute to SLM and governments who are investing a millions of dollar on SLM activities by providing the assessment of hydrological impacts like vegetation cover improvement, land cover dynamics and soil moisture changes gained so far after implementing watershed management and this will create the opportunity to improve and continue the existing SLM interventions. In addition, the findings of this study also contribute to the benefits of science, considering that remote sensing has the potential of evaluating the impact of watershed management.

Due to a lack of sufficient hydrological data and a lack of scientific evidence, watershed management interventions are rarely evaluated on hydrological variables. A recent and novel approach, which is remote sensing, can fill such data gaps. Thus, researchers that apply the recommended approach derived from the results of this study will accurately evaluate SLM intervention on hydrological components. Also, this study will provide new insight into the scientific assessment of gradual changes detection on vegetation densities and soil moisture as caused by a watershed intervention that has been not /limitedly documented to date. Agricultural office and stakeholders who are facilitating the SLM works are also guided by the positive

results recommended from this study and this will further create awareness about the importance of watershed management.

1.6 Scope of the study

It is a lot of work to deal with all hydrological variables, so it's better to limit the scope of the study to its primary objective. This study evaluates the impacts of watershed management measures on vegetation cover, land cover dynamics and soil moisture using Landsat Images in Magera and Wutame micro watersheds. SLM targets both watersheds in 2013/14. Wutame watershed is a part of Magera watershed; because of the small area, it is easy to measure hydrological data's in this watershed; thus, the soil moisture is evaluated only in this watershed. Vegetation cover changes and land cover changes are assessed in Magera watershed because of, all SLM activities are implemented in this watershed. The effect and impact of evaluating watershed intervention on soil moisture distribution don't isolate the impact of climate conditions such as potential evapotranspiration and rainfall.

2. LITERATURE REVIEW

2.1 Remote Sensing to Evaluate Impact of Intervention

The Multi-Spectral Remote Sensing images are very efficient for obtaining a better understanding of the earth's environment (Ahmadi and Nusrath, 2012). Remote sensing is the Art and Science of seeking information and extracting the features in form of Temporal, Spectral and Spatial about some objects, area or phenomenon, such as land cover classification, water resources, vegetation, urban area and agriculture land without coming into physical contact of these objects (Bhandari and Karaburun, 2010). Remote Sensing images has several application areas, including soil moisture measurement, snow mapping, land cover classification, forest type classification, measurement of the liquid water content of vegetation, sea ice type classification and oceanography (Bhandari and Karaburun, 2010). The multispectral remote sensing images carry essential integrating spectral and spatial features of the objects (Chouhan and Rao, 2012).

Remote sensing can identify changes from satellite data using change detection techniques and used for impact evaluation (biophysical changes) of watershed management. Post-classification comparison of pre-and post-implementation satellite imageries is the most common remote sensing approach used for impact evaluation.

As an increasing number of indigenous remote sensing satellites, reasonable pricing of indigenous satellite data and an increasing trained workforce have further use of remote sensing for watershed management (Kumar *et al*., 2010). The use of remote sensing has already begun in prioritizing, developing area-specific watershed development plans, as well as impact evaluation. The standard guidelines have also emphasized the use of advanced tools like remote sensing, GIS and GPS to evaluate intervention of impact (Kumar *et al*., 2010). Various studies have assessed the potential of remote sensing imagery for detecting LULC changes and evaluation the impact of watershed management have shown by several studies (Alemayehu *et al*., 2009; Bakr *et al*., 2010; Abd EI-Kway *et al*., 2011).

Chowdary et al. (2001) analyzed the impact of watershed management on nine watersheds distributed in Koraput, Nawarangpur and Malkanagiri districts of Orissa using Landsat imagery. The effect was assessed based on biomass and LULC dynamics over the pre to post-treatment periods of 1988–1996. The study shows an increase in tree cover, cultivated area, water body and plantation. Shanwad et al. (2008) also evaluated the impact of the integrated watershed

development program in Katangidda Nala watershed, Karnataka, using Landsat imagery. The impact was assessed based on the dynamics of LULC over the pre to post-treatment period of 1995–1997. The result pointed out that there is a significant an increase in agricultural land areas and forest land and decrease in the wasteland area.

Mekuriaw, (2017) evaluated the efficiency of sustainable land management activities on erosion and vegetative cover using remote sensing and GIS techniques in Melaka watershed, Ethiopia

The results demonstrated that agricultural land decreased by 9% whereas grassland and vegetative cover increased by 136 and 96% respectively. As the result, the productivity of the land and availability of forage was much improved which substantially improved people's livelihood. The authors concluded that land resource management measures practiced in the study area were highly effective for reducing soil loss, improving vegetation cover and livelihood of the population.

Kumar et al. (2014) evaluated the impact of watershed management programs in Keetnode village of Barmer district, Rajasthan using satellite imagery. The impact was evaluated based on a dynamics in biomass and LULC using over 2001–2007. The result revealed an increase in scrubland areas, cropland, fallow land, and decrease in sandy areas. Further, Dwivedi *et al.* (2001), evaluated the impact of soil conservation measure in Ghod catchments, using Landsat data of pre and post-monsoon seasons. The effect was assessed based on the change in LULC, soil erosion, biomass, irrigation area. The study noted that the effect of soil and water conservation measures practiced in the watershed in terms of improvement in agricultural land with improvements in eroded lands and groundwater recharge.

Hishe *et al*, (2017) evaluated the effects of soil and water conservation on vegetation cover using a remote sensing in the Middle Suluh River Basin, northern Ethiopia. The authors pointed out that from the remote sensing analysis and field observation results, noticeable increment in vegetation cover have been observed in the last 30 years. These increments are attributable to the implementation soil and water conservation practices, particularly in areas where area of exclosure were defined and protected by the local community.

2.1.1 LULC Change Detection

Digital change detection is defined as the process of identifying changes in LULC properties based on multi-temporal remote sensing data. Many researchers have studied the problem of monitoring LULC change in different geographical areas accurately. To evaluate the land-use

dynamics which typically vary from global to regional scale, remote sensing and GIS are the recent technologies (Csaplovics, 1998; Chowdary *et al*., 2001; Foody, 2002 Dutta *et al*., 2003; Shanwad *et al*., 2008).

Remote Sensing (RS) has been used to generate and map LULC dynamics with different process and data sets. Currently many change detection techniques have been developed that make use of remotely sensed satellite images. Landsat images, in particular, have served a great deal in the classification of different landscape components at a larger scale (Ozesmi and Bauer., 2002). A several change detection process and algorithms have been developed and reviewed for their disadvantages and advantages. Among these post-classification comparisons (PCC), Fuzzy classification, unsupervised classification, Hybrid classification, or clustering and supervised classification are the most widely used techniques in applying image classification (Lu *et al* ., 2004).

Many supervised classification methods have been applied extensively for the LULC dynamics analysis. This technique depends on a combination of background knowledge and personal experience with the greater extent to study area than other areas. Therefore, Jansen (2005) concluded that, per-each pixel signatures are tested and stored in signature files using this knowledge and the raw digital numbers (DN) of each pixel in the image are therefore translated to radiance values.

Several various researchers have applied the supervised classification methods and get highly better results including Rawat and Kumar (2015), who applied supervised classification method to monitor LULC dynamics in India. Moreover, Rawat *et al.* (2013) also applied the supervised classification method for India to track the dynamics observed in the area between the time period of 1990 and 2010. Boori *et al* (2015) also analyzed the LULC disturbance caused by tourism using a number of GIS and Remote Sensing based techniques including supervised classification.

2.1.2 Soil Moisture Detection

Soil moisture is defined as, the amount of water in unsaturated soil profile part, i.e. in between the ground water level and soil surface (van der kwas, 2009). It has many application for example, soil moisture content data is necessary for parameterizing hydrological models, which are further used to quantify evapo-transpiration from land surfaces, and deep percolation for groundwater effect studies. Soil moisture status is important for climate variability studies, for

conducting agricultural applications, for water resource management, soil water balances and for meteorological (Verhoest *et al*., 2008). Therefore, it is highly essential to monitor and estimate the accurate spatial and temporal soil moisture variations.

Soil moisture is widely measured using the point-based method (gravimetric method) by collecting soil samples, but this method is overwhelming and sturdy. It is unable to describe the behavior of its spatial and temporal distribution. Also, the ground measurement of soil water content, in general, is laborious and cannot be easily carried out daily (Younis and Iqbal, 2015). In the modern epoch, technological advancement has presented that soil water content can be estimated by several remote sensing methods (Younis and Iqbal, 2015). Remote sensing techniques have been extensively used for the analysis of soil moisture and have provided alternative tools for obtaining rapid estimates of soil moisture on a large spatial scale (Shimizu *et al*., 2011).

Currently, there are several satellites such as the Soil Moisture Active Passive (SMAP), Soil Moisture and Ocean Salinity (SMOS), METOP-A/B Advanced Scatterometer (ASCAT), Advanced Microwave Scanning Radiometer–EOS (AMSR-E) and the European Space Agency's Climate Change Initiative (ESA CCI) soil moisture products, that have been successfully used to retrieve surface soil moisture at temporal resolution of 2 to 3 days (Ochsner *et al* ., 2013; Chen, and Wang., 2018).

For the purpose of regional and regular determination of surface soil moisture, satellite-based techniques including microwave and optical /thermal remote sensing methods have been used in several various studies over the past many decades (Dubois *et al*., 1995; Liu *et al*, 2012). But microwave RS techniques have received greater attention for monitoring global scale soil moisture dynamics because microwaves can penetrate through the vegetation canopy and underlying soil, especially at lower frequencies (Tabatabaeenejad *et al*., 2015).

Another advantage of Microwave RS can sense the land surface under all-weather conditions without the impact of cloud contamination (Barrett *et al*., 2009). However, this method has several well-known limitations. It has coarser spatial resolution (≥25 km), which is too far from adequate field-scale monitoring owing to the micro watershed like Wutame (Zeng et al., 2019). These limitation can be achieved using thermal/optical remote sensing data, as they have adequate temporal and spatial resolution to capture the seasonal surface soil moisture variation at

large scales and in most case data are easily available free of charge e.g., Landsat series data (Li et al., 2016).

The so-called “trapezoid” model, which is described in Lambin and Ehrlich (1996), is one of the most widely applied approaches to RS of soil moisture utilizing both thermal and optical data. The model is based on the interpretation of the pixel distribution within the VI-LST space, where VI is a RS-based vegetation index and LST is the land surface temperature. The soil moisture index (SMI) is a widely applied thermal/optical infrared remote sensing method that has proven to be feasible in extracting surface soil moisture content over partially vegetated areas (Parida et al., 2008). Zhan et al. (2004), Potic et al. (2017) and Saha et al. (2018) were among to apply the LST- NDVI space for estimating surface soil moisture using SMI model.

2.2 Remote Sensing for LULC Mapping

Land use and land cover terms are often used together. Therefore it is essential to define them clearly. The land cover represents the physical and biological cover of the Earth’s surface, including classes as build-up areas, forests, agricultural areas, wetlands, (semi-)natural areas, water bodies (Gregorio, 2005). On the other hand, land use represents the present and future planned human activities on a territory (Ferance *et al*., 2007), characterized as residential, industrial, commercial, agricultural, forestry and leisure. It is the expression of the human activity developed for social, economic, cultural and political purposes. This means that land cover includes the land use features and they should be represented on different maps.

Land cover can be generated from remote sensing satellite imagery, whereas, land use can’t be generated from satellite imagery. A satellite image often contains information that can readily be analyzed visually.In most cases it is possible to get an idea about the relative importance of urban areas, forests, agriculture etc. just by looking at the image. Nevertheless, it is in some cases necessary to convert the satellite image to a thematic map of different land cover or land use types. This will make it possible to work quantitatively with the characteristics of the area and to analyses and understand the distribution of different land cover types.

Remote sensing data has been applied commonly for classification of various features of the land surface and land cover identification from satellite or airborne sensor. Application of remotely sensed data for land use mapping and land cover and also its changes is fundamental to various applications such as hydrology, agriculture, geology, environment and forestry, etc.

Remote sensing image classification involves grouping the pixels of an image to a (relatively small) set of classes, such that pixels having similar properties have the same class. More of, image classification is based on the detection of the spectral response patterns of land cover classes. Therefore, classification depends mainly on distinctive signatures for the land cover classes in the band set being applied, and the ability to reliably distinguish these signatures from other spectral response patterns that may be present (Eastman *et al*., 2003). The advantage of land cover mapping is to identify the land cover change in different categories of land use and land cover on the watershed. For this reason, remotely sensed imagery has become the primary data source to obtaining information on both temporal trends and spatial distribution of watershed areas and changes over the time dimension for projecting land cover changes but also to support changes impact assessment because of its advantages in fast, cost-effective, synoptic, accurate, flexible and up to date properties and digital data acquisition characteristics (Atasoy *et al*., 2006). To assess the land cover dynamics, to categorize the types of land cover, and to obtain timely land cover information, multi-temporal remotely sensed images are considered useful data sources.

2.2.1 Ground Control Points (GCPs)

Before using satellite image for performing any analysis like LULC mapping, vegetation mapping, image classification, change detection, it is necessary to correct and adapt them geometrically, so that they have comparable resolution and projections as the others set because the raw images taken from satellites are subject to systematic and non-systematic geometric distortions (Environmental, 2005). All satellite imageries are subjected to geometric distortions. Therefore geometric corrections, which are the first preprocessing steps, are normally needed prior to imagery extraction and analysis of information (Lillesand and Kiefer, 2000). Geometric distortion in all satellite images is defined as, the inaccurate feature position of satellite images to the scene on the ground or on map positions. The following are the main sources to all of geometric distortion: rotation of the Earth during image acquisition, curvature of the Earth, and satellite attitude, altitude and velocity variations (Environmental, 2005).

Geometric corrections are applied to remove these distortions so that the geometric representation of the satellite imagery will be as same as to the real environment. Lillesand and Kiefer, 2000 suggested two types of methods to correct various types of geometric distortions. (i) Systematic distortions which is corrected by applying mathematical model to the sources of

distortions. These modeling techniques need a huge knowledge about, the nature and the magnitude of the sources of distortion, the orbit parameters during the image acquisition time. (ii) Random distortions which is corrected by developing mathematical relationship between the coordinates of pixels in the image and the corresponding coordinates of those points on the ground. This relationship is used to correct the geometry of the image irrespective of information about the type and source of distortion.

The second method is most widely used and it doesn't depend on the platform used for image acquisition. This method follows two steps. The first step is the registration step. It includes identifying the images raw coordinates (i.e. row, column) of many clearly visible points, called ground control points (GCPs), in the distorted image, and map them either to coordinates of corresponding points (image-to-image registration), or to their true positions in ground coordinates (e.g. latitude, longitude) measured from a map (image-to-map registration), to georeferenced image (corrected before), through to mathematical transformation, that will convert the raw image coordinates into the desired coordinates (Richards and Jia, 1999). The second step is the resampling techniques to re-analyze the gray pixels level in the already transformed output image based on pixel values in the input image. Resampling can be done through the following three methods: cubic convolution, nearest neighbor and bilinear interpolation (Erdas, 2002).

Several various studies have been conducted on the geometric correction of remote sensing images, either using the first methods (Manadili and Novak, 2009; Dowmann and Dolloff, 2000) or using the second methods (Wu and Lee, 2001; Afity, 2002). Therefore, Baboo and Devi (2011) concluded that, geometric correction is an essential pre-processing step that can be used to correct the inaccuracy between the actual location of ground coordinates and the location of picture elements of coordinates in the image data. This geometric transformation can be assessed by selecting pairs of suitable GCPs on satellite imagery and an appropriate geometric model.

Geometric correction is applied to transform image pixels from coordinate system to another coordinate system related to available reference data (Baboo and Thirunavukkarasu, 2014). Different methods are applied to transform one coordinate system to another coordinate system as polynomial transformation, Helmert transformation, projective transformation, and affine transformation. Polynomial transformation offer many advantages than others such as well-known, understood properties, simple form, and moderate flexibility of shapes. Polynomial

transformation needs the use of reference data with well ground coordinates as ground control points (GCPs) and/or georeferenced image (ERDAS, 2013).

Many researches applied the geometric correction on remote sensing images that deal with main influencing factors of image rectification accuracy as accuracy of control points, number of control points, transformation models and distribution of control points. Santhosh *et al*., (2011) applied the image to map geo-correction using polynomial transformation using sixteen GCPs through ERDAS Imagine 9.1 software. The result revealed that the geometric correction process using a polynomial model resulted in a Root Mean Square (RMS) error equals to 0.6 and it is below the one pixel, which will gives the high-quality georeferenced image (Baboo and Devi, 2011). El Amin *et al*., (2016) analyzed different numbers of GCPs with different densifications for geometric correction of the aerial image. The authors investigated that three GCPs with specific distribution and densification are good enough for geometrical correction of aerial images (Babiker and Akhadir, 2016). Furthermore, Hamza *et al*., (2009) also applied a third-order polynomial using ten GCPs and assessed the impact of the selected location of GCPs and the method of the distribution of the selected GCPs over the distorted image area on geometric correction accuracy. The authors concluded that to get high accuracy of geometric correction of satellite images, the distribution of selected GCPs and location should be taken into consideration, and also the effect of wrong location of selected GCPs is more severe than that of wrong distribution of selected GCPs on the correction accuracy (Eltohamy and Hamza, 2009).

2.2.2 LULC Mapping Methods

Mapping and identifying LULC and its change is the most essential, as well as the most commonly researched topic in GIS and remote sensing. LULC has been used widely to derive several biophysical variables, such as vegetation index, carbon content and biomass.

Mapping LULC accurately and efficiently using remote sensing needs good image classification methods. The essential functions of remote sensing data is the produce LULC maps and can be done by a process called image classification.

Based on the idea that different types land cover have a different spectral reflectance/remittance properties, their recognition can analyzed through the classification process. Lillesand & Keifer (1994) defines image classification as the techniques of grouping all pixels in an image to get a given set of land cover themes. The following steps were followed for general image classification include design image classification pattern, preprocessing of the satellite image,

choosing representative areas of the satellite image and generate training signatures, running of image classification algorithms, post-processing and accuracy assessments (Gong and Howarth, 1990). There are several classification techniques that have been developed and mostly used to generate land cover maps (Aplin & Atkinson, 2004). They are ranging in logic, from parametric to nonparametric to non-metric; supervised to unsupervised, or per-pixel, sub-pixel, pre-field or hard and soft (fuzzy) classification (Jansen, 2005). However, there are two general types of classification steps and each finds application in the processing of satellite images: one is referred to as unsupervised classification and the other one is supervised classification. These can be sometimes used as alternative methods, but are often combined into hybrid methods using more than one method (Richards & Jia, 2006).

Unsupervised image classification is an approach in which the remote sensing image interpreting software identifies a huge number of unknown pixels units in satellite image based on their reflectance units into classes or clusters with no direction from the analyst (Tou & Gonzalez, 1974). There are two common clustering approach used for unsupervised classification: Iterative Self-Organizing Data Analysis Technique (ISODATA) and K-means. These two approaches depends purely on spectrally pixel value-based statistics and incorporate no prior knowledge of the characteristics of the themes being studied.

Supervised classification is an approach in which the analyst defines few areas called training sites on the satellite image, which include the predictor variables estimated in each sampling pixels, and assigns prior classes to the sampling pixels (Cerna & Chytry, 2005). The delineation of training unit representative of a land cover type is most efficient when an image analyst has knowledge of the geography of the study area and experience with the spectral signatures of the cover class (Skidmore, 1989).

The supervised approach has many advantages over the unsupervised approach. In the supervised method, important information categories are distinct first, and then their spectral signature is tested while in the unsupervised approach, the computer software determines spectrally identifiable pixels, and then gives their inform value (Lillesand & Keifer, 1994). Besides, unsupervised classification method is easy to apply, don't require analyst specified training data and is mostly available in satellite image processing and statistical software package; furthermore, it automatically translates raw image data into important information so long as there is better classification accuracy (Langley *et al*., 2001), but one disadvantage of this

classification approach is that the classification techniques has to be repeated if new samples are added. For this reason, mostly researchers suggested to use a supervised classification approach.
A verity of studies has addressed that Supervised Maximum Likelihood classification is the most common method in remote sensing image data analysis. It identifies and locates land cover types that are known a priori through a combination of personal experience, interpretation of aerial photography, map analysis and fieldwork (Jansen, 2005). It uses the means and variances of the training data to estimate the probability that a pixel is a member of a class. The pixel is then placed in the class with the highest chance of membership.

Therefore, Shalaby and Tateishi (2007) concluded that the supervised classification techniques quantitatively assess both covariance and variance of the category of spectral signature patterns when classifying unknown pixels values. For high or medium spatial resolution data having heterogeneous and complex land surface and the high possibility of wide portion of mixed pixel values collecting sufficient number and, training signature is very essential to supervised classification (Lu and Weng, 2007).

2.2.3 Accuracy Assessment

For remotely-sensed data to be beneficial and useful, an appropriate technique of accuracy assessment needs to be performed. Accuracy assessment can be defined as a comparison of a map produced from remotely-sensed data with another map from some other source. Evaluation of the accuracy of classification of remotely-sensed data can fall into one of two general categories: non-site-specific assessment, or site-specific assessment (Campbell, 1987)
Non-site-specific assessment is a simplistic approach to assessing the accuracy of the classification of remotely-sensed data (Campbell, 1987). In this method, a comparison is made between the "known" or estimated area and the area derived through the process of the discrete classification of remotely-sensed data. Non-site-specific error analysis consists of identifying general problems with the resulting classification, but provides no information about the locational accuracy of the assessment (pixel misclassification), or how well each pixel was classified.
Site-specific error analysis takes into account the locational accuracy of the classification (Campbell 1987). This process makes a pixel-by-pixel comparison between the remotely-sensed, data-derived thematic map and a "true" map of the area with the same theme. This accuracy

assessment approach is still prone to errors attributable to control point location error, boundary line error, and pixel misclassification (Hord and Brooner 1976).

Site-specific accuracy assessment can be evaluated for an overall classification or on a per-category basis. The more rigorous and useful approach is to assess accuracy on a per-category basis, which provides more insight into classification errors that may be unique to specific categories. A stratified random method is an appropriate sampling method for accuracy assessment on a per-category basis (Van Genderen and Lock 1976).

The Kappa Coefficient of Agreement, which is a statistical measure of the significance of the difference between observed agreements of two classifications versus agreement due to random chance, is commonly used in both types of assessment and requires a multinomial sampling method. A stratified random sample is a multinomial sampling method, and therefore is an appropriate sampling method to be used with the Kappa statistic.

An error matrix can be useful when evaluating the effectiveness of a discrete classification of remotely-sensed data. An error matrix is a means of reporting a site-specific error (Campbell 1987). The error matrix is derived from a comparison of reference map pixels to the classified map pixels and is organized as a two-dimensional matrix. An error matrix is also referred to as a confusion matrix or contingency table, and in many cases, classification categories are arranged in columns and reference data represented along the rows of the matrix (Janssen and van der Wel, 1994).

From the error matrix, several measures of classification accuracy can be calculated, including the percentage of pixels correctly classified, errors of omission, and errors of commission. In addition, statistical tests such as the Kappa Coefficient of Agreement, Kappa variance, and Kappa standard normal deviate can be calculated from the error matrix. The most commonly used measure of agreement is the percentage of pixels correctly classified. This measure is simply the number of pixels correctly classified from the validation set of pixels divided by the total number of reference pixels. Percentage correct is calculated by dividing the sum of the diagonal entries of the error matrix by the total number of reference pixels. Therefore, the percent correct provides an overall accuracy assessment of a classification.

Errors of omission refer to pixels in the reference map that were classified as something other than their "known" or "accepted" category value. In other words, pixels of a known category were excluded from that category due to classification error. Errors of commission, on the other

hand, means that in the classification map, pixels that were not correctly classified and don't found in the category in which they were assigned according to the image classification. In other words, pixels in the classified image are included in groups in which they don't found.

When evaluating the accuracy of an overall classification, it is best to examine several measures of accuracy, including overall percentage correct, percentage correct by category and also both errors of commission and omission by category.

User accuracy is simply the percentage of pixels in each category of the classification map that are actually that category of the ground (Congalton 1991). Producer accuracy is calculated similarly, with the only difference being that the total number of correctly classified pixels for a category is divided by the total number of pixels in that category in the classification map.

The Kappa Coefficient of Agreement is a statistic suitable for assessing accuracy of nominal data classification. The Kappa Coefficient is a discrete multivariate measure that differs from the usual measures of overall accuracy assessment. The importance of using the Kappa Coefficient is the ability to compare two classifications and determine if the accuracy level between the two classifications is significantly different.

2.3 Application of GIS and Remote Sensing for Vegetation Cover mapping

In recent years, Geography Information System (GIS) and Remote Sensing (RS) have become fundamental tools for characterizing vegetation cover and land use land cover (LULC). The primary source of information about the earth cover is remote sensing images. They are commonly used in monitoring and detecting vegetation cover changes at various scales because of the capability of remote sensing technology to provide repeatable, objective, calibrated and cost-effective data for large and regional areas (Al-Doski et al., 2013). Vegetation cover change detection is the one among the application of remote sensing. Hishe et al. (2017) describe remote sensing as one of the most commonly used technologies for effective discerning correlation of ecosystem properties via the reflectance of light in the spectral and spatial domain. Also, remote sensors such as Landsat, Quickbird, IKONOSs, MODIS and SPOT have the potential of capturing the reflectance from ground surfaces such as from vegetation which have their own unique spectral characteristics.

There are many indices for highlighting vegetation cover areas on remote sensing scene. The most commonly used proxy for vegetation cover and production among the various remote sensing-based vegetation measurement utilized in agricultural monitoring is the Normalized

Difference Vegetation Index (NDVI) (El-Gammal et al., 2014). It is an essential vegetation index, mostly applied in research on climatic change and global environmental (Bhandari et al., 2012). Numerous researchers have studied the use of NDVI for vegetation monitoring.

Gross. (2005), evaluated agricultural biomass using the NDVI time series and noted that NDVI had detected the spatial distribution of vegetation anomalies and vulnerable areas. The author concluded that knowledge of the crop calendar and location of growing regions for the different crop types with NDVI helped accurately to evaluate the agricultural biomass.

Hishe et al., (2017), evaluated the impact of watershed management on vegetation cover using NDVI and SAVI approach in Ethiopia watershed and concluded that NDVI with long term rainfall accurately assessed the watershed management on vegetation cover. EL-Gammal et al. (2014), also detected vegetation cover change using the NDVI threshold in Damietta Governorate, Egypt, and the author noted the potential of NDVI showing the different variability in the percent cover change and the annual rate of difference between the various cover classes.

2.4 Remote Sensing for Soil Moisture Mapping

Accurate estimation of regional soil moisture distributions require direct sensing observations that capture discontinuities in soil moisture fields (Hendrickx *et al*., 2010). Analyzing the spatial and temporal soil moisture variability is hence important for various scientific issues and applications (Famiglietti *et al.,* 2008). From that perspective, a huge number of soil moisture sensing methods have been developed and used for the last 50 years (Robinson *et al*., 2008).

Currently direct measurement of soil moisture are restricted to discrete measurements at specific locations and such direct measurements don't represent the spatial distribution of soil moisture, because soil moisture is extremely variable both temporally and spatially (Engman 1991). Advancement in remote sensing technology has provided a several techniques for estimating soil moisture across a large area continuously over time (Engman 1991). In the mid-1970s, studies on soil moisture remote sensing began shortly after the rapid advancement in satellite remote sensing.

Several studies have reported that soil moisture content can be measured by thermal infrared and optical remote sensing, as well as active and passive microwave remote sensing techniques (Njoku and Kong 1977). The primary difference among the techniques are the region of wavelength of the electromagnetic spectrum used, the response captured by the sensor, the

source of the electromagnetic energy and the physical relationship between the soil moisture and reaction (O'Neill *et al*., 2003).

Soil moisture cannot be estimated directly by remote sensors but, mathematical models are developed to know the relation between the soil moisture content and measured signal (De Troch *et al*., 1996). Nowadays, development in technological remote sensing has shown that soil moisture can be analyzed by a number of remote sensing techniques on wide scale; each has its own strengths and weaknesses (Liand Islam 1999). Optical/IR and microwave regimes techniques have received more attention. Finer spatial resolution is provided by Optical/IR techniques to estimate soil moisture content. Microwave remote sensing has shown a quantitative ability to analyze soil moisture content physically for wider ranges of vegetation cover. However, the spatial resolution and the channel frequencies of current remote sensing microwave radiometers are not good enough for land remote sensing due to practical problems in supporting wide, low-frequency antenna in space (Zhan *et al*., 2002).

Hence the swivel task was to use the novel optical/IR approaches the so-called trapezoid or method proposed by Sadeghi *et al*. (2017). The model is also known as Thermal-Optical Trapezoid Model (TOTRAM) is interpreted based on the pixel distribution within the VI-LST space, where VI is a RS-based vegetation index and LST is the land surface temperature.

Vegetation indices (VIs), which are mathematical combinations of different spectral bands from satellite remotely sensed data, have been utilized to estimate soil moisture (Chen *et al*., 2015). The normalized difference vegetation index (NDVI) is the standardized reflectance difference between the near-infrared (NIR) and visible red (R) bands (Tucker *et al*.,1979), which measures changes in chlorophyll content. As a result, it is considered a function of vegetation strength, which changes as vegetation interacts with soil moisture. The normalized difference water index (NDWI) is a more recent satellite-derived index from the NIR and short-wave infrared (SWIR) channels that reflects changes in both water content and spongy mesophyll in vegetation canopies (Gao, 1996). This index has been employed for the determination of vegetation water content and stress and is therefore expected to be linked to soil moisture due to its impact on vegetation water stress. Moreover, land surface temperature (LST) can rise rapidly with water stress (Goetz, 1997), which is directly related to soil moisture. Accordingly, LST is also widely used as a soil moisture indicator (Carlson, 2007).

The VI-LST relationship shows an inverse relationship typically, resulting in trapezoid-shaped VI-LST plots at different spatial scales (Goetz, 1997). Based on the VI-LST correlation, the soil moisture index (SMI), computed from the NDVI-LST relationship, has become a widely used moisture index to estimate surface soil moisture (Parida et al., 2008). For example, Hao and Dasgupta (2007) applied NDVI-LST produced from moderate resolution imaging spectroradiometer (MODIS) data to investigate the correlation with soil moisture determined by field measurements. The results revealed that NDVI-LST is strongly correlated with soil moisture and can be used to generate soil moisture estimates. Saha et al. (2018) used the SMI (NDVI-LST) derived from Landsat-8 OLI data to estimate soil moisture and found that the SMI can reflect the soil moisture status under different tree species.

2.5 Impacts of Land Degradation on vegetation Cover and Soil Moisture

Land degradation and desertification are processes characterized by the deterioration in land quality in terms of its capability to support selected land use and associated flora and fauna functionally. Land degradation is usually associated with sparse vegetation of low biodiversity. Many researchers defined and explained land degradation in different ways based on their impacts and causes. Taddese. (2001), describes land degradation is the loss of land productivity, quantitatively or qualitatively through various processes such as wind and soil erosion, salinization, waterlogging, and depletion of soil nutrients and soil contaminants. UNCCD. (1994) also explains land degradation as the destruction of vegetation cover, soil loses, soil erosions, biological reduction of forests, pastures and woodlands resulting from natural and human activities. Nunes et al. (2012) further demonstrate land degradation as the reduction in soil moisture contents to changes in chemical, biological and physical properties caused by soil erosion.

In the whole world, land degradation was started over the past many decades. Since then, many of the land areas are degraded. According to FAO (2015) estimate, the global degraded land area is about 33% of the total area. From this total global degraded land area, Bai et al. (2008) point out that cropland degradation accounts for approximately 18% and forest degradation accounts for approximately about 47% of the global total degraded area. Furthermore, Naseer and Pandey (2018) showed on their studies that roughly about 1.9 billion hectares of land and two billion people and are affected by land degradation globally.

The leading cause for such land degradation are different factors such as climate changes which decrease the natural ability of land to recover economic activities, deforestation and vegetation cover changes and losses, poor watershed management practices like overgrazing and over-cultivation of soils and other factors like soil and water pollutions (Lanfredi et al., 2015; Naseer and Pandey, 2018). Land degradation has a direct negative impact on vegetation densities and soil moisture content. Several previous studies suggested the negative effects of land degradation in altering the hydrological systems, for example, Conacher and Sala. (1998), indicated that land degradation could cause vegetation degradation, which means the permanent or temporary reduction in structures, densities or species composition of vegetation cover. In addition, the authors further pointed out that vegetation degradation can be caused by extreme climate changes, less soil moisture, overexploitation and unfortunate watershed management activities.

Ali. (2007) also demonstrated the impact of land degradation on soil moisture by relating it with ecosystem alteration like soil degradation and can be manifested by vegetation loss, and this, in turn, causes the land to lose its production and stability. This further also causes deterioration of biodiversity, negatively affecting the balance of the ecosystem and finally creating the ecosystem alteration such as energy and water regulations. Further, the author digs out, degraded land has less soil holding capacity, this increases the runoff of volume by reducing infiltration, thus increasing the risk for flood and high drainage also can cause river siltation and sediment load. Therefore, Nunes et al. (2012) concluded that the main impacts of land degradation are the loss of soil productivity that results from decreases in soil moisture, soil organic matter, soil biodiversity and water quality and further, this process decreases soil microbial biomass and consequently, soil microbial processed.

2.6 Impact of Interventions in Ethiopia

Integrated watershed management (IWSM) is a multi-objective and multi-disciplinary approach to solving natural resource management and food security problems in rural communities, particularly in dry and semi-arid areas where rainfall is scarce (Igbokwe and Adede, 2001). The overall aim of integrated watershed management is, therefore, to ensure sustainable natural resource use and equitable growth of communities. The replicability of land resource management can be justified if the intervention approach and the impacts are well assessed and studied (Alemayehu et al., 2009).

In Ethiopia, impact of the watershed intervention is rarely evaluated. Here are some articles which tell the evaluation of watershed intervention in Ethiopia.

Mekonen and Tesfahunegn (2011) evaluated the Impact of soil and water conservation measures at Medego watershed in Tigray, northern Ethiopia. The study demonstrated that terraces and check dams were filled with soil up to 1.5 m deep, gullies started to stabilize, water supplies and irrigation increased in many folds, the seedling survival rate rose to over 45%, and the vegetation density and coverage are improved by more than 30%. Also in hand-dug wells water levels increased up to 2 m. In addition, many springs and shallow wells emerged by more than 100 times after impact of SWC measures implemented in the watershed. Finally, the authors concluded that evaluation of watershed management intervention is very important to understand the failure and the success of previous watershed management measures and to readjust it accordingly for the future plan.

Yaebiyo *et al*. (2015) assessed the socio-economic impact of integrated watershed management in Sheka watershed, Ethiopia. The result revel that after watershed management there were significantly higher yields gain in the treated watershed than the untreated watershed. Also, honey bee yield and milk yield of local dairy cow was increased by 24.24% and 12.3%, respectively. The better annual income was get from the users who applied both the improved livestock and irrigation. The main source of annual income generation for households were using irrigation access, livestock number, cultivated land and off-farm income. Authors concluded that integrated watershed management not only improved crop and livestock production but also improved the household's annual income generation.

Adimassu and Langan (2016) assessed the Comprehensive impact of watershed management interventions in Ethiopia. The study was conducted in four agricultural watersheds located in four regions of Ethiopia. Embahasti watershed is located in the Northern part of the country in Tigray Region, Alekit –wonz watershed is located in Northwest Ethiopia of Amhara Region, Borodo is located in the central Ethiopia of Oromia Region, Jawe-gumbura watershed is located in the Southern parts of the country in the SNNP Region. In that watershed management interventions (mainly soil and water conservation practices) improve soil nutrient and soil moisture. The majority of the interviewed farmers responded that soil and water practices reduced soil erosion and increased crop yield.

Mena *et al*. (2018) assessed the impact of community adoption of watershed management practices at Kindo Didaye district Wolayita, Southern Ethiopia. The findings this study revealed that almost 100% respondents have got knowledge about the problems watershed degradation; and the response achieved by only the implementation of watershed management practices. The key finding of this research presents that due to watershed interventions the life of the community was improved and enhanced especially; food availability, water, income, forest cover and crop productivity.

2.6.1 LULC Change

LULC change refers to human modification of the terrestrial surface of the Earth (Ellis, 2006). The dynamics in LULC can either can cause positive or negative effects depending on what drives the changes. Apparently, the dynamics is driven by either institutional or political factors, biophysical, anthropogenic factor and socio-economic, which can be grouped as proximate and underlying causes (Lambin& Geist 2002). Human activities that causes conversion of vegetated area to urban and agricultural may result in negative impacts; while human activities which causes conversion of bare land to vegetation cover or agroforestry may result in improvement of land cover (WRI, 2001). Improvement in vegetation cover and land cover can be achieved via implementation of different natural resource management approaches among which sustainable watershed management is the principal one.

Various authors addressed LULC change in Ethiopia, their focus varying greatly in terms of thematic area as well as spatial locations (Tsegaye *et al*., 2010; Teferi *et al.,* 2013; Mengistu and Waktola, 2016). However, comprehensive and national scale analysis was conducted by the Woody Biomass Inventory and Strategic Planning Project, which has produced land use and land cover maps for Ethiopia (WBISPP, 2005). All of these studies showed that LULC dynamics has an effect on local livelihoods, water resources , biodiversity and forest among others. The main cause of dynamics are linked to population growth and farmland expansion.

Here is some of the reviews related to the impact of watershed management on LULC change in Ethiopia. Legesse *et al*., (2108) evaluated impacts of community-based watershed management on LULC Change at Elemo micro-watershed, Southern Ethiopia. The authors demonstrated that before the watershed management activities the proportion of shrub land and agroforestry was 171 ha and 34 ha respectively. This was later increased to 617 ha and 152ha respectively after

the intervention. The result also showed that the implementation of community-based watershed intervention resulted in the restoration of biodiversity and improvement in soil fertility.

Haregeweyn *et al*., (2012) also assessed the effectiveness of watershed management to curb land degradation in the Enabered watershed in Northern Ethiopia. The study demonstrated that Land use and land cover, runoff, and soil losses were compared before (2004) and after (2009) the interventions.The resulst revealed that plantations and exclosures increased significantly at the expense of grazing lands and bush land. Runoff and sheet and rill erosion decreased by 27 and 89 %, respectively, and gully channels were reclaimed.

Alemayehu *et al*. (2009) evaluated the impact of watershed management on LULC dynamics in eastern Tigray, Ethiopia. The dynamic in LULC was assessed by integrating GIS and remote sensing. The results reveal that there is a conversion of LULC and significant modification was observed in the watershed. The irrigated areas undergo increased from 7 ha to 222.4 ha post-intervention. The forested areas also undergo increased from 32.4 ha to 98 ha. This study further showed that management measures, increased soil moisture, decreased soil erosion, reduced runoff and sedimentation. Also after intervention stabilization of gullies and river banks, rehabilitation of degraded lands was observed.

2.6.2 Soil Moisture and Ground Water Change

The main objective of watershed management is to rehabilitate degraded land, protecting soil moisture dryness and sustaining the ecosystem. On the other hand, overgrazing and improper land resource management are the principal causes of increased runoff, low soil moisture content, soil erosion and low groundwater availability in Ethiopia. But it could be reversed through watershed management intervention with a positive impact on groundwater balance as well as soil moisture.

In Ethiopia impact of watershed management on soil moisture change and groundwater change is not yet evaluated. But some previous related study on soil moisture and groundwater change using remote sensing in Ethiopia are here.

Hishe *et al*. (2017) evaluated soil and water conservation effect on soil properties in the Middle Silluh valley, northern Ethiopia. In their study, they considered conserved landscapes (terraced hillside, terraced farmland and exclosure area) and non- conserved landscapes (non-terraced hillside, non-terraced farm and open grazing land) for comparison using a one-way analysis of variance (ANOVA). The results indicated that mean bulk density was low on a terraced hillside,

non-terraced hillside and exclosure area. A higher mean organic matter was observed in the conserved landscape, as compared with the corresponding non-conserved landscape. The authors concluded that the results show that soil and water conservation had significantly positive effects on the soil's physical and chemical properties in the study area.

Demisachew and Dananto, 2018 quantified the impact of integrated watershed management on groundwater availability in Gerduba watershed, Yabello district, Ethiopia. The result noted that as the result of watershed management measures, the surface runoff volume become reduced from 45.98 to 33.44% of the mean annual rainfall of the catchment. Inversely, the groundwater level increased from 12.8 to 55.14% of the mean annual rainfall of the watershed. The difference in groundwater level in the cistern and hand-dug wells in post interventions was found to be 1.1 and 1.3 m, respectively. Finally, the authors concluded that the construction of additional physical conservation structures is suggested to further improve the groundwater availability in the area.

Here are also some similar previous studies in impact evaluation of watershed management on groundwater. According to a study carried out by Bierman and Rosen (2005), introducing biological and physical soil conservation measures can restrict runoff and reduce erosion then increases groundwater recharge. Nyssen *et al*. (2010) demonstrated that good watershed intervention resulted on increased in infiltration rate and a reduction in volume of direct runoff by 81%, which had a significantly positive influence on the catchment water balance, because some of the rainfall is divided between the atmospheres through evapotranspiration and deeply percolates downward, with some re-emerging as stream flow, while the remaining recharges the groundwater as a result of watershed intervention which may balance the discharging and recharging (Kumar, 2003).

Singh *et al*. (2014) also studied at Garhkundar- Dabar watershed in India the effect of treated and untreated watershed and compared the result. The result shows that treated watershed decreased rainstorm flow (21 vs. 34%) together with increased base flow (4.5 vs. 1.2%) and groundwater recharge (11 vs. 7%) relative to total rainfall received. These led to minimizing of the velocity of surface runoff generation and created opportunities for percolation and recharge of groundwater.

3. MATERIAL AND METHOD

3.1 Description of the study area

Wolayita Zone is one of the rapidly growing zones in the SNNPR and has 12 Woredas. Boloso Bombe Woreda is one of these. Bombe is a capital town of the woreda, situated in along Ajora falls, which is located 325km and 55 away from Addis Ababa and Sodo town, respectively. The geographic location of the woreda is 37.44-37.66 East and 7.03-7.19 North with an altitude varying from 501-2500 meters above sea level. The woreda is located at the north, Kambata Tambaro, at South, Sodo Zuria, and Kindo Koysha Woreda, at East Boloso Sore Woreda and at West Damot Sore Woreda (Honja et al., 2016; WZFEDD, 2014).

Out of 21,859 ha of total area, 13,592 ha (62%) is cultivable land, 1560 ha is grazing land and 3207 ha is forest land. The remaining 3500 ha land is found to be uncultivable. The dominant form of economic activity is agriculture, especially crop production. Ginger production takes a lion share followed by cereals like maize, teff, etc. and root crops such as enset, sweet-potato and potato (Jokka, 2019)

The mean yearly temperature of the woreda is ranging from 12.6-25^{0}c. The rainfall also varies in amount, duration, and intensity. The area gets a mean annual rainfall of 1200-1600 mm per year. The Woreda has diverse agro-ecological zones ranging from *Kola* to *Dega*. From the total area, *Kola* account for 62.28 %, *Dega* accounts 14.28%, and *Woyna Dega* accounts for 23.44% (Honja *et al.*, 2016; WZFEDD, 2014).

Farawocha kebele, the study area, is one of 18 kebele in Boloso Bombe Woreda located at North Adila kebele, at south Udula Matala kebele, at East Matala Walana kebele, at west Bombe 01 kebele. The total area of the kebele is 1126.04ha, out of the total area 956ha (84.8%) used for Agricultural, forest and shrub 49.47ha (4.4%), grazing land 81.17ha (7.2%) and bare land 30.9(3.49 %.) according to the SLMP report. The figure below shows Wutame micro watershed, which is 2.4 square kilometer and Magera micro watershed, which is 38.1 square kilometer covers Farawocha kebele and found in Omo Gibe Basin. Wutame stream flows into Magera River and finally flows to Omo River. It has an altitude varying from 1583 - 1950m above mean sea level. Magera watershed has an altitude varying from 1580 - 2329m above mean sea level.

Geographically, the watershed is located in between 7º2'30" - 7º7'41" North and 36º36'25" - 37º39'15" East.

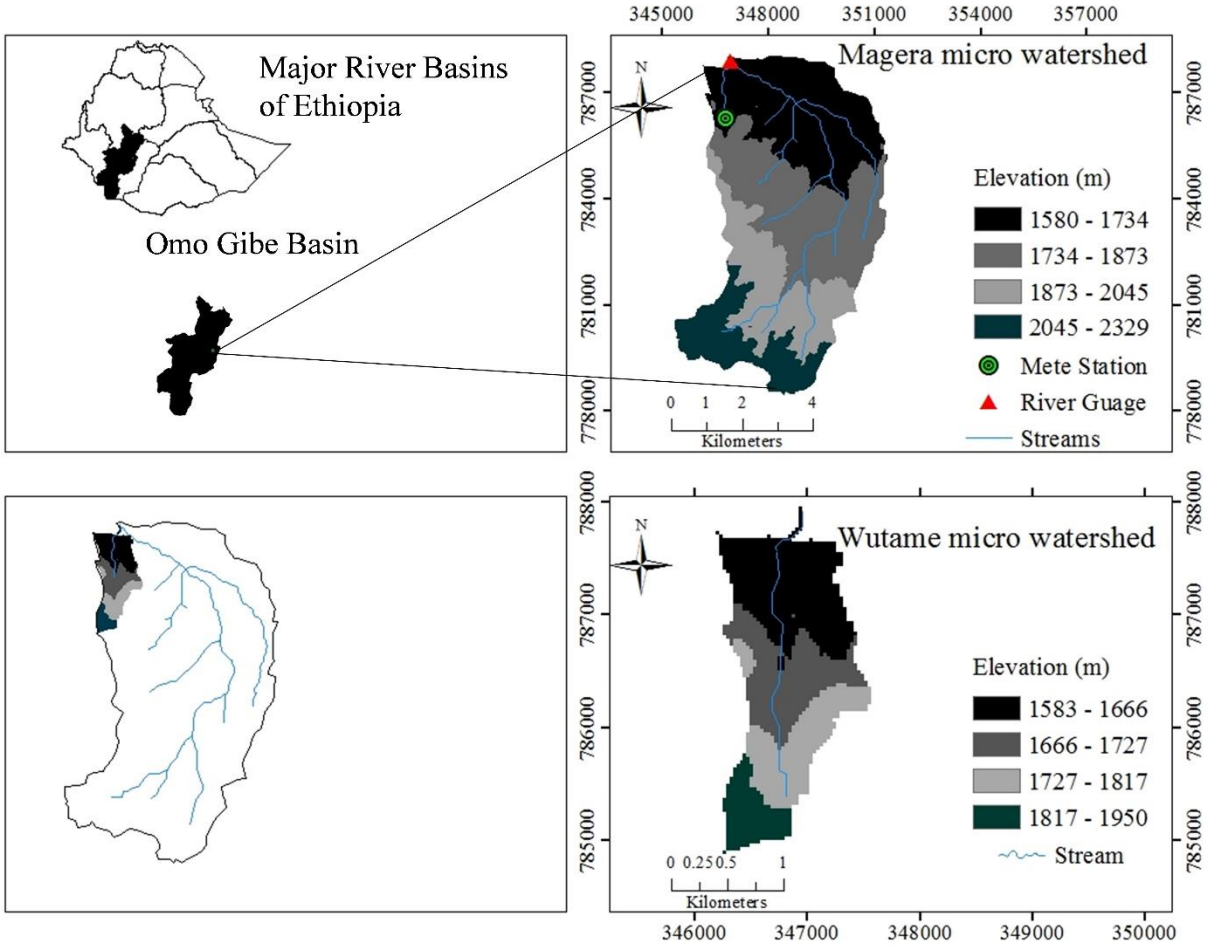

Figure 3.1: Description of the study area

3.2 Methods

In order to achieve the objective of this study, the following procedures were followed. The changes in land use/land cover, vegetation cover and soil moisture as a result of the SLMP interventions were evaluated using remote sensing-based analysis. Remote sensing information is obtained from Landsat images. For this study, Landsat images are used because of Landsat satellite provides high- quality, multispectral imagery of the surface of the earth. While many other satellite provides imagery, Landsat image are unique in three ways: those are; they provide global coverage on a regular basis, they are now available for free and Landsat's image archive reaches back to 1972.

3.2.1 Data Collection

For this study primary and secondary data were collected from field and remote sensing (RS) respectively.

3.2.1.1 Remote sensing data

To delineate watershed, Digital Elevation Model (DEM) from Shuttle Radar Topographic Mission Digital Elevation Model (SRTM-DEM) with 30m spatial resolution was obtained from USGS Earth Explorer, the NASA website (https://earthexplorer.usgs.gov/). Satellite data are used for land cover mapping and vegetation change detection. Landsat-8 houses the Operational Land Imager (OLI) and the Thermal Infrared Sensor (TIRS), which image the land surface at 11 spectral bands in the optical and thermal infrared domains with 30- to 100-m spatial resolution and 16-day temporal resolution. Because of the smaller size of the watershed, it is difficult to classify the watershed accurately into different land use classes and to produce accurate LULC maps, vegetation cover maps using coarser resolution satellite imagery. So, a recent SPOT 7 2016 imagery is used for georeferencing and for easily visualizing the different land use classes, utilizing its higher resolution of 6m. SPOT 7 2016 satellite imagery was purchased from Geospatial Institute of Ethiopia.

3.2.1.2 Field data

Field data, such as rainfall data, streamflow data, groundwater level data, springflow data, Ground Control Points (GCPs), are used for this study. Historical rainfall data was collected from the National Metrological Agency (NMA) of Ethiopia, whereas groundwater level, streamflow and springflow data are monitored in the study area through the support of International Water Management Institute (IWMI) of Ethiopia.

3.2.2 Field Work

During the fieldwork period, different activities were carried out. Intensive fieldwork was carried out to collect the ground truth LULC information and soil moisture sample. A portable sensor HH2 meter was used to sample soil moisture from the same ground reference point and is received from IWMI of Ethiopia. Auger is also used to take soil samples in the field and received from Arba Minch University. Global Positioning System (GPS) is used to collect ground truth information and also received from IWMI.

3.2.2.1 GCP for land cover mapping

Geo-referencing of the images requires the collection of GCPs of features that can be accurately located on the digital imagery. Such features include road intersection, drainage junction, and isolated features like check dams. Intensive field work is carried out to manually collect the ground LULC cover information using handheld GPS. The minimum number of GCPs for Landsat is six per images and the recommended number is 10 to 15 per image (OrthoEngine, 2017). For this study, 15 GCPs per Landsat image were used for georeferencing. Overall, 200 GCPs were collected randomly from February to May 2019, for georeferencing and training of image classification. The spatial distribution of GCPs collected is shown in figure 3.2. Out of these, 80% of data points were used for training of image classification algorithms and 20% for the validation.

Firstly, SPOT 7 2016 was georeferenced using well-collected GCPs with a first-order polynomial in Arc GIS 10.5 and the rectified image was obtained. This image was used as the reference to rectify the all Landsat images. The rectification of Landsat images was done by registering to SPOT image using image to image registration in ERDAS Imagine 2016, with second-order polynomial (Annex figure 7)

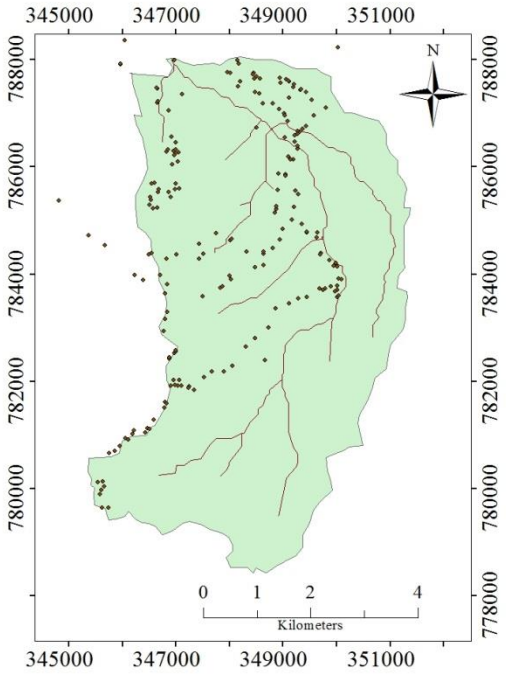

Figure 3.2. Spatial distribution of GCPs data collected from the field

3.2.2.2 Sampling soil moisture

Soil water content is an expression of the mass or volume of water in the soil, while the soil water potential is an expression of the soil water energy status. The relation between soil water content and soil water potential depends on the characteristics of the soil, such as soil density and soil texture.

Soil water content on the basis of mass is expressed in the gravimetric soil moisture content, θ_g(gg^{-1}), defined by:

$$\theta_g = \frac{M_{water}}{M_{soil}} \quad \text{.....(3.1)}$$

Where M_{water} (g) is the mass of water in the soil sample and M_{soil} (g) is the mass of dry soil after oven dried that is contained in the sample.

The volumetric soil water content of the soil is often useful and it can be expressed as:

$$\theta_v = \frac{V_{water}}{V_{sample}} \quad \text{.....(3.2)}$$

Where θ_v is volumetric water content, V_{water} is the volume of water in the soil sample and V_{sample} is the total volume of (drysoil+air+water) in the sample. The unit of V_{water} and V_{soil} is cm^3 and θ_v is cm^3cm^{-3}

The relationship between gravimetric and volumetric water content is expressed as:

$$\theta_v = \theta_g * G = \theta_g * \left(\frac{\rho_b}{\rho_w}\right) \quad \text{.....(3.3)}$$

Where G is the specific gravity of soil, ρ_b is the dry bulk density (gcm^{-3}) and ρ_w is soil water bulk density (gcm^{-3})

The following points were considered before taking soil moisture sampling: (i) the sampling site will be selected as much as possible at homogeneous land cover and also relatively uniform slope. This to minimize the variation of soil water content and to minimize on the effect of topography; (ii) the measurement will be taken at the time of the satellite overpass. This helps to correlate ground measured soil moisture with remote sensing data; (iii) spatial variability of soil moisture at the pixel level must be taken into account while locating the sampling site. By considering the above criteria, eight sample plots, four in the upstream, two in the middle and two in the downstream of the watershed were randomly selected for sampling soil moisture.

Forty soil samples, five from each of eight sample plots from vegetation and bare land, were collected using auger at 0-15cm depth in each sampling day. Soil sampler kit was also used to

measure soil moisture from the same reference at the same time and latter calibrated with laboratory result. The instrument is also named as moisture meter HH2 type, Delta-T version 4. Collecting of soil sample was started on 08/02/2019 and continued for every 16 days, which is the same as Landsat 8 revisiting date. Overall, 210 sample points were collected from all subplots and five subplots are averaged; 40 averaged samples were collected from Feb.8, 2019 to May.31, 2019. The spatial distribution of the soil samples collected and different land cover in which soil sample was taken is shown in figure 3.3 and annex figure 1. Larger 30 m x 30 m sample areas, corresponding to the spatial resolution of Landsat 8 images (30 m x 30 m pixel size) used for linear regression analysis, were divided into five subplots for collecting soil samples. Each soil sample was georeferenced using a handled GPS.

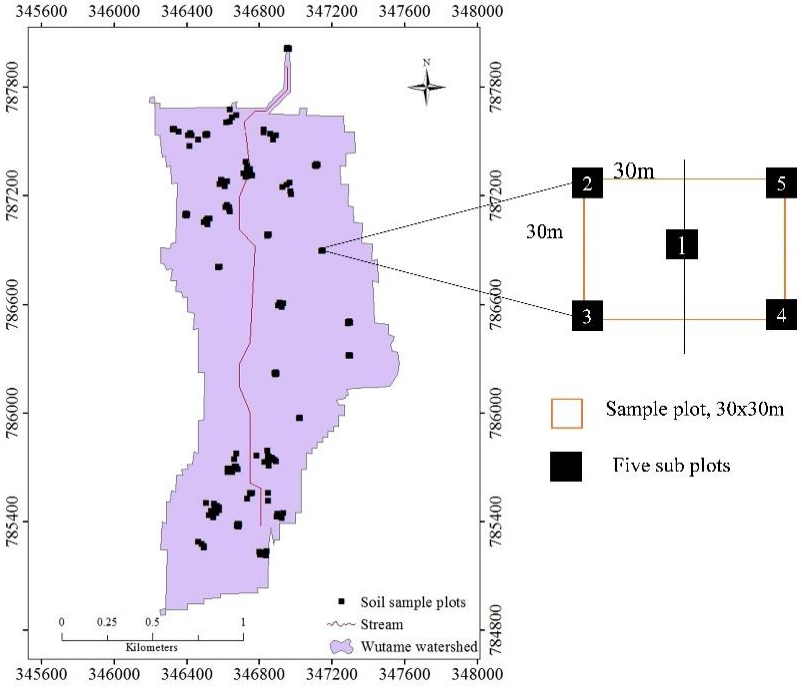

Figure 3.3. Soil sampling site within Wutame watershed.

3.2.2.3 Sampling soil texture

One of the methods to analyze the soil moisture content (SMC) of the study area accurately and precisely is analyzing its soil texture and establishing the relationship between soil moisture content and soil texture. Soil texture refers to the composition of the soil in terms of the proportion of small, medium, and large particles (clay, silt, and sand, respectively) in a specific

soil mass. For example, a coarse soil is sand or loamy sand, a medium soil is a loam, silt loam, or silt, and fine soil is sandy clay, silt clay, or clay.

Water holding capacity is controlled primarily by soil texture and soil porosity. Soils with smaller particles (silt and clay) have a larger surface area than those with larger sand particles, and a large surface area allows soil to hold more water. In other words, a soil with a high percentage of silt and clay particles, which describes fine soil, has a higher water-holding capacity. Thus, soil texture has an important role in defining the soil moisture retention and its redistribution in the soil profile. Hence, analyzing the soil texture is very important to verify which part of the watershed has high soil moisture content and has low moisture content.

3.2.3 Laboratory Work

Laboratory analysis is conducted to estimate soil moisture content and soil texture analysis, this result later used to validate the soil moisture estimated by the remote sensing.

3.2.3.1 Methods to determine soil moisture content

A. Gravimetric method (direct method)
B. Instrumental method (indirect method

A. Gravimetric method (direct method)

Soil samples were collected from each of the five subplots, which are representative of the soil within each plot. Each soil sample was placed in a plastic container and sealed tightly for further laboratory analysis. In the lab for analysis of gravimetric soil moisture, first, the soil sample weighed (wet weight in grams) using a standard laboratory scale and placed them in drying oven at 105 ^{o}C for 24 h (Gardener, 1986). The dried soil samples were weighed and the percentage gravimetric soil moisture was calculated using Eq. (3.4):

Soil moistute = $\frac{wet\ weight - dry\ wet}{dry\ wet} x100\%$ ……3.4

Five soil moisture measurements from each of the five subplots within each sample plot were averaged to obtain representative soil moisture for each 30 m^2 site, corresponding to the spatial resolution of Landsat 8 images. The averaged soil moisture data from 40 sample plots were used for both training (80%) and validation (20%) data. The results showed a range of 11.89-23.81% gm soil moisture of the study area (see annex table 1).

B. Instrumental method (indirect method)

During the fieldwork, a soil moisture meter HH2 type, Delta-T Version 4 was used to measure soil moisture. This moisture meter measures in volumetric soil moisture content. Volumetric soil moisture content is the ratio between the volume of water present and the total volume of the sample. This is a dimensionless parameter, expressed as a percentage (%vol). The soil moisture kit can measure up to 100mm depth. For this specific study, the moisture measurements was taken from 10-15cm using soil moisture sensor from the same reference point at the same time with gravimetric moisture measurement. The results showed a range of 0.54%vol- 21%vol soil moisture for sampling date Feb.8, 2019 of the study area (see annex table 1). The instrument latter calibrated with gravimetric moisture content obtained from laboratory analysis.

Field calibration of the sensor

For analyzing the moisture content of the study area spatially, several sampling points are required. The laboratory method (gravimetric method) is used to measure moisture content accurately and precisely. However, the laboratory method is costly, time-consuming and difficult to analyze the moisture content for several sampling points. Soil moisture sensor HH2 helps to minimize these limitations because it is easy to handle and easily movable. So, soil moisture meter HH2 was used to measure moisture from the same reference point with the laboratory method. Once the soil moisture was analyzed using a laboratory method and measured using a moisture sensor, the moisture measured using a moisture meter is calibrated with laboratory results by developing a linear regression equation.

After the instrument calibrated, no need of doing several laboratory analysis, Ruther than taken a number measurement using moisture meter at a satellite acquisition date and substitute in the developed equation. Before calibrating the instrument, the standard unit measuring in both cases (HH2 sensor meter and laboratory method) must be the same because moisture measured using sensor meter is in volumetric water content (%vol) and using laboratory method is in gravimetric method (%gm.). To do this, moisture content analyzed using a gravimetric laboratory method is converted into volumetric moisture content. The conversion into a volumetric equivalent can be done multiplying the gravimetric water content by the dry bulk density of the sample, with a knowledge density (the density of water was assumed to be 1g/cm^3). The volumetric water content was calculated using equation (3.5) below:

$$\theta_v = \theta_g * (\rho_b) \quad \text{.....(3.5)}$$

Where θ_v is volumetric water content ($cmcm^{-3}$), θ_g is gravimetric water content (gg^{-1}), ρ_b is the dry bulk density (gcm^{-3}).

Dry bulk density must be calculated for each soil sample. Dry bulk density is the ratio of dry soil mass to sample volume. After determining the values of dry bulk density (dbd) for all soil samples, substitute in the equation (3.5) to obtain volumetric moisture content. The result obtained is in the range of 7.76-25.96%vol (see annex table 1). The coefficient of correlation (r), which represents the degree of association between the moisture content measured in the field and laboratory, Mean absolute percentage error (MAPE) is the average of absolute errors divided by actual observation value were used to evaluate the field and laboratory calibration equation and also to evaluate the errors between them. Out of 40 averaged soil moisture sampling point, 34 were measured by both direct (lab) and indirect (portable sensor). These data are used for calibrating the HH2 sensor. Six sampling points were measured only by indirect (sensor), latter re-adjusted by a calibrated equation. Detail of calibrating of the instrument is in the annex table 2. The mean absolute error is calculated as follows:

$$\text{MAPE} = \frac{\sum_{t=1}^{n}\left|\frac{A_t - F_t}{A_t}\right|}{n} \times 100 \ldots\ldots(3.6)$$

Where, A_t is actual observation (lab); F_t is the forecasted value (field); n is a number of observation. Excel is used to calculate the MAPE (see annex table 2). Furthermore, the values of soil moisture measured by moisture meter were plotted versus the soil moisture analyzed by the laboratory to establish the field calibration equation. The established relationship between the moisture measured by the lab and portable sensor is shown in annex figure 4.

3.2.3.2 Soil texture analysis

The soil texture of the study area is analyzed by combine reading of sieve analysis and hydrometry analysis. The distribution of particle sizes larger than 75 μm (retained on the No. 200 sieve) is determined by sieving, while the distribution of particle sizes smaller than 75μm is determined by a sedimentation process, using a hydrometer. Eleven spatially distributed soil samples are taken to analyze soil texture from the same reference point with soil moisture sample. The soil sample was taken from 1m depth. The samples were weighed before and after dried in oven for 24h at 105°C. Sieve analysis and Hydrometry analysis are as follows:

Sieve analysis

After the sample dried in an oven for 24hr, 1000g of soil are taken and socked for 1hr. Transfer the material on the No. 200 sieve to a suitable container, dry in an oven at 115 ^{o}C and record the weight retain soil on each series of sieves. Sieve analysis is used to determine the distribution of coarser particles (see annex figure 2b).

Hydrometry analysis

For Hydrometry analysis, after the sample dried in an oven for 24hr the soil are sieved with a diameter 4.25mm, 50g of soil are taken from a soil pass with 4.25mm diameter sieve and socked for 1hr and then take hydrometer readings at the following interval time: 0.5min, 1, 2, 5, 15, 30, 60, 360 and 1440min(see annexfigure 2a).

Soil gradation is a classification of a coarse-grained soil that ranks the soil based on the different particles sizes contained in the soil. Soil gradation is determined by analyzing the combined results of a sieve analysis and a Hydrometry analysis. To plot the gradation curve, orderly combine the results of sieve size (mm) with grain size (mm) and percent passing with percent finer combined from sieve analysis and Hydrometry analysis, respectively(see annex figure 3).

3.2.4 Intervention impact on land cover

LULC change as the result of SLMP intervention was evaluated with the following procedures.

3.2.4.1 Land cover classification

This study is divided in two parts. The first part deals with land cover classification, post-classification analysis and change detection over 2010-2019. The second part deals with remote sensing data of the year 2010, 2014 and 2019 will be used to calculate NDVI, and subsequently, the NDVI is used during the classification stage. In this study, the maximum likelihood classification algorithm is selected for supervised land cover classification. This classification algorithm was chosen since it results in a minimum error of misclassification and is the most accurate classifying method as it's unbiased to any class (Thakkar *et al*.,2017).

The Landsat images will be pre-processed before use. The processing will include geometric correction, radiometric correction, and sun angle correction. Ancillary data are any type of spatial or non-spatial information that may be of value in the image classification. It consists of elevation, slope, soil, hydrology, aspect, geology, DEM, derived indices (Thakkar *et al*.,2017). Several various studies were applied to improve the accuracy of classification using ancillary

data (Shalaby and Tateishi, 2007). In this study, the ancillary data of NDVI and SPOT 6 were utilized to improve the classification accuracy of the heterogeneous landscape region of the study area

3.2.4.2 Accuracy assessment

Accuracy assessment is an imperative part of digital image classification. It increases the authenticity and usefulness of classified LULC maps in the decision-making process (Thakkar et al., 2017). To evaluate the accuracy of the land cover map, error matrix was used. The formation error of the matrix is the most common way of representing the outcome of accurate assessment (Foody, 2002). The error matrix was evaluated using the accuracy parameters with overall accuracy, producer's accuracy, user's accuracy and kappa coefficient. Percentage correct is calculated by dividing the sum of the diagonal entries of the error matrix by the total number of reference pixels.

$$PC = \frac{\sum_{i=1}^{r} X_{II}}{\sum_{i=1}^{r} X_i} \quad \text{.....(3.7)}$$

Therefore, percent correct provides an overall accuracy assessment of a classification (Senseman *et al*., 1994). User and producer accuracy are directly related to errors of commission and errors of omission, respectively (Janssen and Van der Wel, 1994). These relationships are: User's Accuracy (reliability) = percentage correct by category = 100%-error of commission (%) and Producer's Accuracy = 100%-error of omission (%).

The Kappa Coefficient is a discrete multivariate measure that differs from the usual measures of overall accuracy assessment, basically in the following way. The calculation takes into account all of the elements of the error matrix, not just the diagonals of the matrix (Foody, 2002).

The Kappa Coefficient of Agreement, K, is calculated as:

$$K = \frac{N\sum_{i=1}^{r} X_{ii} - \sum_{i=1}^{r}(X_{I+} * X_{i+})}{N^2 - \sum_{i=1}^{r}(X_{i+} * X_{+i})} \quad \text{.....(3.8)}$$

Where:

r = the number of rows in the error matrix

X_{ii} = the number of observations in row I and column I

X_{i+} = the marginal totals of row i

X_{+1} = the marginal totals of column I

N = the total number of observations (Bishop *et al*., 1975).

3.2.4.3 Change detection

The post-classification comparison (PCC) was used to detect changes as it is a very common and effective approach to quantify LULC changes over a given period. It involves a comparative analysis of two independently categorized maps for different dates (Lunetta *et al*., 2004). In the present study, the PCC of LULC maps generated for the year 2010, 2014 and 2019 has been carried out at the micro watershed. Also, to describe the extent of change between two points percentage changes of individual LULC types were computed using the following equation (Long et al., 2009; Berihun et al., 2019):

$$\text{Percentage change (\%)} = \left(\frac{A_2 - A_1}{A_1}\right) * 100 \quad \text{.....(3.9)}$$

Where A1 is the area in year 1 and A2 is the area in year 2 of a LULC type.

3.2.5 Intervention impact on vegetation cover

3.2.5.1 Normalized difference vegetation index (NDVI)

Vegetation coverage was analyzed through the Normalized difference vegetation index (NDVI). NDVI quantifies the vegetation by measuring the difference between near-infrared (which vegetation strongly reflects) and red light (which vegetation absorbs). It is computed using the red band (0.64-0.67 μm) and near-infrared (0.85-0.88μm) data as,

$$NDVI = \frac{NIR - RED}{NIR + RED} \quad \text{.....(3.10)}$$

Where, NIR is Band 5 and RED is Band 4 in the Landsat 8 imagery.

Before calculating the NDVI, Digital Number (DN) is converted into atmospheric reflectance.

3.2.5.2 Retrieval of NDVI from Landsat 5 and 7 Imageries

Conversion to ToA Reflectance

The conversion from DNs to top of atmospheric (ToA) reflectance for the TM band requires using a two-step process.

The following equations were used

$$L_\lambda = \left(\frac{(LMAX_\lambda - LMIN_\lambda)}{(QCALMAX - QCALMIN)}\right) \times (QCAL - QCALMIN) + LMIN_\lambda \quad \text{.....(3.11)}$$

where, L_λ= spectral radiance at the sensor's aperture in watts/ (meter squared*ster*μm); QCAL= the quantized calibrated pixel value in DN; $LMAX_\lambda$= the spectral radiance scaled to QCALMAX in watts/ (meter squared*ster*μm); $LMIN_\lambda$= the spectral radiance scaled to QCALMIN in watts/ (meter squared*ster*μm); QCALMIN=the minimum quantized calibrated pixel (typically 0 or 1); QCALMAX=the maximum quantized calibrated pixel value (typically =255).

Conversion of radiance to reflectance

Radiances are converted to reflectance using the Sun zenith angle cosine interpolated at the pixel and the Sun spectral flux.

$$\rho_p = \frac{\pi \times L_\lambda \times d^2}{ESUN_\lambda \times \cos\theta_S} \quad \text{.....(3.12)}$$

Where, ρ_λ=unit less planetary reflectance; L_λ= spectral radiance (from the above equation 3.12); d=Earth-Sun distance in the astronomical unit; $ESUN_\lambda$=mean solar exo-atmospheric irradiances; θs= solar zenith angle.

3.2.5.2. Retrieval of NDVI from Landsat 8 Imageries

Conversion to ToA Reflectance

Operational Land Imager (OLI) spectral radiance data can be converted to ToA planetary reflectance using the reflectance rescaling coefficient provided in the Landsat 8 OLI metadata file. The following equation is used to convert DN to ToA reflectance for OLI image:

$$\rho\lambda' = M\rho \times Qcal + A\rho \quad \text{.....(3.13)}$$

where, $\rho\lambda$'= ToA planetary reflectance, without correction for solar angle; $M\rho$= represents the band-specific multiplicative rescaling factor from the metadata (REFLECTANCE_MULT_BAND_x, where x is the band number); *Qcal*= quantized and calibrated standard product pixel value (DN); $A\rho$= represents the band-specific additive rescaling factor from the metadata (REFLECTANCE_ADD_BAND_x where x is the band number).

ToA reflectance with a correction for sun angle is then:

$$\rho_\lambda = \frac{\rho_{\lambda'}}{cos(\theta_{SZ})} = \frac{\rho_{\lambda'}}{sin(\theta_{SE})} \quad \text{.....(3.14)}$$

where, ρ_λ= ToA planetary reflectance; θ_{SE}: local sun elevation angle. The scene center sun elevation angle in degrees is provided in the metadata (Sun Elevation); θ_{SZ}: local solar zenith angle, θ_{SZ}= 90^o- θ_{SE}.

To easily readable in GIS, the angle given in degrees was converted to radian.

3.2.6 Trend test

The non-parametric Mann-Kendall test was used in this study and is commonly employed to detect monotonic trends in a series of hydrological data and climate data (Mann, 1945; Kendall, 1975). The reason for using Mann-Kendal tests is that, compared with parametric tests, the factors were thought to be more suitable for non-normally distributed data, which were more frequently encountered in the NDVI time series. The Mann-Kendall test statistic is calculated according to:

$$S = \sum_{k=1}^{n-1} \sum_{j=k+1}^{n} sgn(X_j - X_k) \quad \text{.....(3.15)}$$

With

$$sgn(x) = \begin{cases} 1 & if \quad x > 0 \\ 0 & if \quad x = 0 \\ -1 & if \quad x < 0 \end{cases} \quad \text{.....(3.16)}$$

Where n is the data set record length and x_j and x_k are the sequential data values.

There are two basic parameters in the Mann-Kendall test to detect the trends, the slope magnitude estimate, is to indicate the magnitude and direction of the trend and the significance level, and is to detect trend strength. If S has a mean of zero and a variance of

$$Var(S) = \frac{n(n-1)(2n+5)}{18} \quad \text{.....(3.17)}$$

Then the null hypothesis of an upward (or downward) trend in the data cannot be rejected and is asymptotically normal. The normal z-test statistics is

$$z = \frac{S}{[Var(S)]^{0.5}} \quad \text{.....(3.18)}$$

To detect whether there is a trend in the data up to *i* the statistics, z can be compared for any values of *i* at chosen level of significance using the z-test. In testing the statistical significance for the null hypothesis, the two-tailed significance test is used. Hirsch et al., (1982) developed the equation to estimate the magnitude of the slope β as:

$$\beta = Median \left[\frac{(x_j - x_k)}{j-k} \right] \quad for\ all\ k < j \quad \text{.....(3.19)}$$

An upward trend is represented by a positive value of β and a downward trend is represented by a negative value. Linear regression was performed to confirm the result obtained from Mann-Kendall test.

3.2.7 Change point analysis

In order to avoid any possible sensitivity in the change-point tests, multiple change-point analyses were carried out to detect the changes in vegetation cover using the NDVI time series. In this study, Pettit's test, Buishand's test and Standard normal homogeneity test (SNHT) are applied.

3.2.7.1 Pettitts test

Pettitt's test is a non-parametric test that is commonly used to detect a single change point in hydrological series or climate series with continuous data (Pettitt. 1979). This test detects a significant change in the mean of a time-series when the exact time of the change is unknown. Considering a time series x_i $(1 \leq i \leq N)$, the test uses a version of the Mann-Whitney statistic $U_{t,N}$, that verifies if two samples $x_1,\ldots\ldots, x_t$ and $x_{t+1},\ldots., x_N$ are from the same population or not. The $U_{t,N}$ statistic counts the number of times a member of the sample exceeds a member of the second sample and is given by

$$U_{t,N} = U_{t-1,N} + \sum_{j=1}^{N} sgn(x_t - x_j) \quad for\ t = 2, \ldots \ldots N \qquad (3.20)$$

where, sgn(X) = 1 if X > 0; sgn(X) = 0 if X = 0; sgn(X) = -1 if X < 0.

The null hypothesis of Pettitt's test is the absence of a changing point. It's statistics k (t) and the associated probabilities used in significance testing are given by

$$k(t) = max_{1\leq t\leq N}\left|U_{t,N}\right| \qquad (3.21)$$

and

$$p \cong 2exp\{-6k(t)^2/(N^3 + N^2)\} \qquad (3.22)$$

respectively.

3.2.7.2 Buishand's test

Buishand's test (1982) can be used on variables following any type distribution. Let X denote a normal random variate. Then the following model with a single shift (change-point) can be given by:

$$\begin{cases} \mu + \epsilon_i & i = 1, \ldots \ldots . m \\ \mu + \Delta + \epsilon_i & i = m + 1, .., n \end{cases} \qquad (3.23)$$

$\epsilon \approx N(0, \sigma)$. The null hypothesis $\Delta = 0$ is tested against the alternative $\Delta \neq 0$. In the Buishand range test (Buishand, 19820), the rescaled adjusted partial sums are calculated as

$S_k = \sum_{i=1}^{k}(x_i - \hat{x}) \qquad (1 \le i \le n)$

The test statistic is calculated as:

$R_b = \frac{\max S_k - \min S_k}{\sigma}$ ……...…(3.24)

The *p* value is estimated with a Monte Carlo simulation using *m* replicates.

3.2.7.3 Standard Normal Homogeneity Test (SNHT)

In the Standard Normal Homogeneity Test, the null hypothesis is the same as in the Buishand's Range Test. The test statistics is

$T_k = kz_1{}^2 + (n-1)\, z_2{}^2 \quad (1 \le k \le n)$ ……..….(3.25)

where,

$z_1 = \frac{1}{k}\sum_{i=1}^{k}\frac{x_i - \bar{x}}{\sigma} \qquad z_2 = \frac{1}{n-k}\sum_{i=k+1}^{n}\frac{x_i - \bar{x}}{\sigma}$……...……(3.26)

The critical value is:

$T = maxT_k$…….……(3.27)

The *p* value is estimated with a Monte Carlo simulation using *m* replicates.

3.2.8 Intervention impact on soil moisture

3.2.8.1 Remote sensing for soil moisture estimation

The changes in soil moisture as the result of SLMP intervention was evaluated using soil moisture index (SMI), which is resulted in a trapezoid shape (fig.3.4) of the scatter plot of remotely sensed LST and NDVI space. The upper envelope of the trapezoid, A-C, is representing the dry condition named as the "warm edge"- the upper limit of surface temperature for a given vegetation cover. The lower limit of trapezoid B-D, corresponding to the well-watered condition, was named as the cold "cold edge." Soil moisture index is based on an empirical parameterization of the relationship between land surface temperature (LST) and normalized difference vegetation index (NDVI) and calculated based on the proportion between line M-E and M-N in Eq. 3.28 (Zeng *et al*., 2004; Parida *et al*., 2008, Wang *et al*., 2009):

SMI = $(\frac{LST_{max} - LST}{LST_{max} - LST_{min}})$…….(3.28)

Where LST_{max} and LST_{min} are the maximum and minimum surface temperature for a given NDVI and LST is Land Surface Temperature, the surface temperature of a pixel for a given

NDVI derived using remotely sensed data. Two inputs must be calculated (LST and NDVI) to be able to calculate LST_{max} and LST_{min}.

LST_{max} and LST_{min} are calculated using following Eq 3.29 and 3.30, respectively (Zhan *et al*., 2004; Parida *et al*., 2008):

$LST_{max} = a_1 * NDVI + b_1$ .....(3.29)

$LST_{min} = a_2 * NDVI + b_2$ .....(3.30)

Where a1, a2, b1 and b2 are the empirical parameter obtained by the linear regression (a present slope and b present intercept) defining both dry and wet (warm and cold) edges of the data (Fig. 3.4).

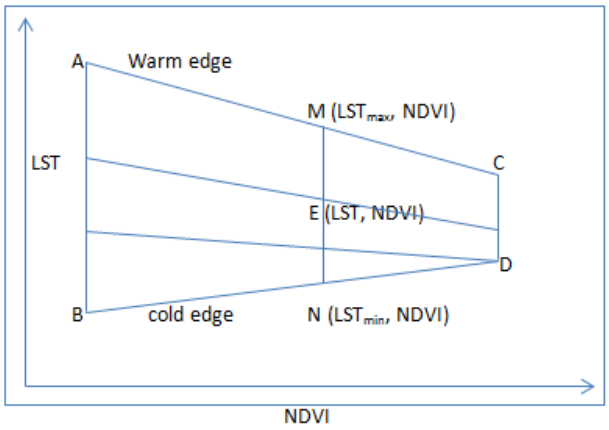

Figure 3.4: Definition of SMI, Scatterplot in LST-NDVI space (Parida *et al*., 2008)

Following the concept illustrated in figure 3.4, the LST and NDVI data were combined to form an index for identifying soil moisture. A soil moisture index (SMI) based on the pixel location in LST-NDVI spaces was defined in a scatter plot.

The first step in SMI calculation is the retrieval of land surface temperature (LST) and normalized vegetation index (NDVI) from Landsat 8 Images. NDVI was analyzed in the earlier section for vegetation analysis.

3.2.8.2 Land Surface Temperature (LST)

The land surface temperature (LST) is the radiative skin temperature of the ground, which depends on albedo, vegetation cover and soil moisture of the land surface. The measurement of LST could be affected by the differences in temperature between the ground and vegetation cover.

Retrieval of LST from Landsat 8 Imageries

Conversion of DN to ToA Radiance

OLI and TIRS can be converted to TOA spectral radiance using the radiance rescaling factors provided in the metadata file (Lwin 2010):

$$L_\lambda = M_L Q_{cal} + A_L \quad (3.31)$$

where, L_λ = ToA spectral radiance (Watts/ (m2×srad×μm)); M_L= band-specific multiplicative rescaling factors from the metadata (RADIANCE_MULT_BAND_x, where x is the band number); A_L=band-specific additive rescaling factors from the metadata (RADIANCE_ADD_BAND_x, where x is the band number); *Qcal*= Quantized and calibrated standard product pixel values (DN).

Conversion to Top of Atmospheric Brightness Temperature

TIRS bands data can be converted from spectral radiance to top of atmospheric brightness temperature using the thermal constants provided in the metadata file

$$TB = \frac{K_2}{\ln\left(\frac{K_1}{L_\lambda}+1\right)} \quad (3.32)$$

where, *TB*= Top of atmospheric brightness temperature (K); L_λ= ToA spectral radiance (Watts/ (m2×srad×μm)); K_1= Band specific thermal conversion constant from the metadata (*K1*_CONSTANT_BAND_x, where x is the thermal band number); K_2= Band specific thermal conversion constant from the metadata (*K2*_CONSTANT_BAND_x, where x is the thermal band number)

TB in Kelvin (K) is converted into degree Celsius (^oC) using the following equation:

$$TB = \frac{K_2}{\ln\left(\frac{K_1}{L_\lambda}+1\right)} - 273.15 \quad (3.33)$$

Estimating proportion of vegetation and emissivity

Land surface emissivity is an average emissivity of an element of the land surface temperature (LST) and radiance. Before calculating the land surface emissivity, the proportion of vegetation or vegetation fraction from the NDVI output is calculated. The following equation is used to calculate the proportions of vegetation:

$$Pv = \left(\frac{NDVI - NDVI_{min}}{NDVI_{max} - NDVI_{min}}\right)^2 \quad (3.34)$$

where, $NDVI_{min}$, and $NDVI_{max}$, correspond to the values of NDVI minimum and NDVI maximum in an image respectively; *Pv*= proportions of vegetation.

The land surface emissivity is computed using the following equation:

$\varepsilon mmisivity = 0.004Pv + 0.986$ ……..……(3.35)

LST is essential to estimate the amount of vegetative cover, land cover changes and soil development. The natural phenomena on the earth's surface have no homogenous characteristics in terms of land surface emissivity. Hence surface emissivity is highly dependent on the type of vegetation cover, soil and topography. The LST results are all in degree Celsius.

Conversion from At-Satellite Temperature to Land Surface Temperature

Now At-Satellite brightness temperature is converted to land surface temperature using the following equations (Weng *et al*., 2004):

$$LST = {}^{TB}\Big/\left[1 + \left(\lambda * {}^{TB}/_{C_2}\right) * \ln(e)\right] \quad \text{……(4.36)}$$

where, *LST*= land surface temperature; *TB*= Top of atmospheric brightness temperature (℃) λ= wavelength of emitted radiance (10.8); C_2 = h×c/s = 1.4388×10^{-2} m K = 14388μm K; *h*= Planck's constant = 6.626×10^{-34} Js; *s*= Boltzmann constants = 1.38×10^{-23} J/K; *c*: velocity of light = 2.998×10^{8} m/s; *ln (e)* = log of spectral emissivity value.

The final step is the determination of empirical parameters by linear regression. Linear regression value range from 0 at the "dry edge" (limited water availability) to 1 at the "wet edge". Pixels close to the dry edge are drier relative to the wet edge, which is wetter (Maximum evapotranspiration- unlimited water access (Potic *et al*., 2017). The parameters are implemented in the Equation 3.29 and 3.30

3.2.8.3 Soil moisture model and validation of remote sensing-based soil moisture

Soil moisture estimation model established by Burapapol and Nagasawa (2016) was used in this study. The model was developed based on a collection of field sampling and remote sensing data. A regression approach was to assess the relationship between field soil moisture data and remote sensing data, i.e., SMI was used as independent variables. The model was computed using the following regression formula;

Estimated soil moisture = $a + b(SMI)$ ……(4.38)

Where, the estimated soil moisture is given by cm^3cm^{-3} and a, b are coefficients of the regression lines of SMI.

The model was validated by ground and remote sensing data. Actual soil from the field measurements was used to evaluate the accuracy of the predictive model by statistical inferences: (i) adj-R^2, (ii) root mean squared error (RMSE), (iii) absolute average difference (AAD), and the precision model (Burapapol and Nagasawa, 2016). The precision model is calculated as:

$$\text{Precision} = \sqrt{\frac{\sum\left[\frac{(Y_i - Y'i)}{Y'_i}\right]^2}{N}} x100\% \quad \text{.....(4.39)}$$

Where, Y_i is the actual soil moisture of the field samples (cm^3cm^{-3}), Y'_i is the estimated soil moisture from remotely sensed data (cm^3cm^{-3}), N is sample size.

In the final step, the validated model was used to estimate and map the spatial and temporal soil moisture of the study area.

3.2.8.4 Soil moisture change detection

Soil moisture index (SMI)

The algorithm that applies to the calculation of SMI function is based on the utilization of the NDVI and LST which are calculated using multispectral satellite imagery for each pixel. There are different methods of presenting modes for SMI. Saha et al. (2018) present SMI values from 0 to 1 where higher values close to 1 represent higher estimated soil moisture levels. Potic *et al*. (2017) also present SMI values from 0 to 1. Parida *et al*. (2008) applied SMI to detect drought prone areas with SMI values > 0.3 were not to be drought or favorable soil moisture conditions and SMI values ≤ 0.3 were classified as slight, moderate and severe drought. In presented works, continuous SMI data ranged between 0 to 1 best describes the level of soil moisture. Therefore, Saha et al., (2018), Potic et al. (2017) and Parida et al.(2008) were used to present a mode of SMI.

The result from Equation 3.28 is presented with the value range from 0 to 1, where value near 1 is the regions with a high amount of vegetation and low surface temperature and presents high level of soil moisture. The values near 0 are the areas with a low amount of vegetation and high surface temperature and present the low level of soil moisture (Zhan *et al*. (2004) and Parida *et al*. (2008).

4. RESULTS AND DISCCUSION

4.1 Vegetation cover change detection using NDVI approach

The vegetation cover of the study area is analyzed from 2010 up to 2019 using the NDVI approach. Since no standardized rule is specified to fix the threshold value of NDVI, firstly, the thresholds were set based on the literature, to compute the NDVI. The study reported by Gross (2005) noted that shallow values (0.1 and lower) correspond to barren areas of sand, rock and snow. Moderate values (0.2 to 0.3) indicate grassland and shrub land, while high NDVI values (0.6 to 0.8) indicate temperate and tropical rainforests. EL-Gammal et al., (2014) also classified NDVI in low values (0 and lower) as no plant cover, moderate values (0.01 to 0.3) as weak plants and high values (0.31 and higher) as healthy plants. Following this literature, NDVI values are calculated for every year, considering three land cover groups – (i) "no plant cover" which includes degraded land, bare soil and barren areas of soil and rock, with NDVI ranging from minimum value to 0.2 (shown in red in Figure 4.1); (ii) "weak plants" which includes, grassland and shrubland, with NDVI ranging from 0.2 to 0.4 (shown in yellow in Figure 4.1); and (iii) "healthy plants" which includes natural forest and indigenous forest such as Eucalyptus tree, Zigba and Tid, with NDVI ranging from 0.4 to maximum value (shown in green color in Figure 4.1). LULC map of 2019 (figure 4.8) is used to fix these thresholds and are validated by SPOT 7 images (annex figure 7), with a focus on healthy plants.

The spatial patterns of vegetation cover distribution, along with the threshold values before intervention, are illustrated in figure 4.1. Evidently, moderate healthy plants and high weak plant cover are seen in February 2010, with negligible bare land/no plant. However, the NDVI values tend to significantly decrease in the subsequent years, with a higher area of bare land/no plants and very little healthy plants/forests in February 2012 and 2013. As mentioned before, the period 2013/14 was the beginning year of SLM intervention.

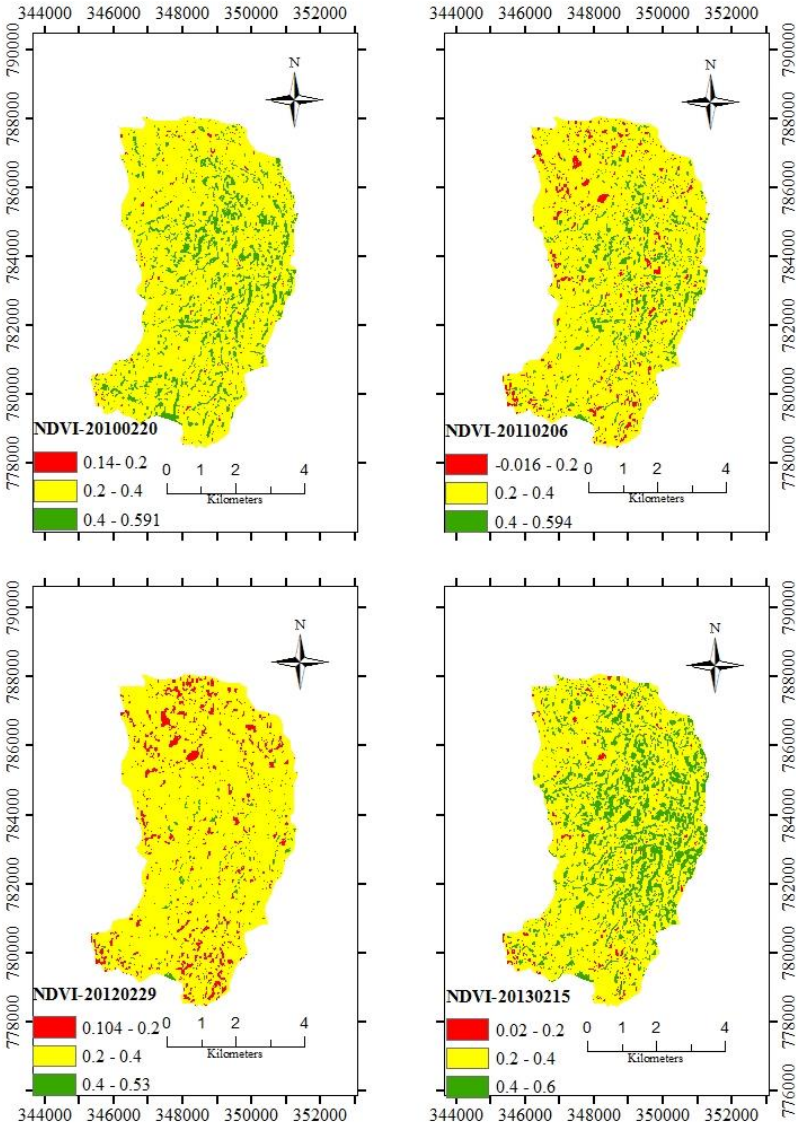

Fig 4.1. Spatial distribution of three vegetation classes, with varying NDVI values in the Magera before intervention

The density of greenness radically started with a significant increase (NDVI value of 0.61), since February 2014. Significant increments in NDVI values are observed in February 2015. Most of the area with no plant cover existed in 2012 is completely changed to weak plants/healthy plants area. It is known through discussions with village elders and focal persons that free grazing is prohibited through a law agreed by community, since 2015. The gradual increments in vegetation cover continued from -0.016 in 2011 up to 0.67 in 2017, which proves the conversion of no plant covers into healthy vegetation. NDVI shoots up to 0.64 in 2018; however, there is a lot of red colors, which could be attributed to the effect of cloud cover in the imagery. The

consistent increase in the green cover is evident from the consistent increase in NDVI area from 1.5% in 2012 to 33% in 2019.

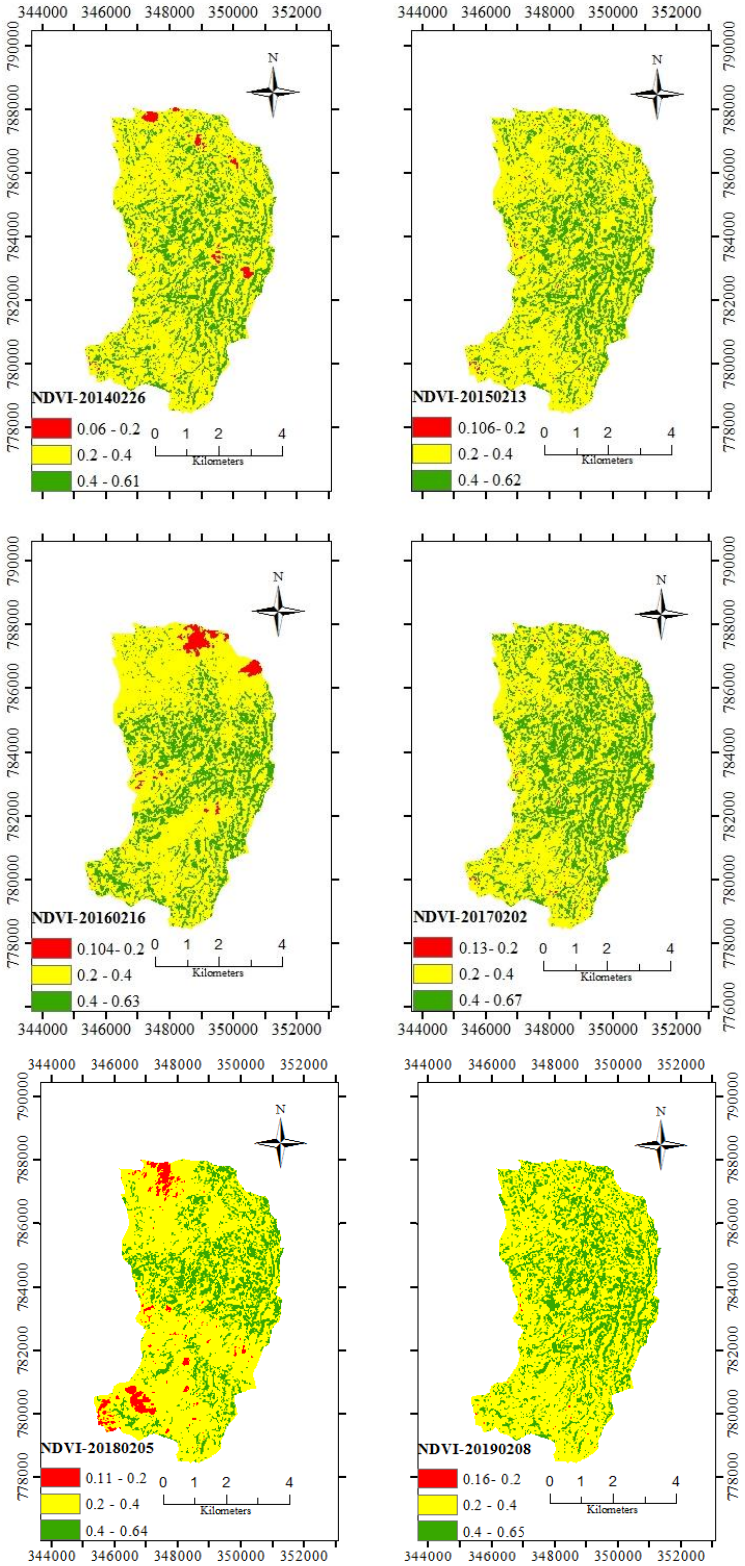

Fig 4.2. Spatial distribution of three vegetation classes, with varying NDVI values in the Magera after intervention

Table 4.1 shows the quantified variation of each vegetation cover classes in terms of the area occupied, from 2010 to 2019, as obtained from the images shown in Figure 4.1 and 4.2. The classified images of 2010 showed that the vegetation cover is dominated by "weak plants," which accounts for around 84.4% of the total basin area, followed by "healthy plants," which accounts for only 14.6%. However, starting from this year, the vegetated area is found to be decreasing dramatically. In 2012, reached "healthy plants" reduced to 1.5%, whereas "no plant" increased to 8.1%. As mentioned earlier, SLMP has started the watershed management activities in 2013/2014. The dramatic decreased in vegetation cover visible till 2013 ("no plants" increased to 40.1% in 2013), was reverted back gradually over the years. In 2014, "healthy plant" started increasing and on the other hand, "no plant" started decreasing. The situation almost reversed in 2017, when compared to 2013. 1.9% "healthy plant" and 40.9% "no plant" in 2013 has changed to 35.6% "healthy plants" and 0.4% "no plant" in 2017. The continuous increase in the area coverage of healthy plants and the continuous decrease in the area of bare land since 2013 could be attributed to the appropriate watershed management practices carried out in the watershed. The increament in vegetation cover shown after watershed intervention for Magera micro watershed is also shown increament for Wutame micro watershed.

Table 4.1: Vegetation class cover classified using the NDVI thresholds, for the period 2010 to 2019 (imagery for February month)

Class cover		No plant	Weak plant	Healthy plant
2010	Area (Km^2)	0.4	32.2	5.6
	(%)	1.0	84.4	14.6
2011	Area (Km^2)	1.4	33.9	2.8
	(%)	3.7	89.1	7.3
2012	Area (Km^2)	3.1	34.5	0.6
	(%)	8.1	90.4	1.5
2013	Area (Km^2)	15.6	21.8	0.7
	(%)	40.9	57.2	1.9
2014	Area (Km^2)	6.1	28.5	3.5
	(%)	16.1	74.7	9.2
2015	Area (Km^2)	0.2	27.0	11.0
	(%)	0.4	70.8	28.8
2016	Area (Km^2)	0.9	26.9	10.2
	(%)	2.5	70.6	26.9
2017	Area (Km^2)	0.2	24.4	13.6
	(%)	0.4	64.0	35.6

2018	Area (Km^2)	1.4	28.4	8.4
	(%)	3.6	74.4	22.0
2019	Area (Km^2)	0.2	25.3	12.6
	(%)	0.6	66.4	33.0

4.2 Seasonal variations of NDVI for three vegetation cover classes

Because the vegetation is expected to be significantly varying across the seasons, it is better to monitor NDVI over different seasons. In Ethiopia, there are four major seasons, Bega (Autumn) - December, January and February is the dry season, Tseday (Spring) – March, April and May is autumn season, Kiremt or Meher (Summer) – June, July and August is summer season. Heavy rains fall in these three months of the summer season, Belg (Autumn) – September, October and November is the spring season or harvest season. Since there will be a large variation in the vegetation (and hence, NDVI), NDVI is analyzed for the four seasons separately.

The seasonal variation of NDVI for three vegetation cover classes, over the period 2010 to 2019 is shown in figure 4.3. Evidently, for forests, the NDVI area for four seasons is significantly increasing from 2014/15 to 2019. However, the NDVI area was significantly decreasing from the baseline to 2013/14. It is apparent that reducing in NDVI area started from baseline to 2013/14 in every year is curved by watershed management intervention unless the decreasing in the NDVI area maybe continues to 2019. Especially for the season SON (September, October and November), the NDVI area clearly showed the increment in forest or vegetation cover. The reason was, this season in Ethiopia is called Belg season, which is agricultural lands that are fully covered with crops and green forests also include the resting place. Even the satellite images in this season provide the information without cloud affected images. Next to SON, JJA (June, July and August) has also resulted in a higher NDVI area, which is the wettest season. It is evident that the least NDVI area was results in DJF because of the driest seasons; however, the vegetation cover is increasing in every year from 2014/15 to 2019.

For no plant or bare land, the NDVI area was increasing from 2010 to 2013/14 for four seasons. But the NDVI area started decreasing from 2014/15 to 2019 (figure 4.3). One of the objectives of SLM intervention is to curb degraded land. So, the dropping of the NDVI area for bare land indicates the result of watershed management interventions. For shrubland or weak plant, the NDVI area was higher in 2010 and continued increasing to 2103/14. However, the NDVI area started decreasing in 2014/15 (figure 4.3) indicates the area under shrubland is on conversion to forest land. During the field visit, also have seen that SLM began to soil and water conservation

activities from area exclosure of shrubland and plating some indigenous plants to translate the area covered by shrubland to forest or vegetation cover.

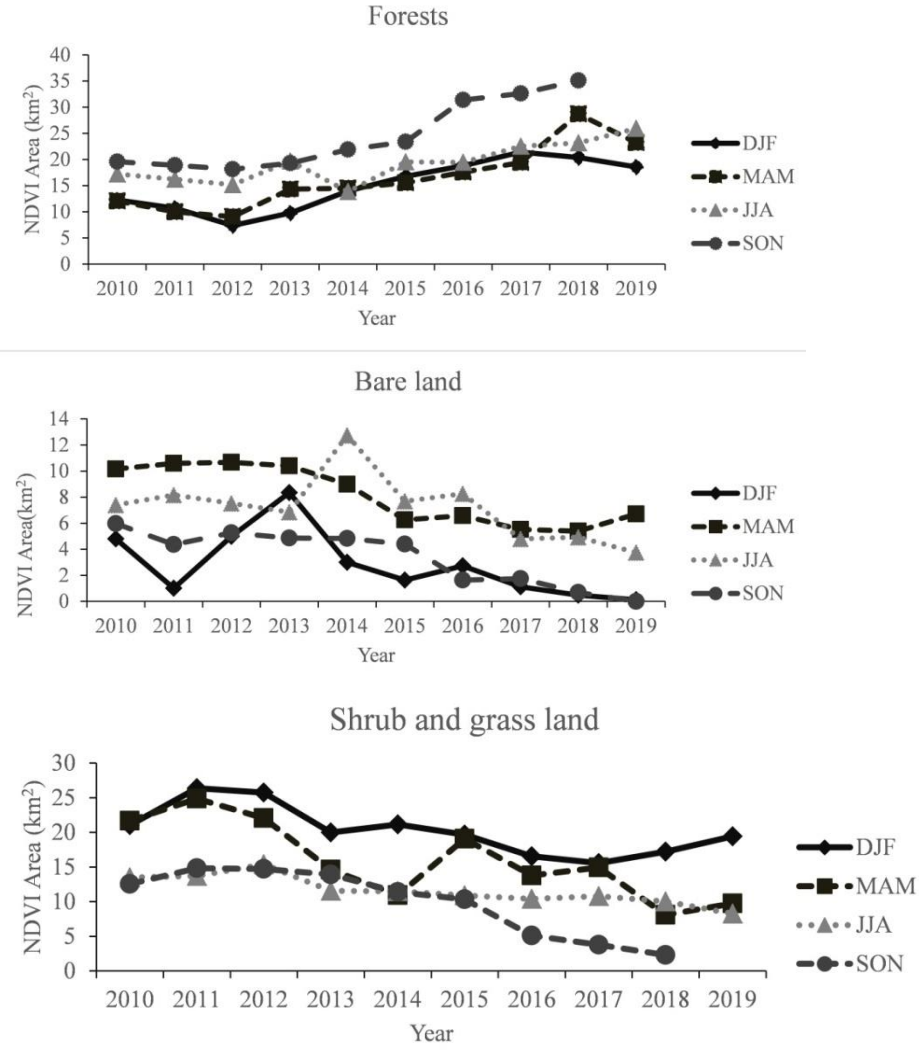

Fig 4.3. Seasonal variation of NDVI for three vegetation cover classes, over the period 2010 to 2019

4.3 Trends in NDVI time series for vegetation cover classes

Monthly NDVI trends were tested using the MK test and regression analysis for forest land or healthy plant. The results of MK tests show there is a significant increase in trends in monthly NDVI time series (figure 4.4 and table 4.2). As computed p-value (< 0.0001) is lower than the significance level alpha (α)=0.05, the null hypothesis H_0 of no change in monthly NDVI time series can be rejected and the alternative hypothesis H_a of there is significantly increasing trend

in NDVI is accepted. The regression analysis also indicates there is a moderately increasing trend in NDVI time series.

The MK test also suggests that there is a significant trend at the 5% significance level in the NDVI time series but the decreasing trend from regression analysis for shrub and grassland or weak plant. For no plant or bare land, the null hypothesis of no change in monthly NDVI time series also can be rejected at the 5% significance level because the computed p-value (0.0017) is lower than the NDVI time series is accepted. Despite the regression analysis showing a weak correlation, there is a decreasing trend in the NDVI time series.

Hence, the increase in the NDVI area for forest land indicates that there is a significant increase in vegetation cover. However, the decreasing in the NDVI area for bare land means the bare land is disappearing. The shrubland is in converting into forest land; that is why the NDVI area for shrubland is decreasing also. Therefore, the significant increase trend in NDVI time series and the decreasing trend is attributable to soil and water conservation interventions guided by the environmental rehabilitation strategy of Boloso Bombe woreda agriculture and rural development office.

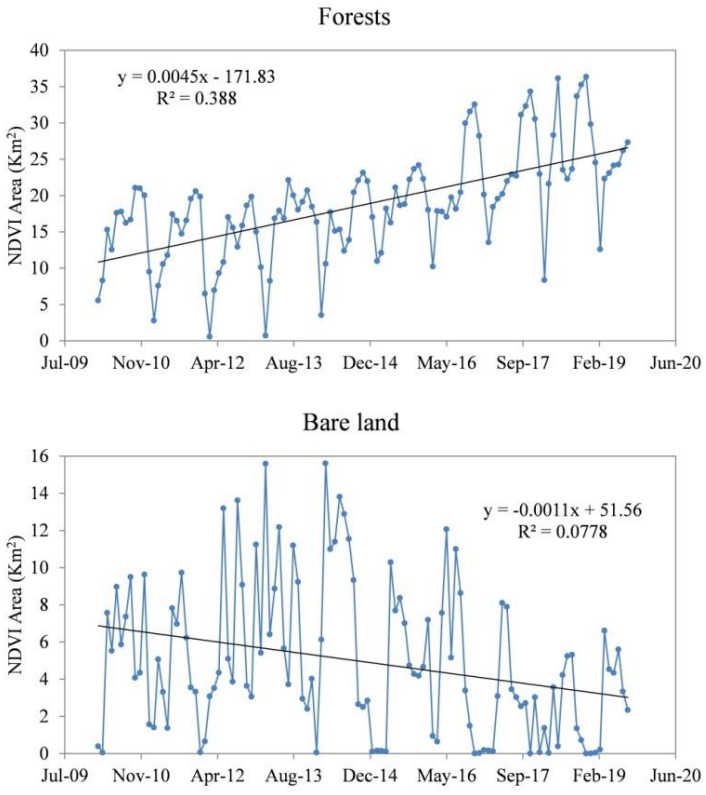

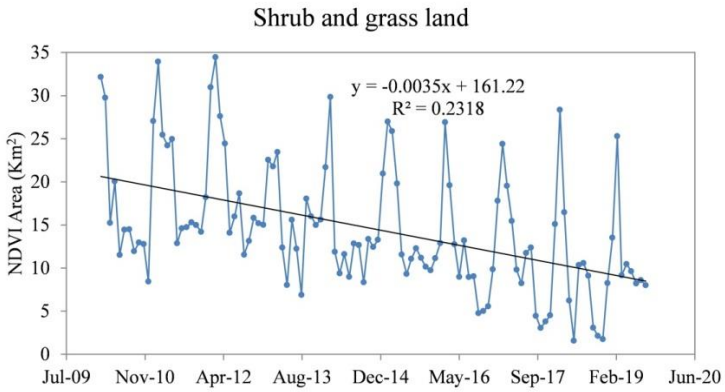

Fig 4.4. Mann-Kendal Trend test for NDVI time series for each vegetation cover

Table 4.2: Summary of Mann-Kendal trend test statistics for vegetation cover classes

	Mann-Kendall trend /Two-tailed						
	Kendall's tau	S	Var (S)	p-value	alpha	Sen's slope	H_o
Forest	0.478	3134	171155	< 0.0001	0.05	0.133	R
Bare land	-0.1979	-1297	171156	0.0017	0.05	-0.0314	R
Shrub & grass land	-0.373	-2448	171157	< 0.0001	0.05	-0.097	R

4.4 Change-point analysis using three deferent methods

Pettitt's test, Buishand test and SNHT test for homogeneity trend were, applied to monthly NDVI time-series data for each vegetation cover class between 2010 and 2019.

For forest or healthy plants, Pettitt's test showed no homogeneity in monthly NDVI time series, indicating that the NDVI time series has changed significantly over the study period. The null hypothesis H_0 of no changes point in monthly NDVI can be rejected at the 5% significance level because, the computed p-value (<0.0001) is lower than the significance level of alpha (α)=0.05, the alternative hypothesis Ha of there is change point in NDVI time series is accepted.

The Pettitt's test applied to the monthly NDVI time series showed a change point in May-2015 (figure 4.5 and table 4.3). Based on these change points, the time series NDVI data was divided into two periods: period 1 (mean value of NDVI in km^2=14.7) for 2010-2014, period 2 (mean value of NDVI in km^2=23.6) for 2016-2019. For bare land or no plant, Pettitt's test showed a change point in August-2016, with mean value decreased from (6.082) in period 1 to (2.459) in period 2. The mean value for shrub and grassland or weak plant also decreased from (17.59) in period 1 to (10.86) in period 2 with a change point in April-2015 (figure 4.5 and table 4.3). The change point year for forests and shrubland is the same in 2015 and for bare land in the year 2016, which indicates almost a similar change point is detected.

Note that, physical and biological soil and water conservation activities were started in 2013/2014 in this watershed. The change point for the forest in May-2015, which is two years after the start of SLMP interventions, indicates there is an increment in vegetation cover as the result of watershed management interventions. Reducing or curbing bare land is one the objectives for SLMP; reduction in bare land started in August-2016 also indicates the impact of the response. Decreasing in shrubland in 2015 suggests the conversion of shrubland into forest land, which is also the result of soil and water conservation activities.

SNHT and Buishand's test showed almost similar change point with Pettitt's analysis, especially the bare land and shrubland for Pettitt's and SNHT is the same year and forest land shrubland for Pettitt's and Buishand's is same (table 4.3).

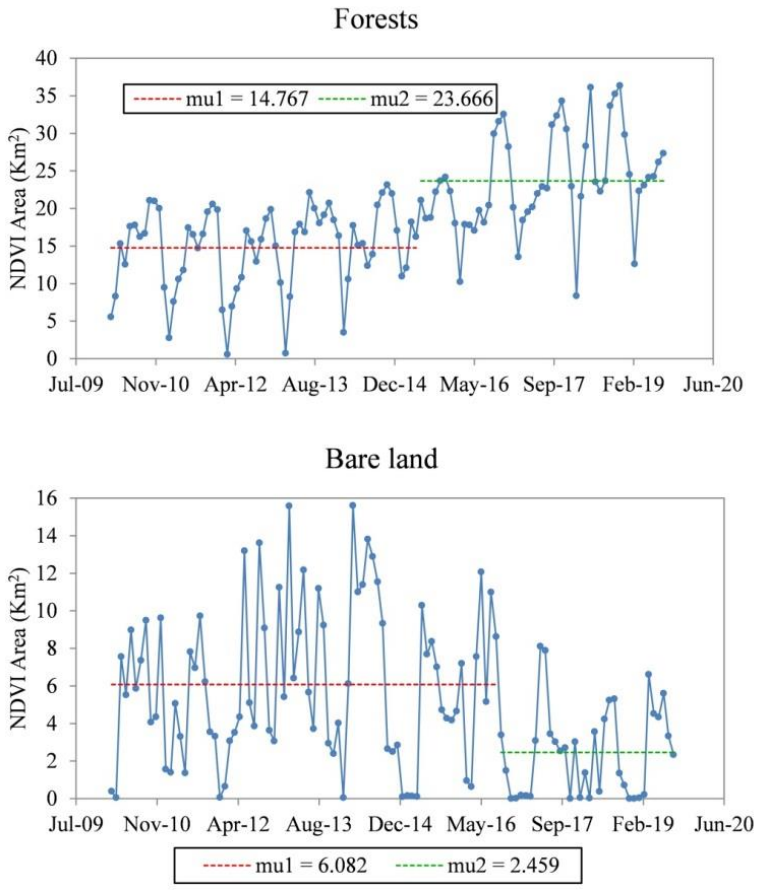

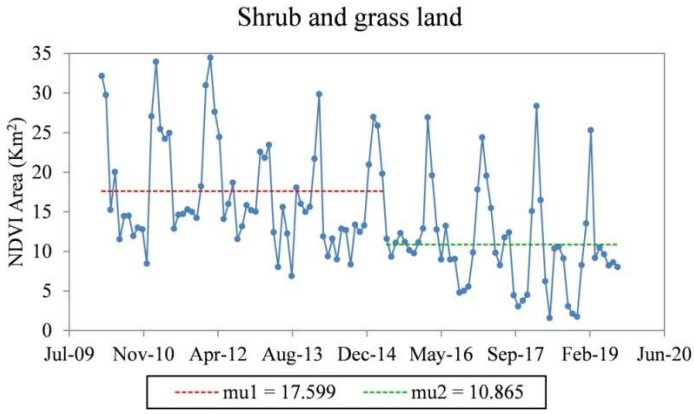

Figure 4.5: Changepoint analysis using Pettitt's test

Table 4.3: Summary of statistics for three change-point analysis methods

		Forest	Bare land	Shrub and grass
Pettitt's test	K	2439	1542	1954
	t	15-May	16-Aug	15-Apr
	p-value (Two-tailed)	<0.0001	0.0001	< 0.0001
	alpha	0.05	0.05	0.05
Standard normal homogeneity test (SNHT)	T0	43.62	19.88	23.79
	t	16-Aug	16-Aug	15-Apr
	p-value (Two-tailed)	< 0.0001	0.0005	< 0.0001
	alpha	0.05	0.05	0.05
Buishand's test	Q	34.29	22.48	26.15
	t	15-May	14-Sep	15-Apr
	p-value (Two-tailed)	< 0.0001	0.0001	< 0.0001
	alpha	0.05	0.05	0.05

4.5 Possible influence of rainfall in the increased vegetation

It was evident that vegetation or forest is highly dependent on rainfall, which means that when the rainfall increase, the vegetation cover also increases. However, this is not always true because vegetation also depends on other factors means that other than rainfall, factors are contributing to the vegetation cover increment. The variation of NDVI and precipitation are shown in figure 4.6. There is a significant positive increment trend in the monthly NDVI area at a 5% significance level, for forest or healthy plant (R^2=0.393). On the other hand, the pattern of

rainfall from Areka stations from 2010 to 2017 shows, there is a significant positive trend in time series but a very weak correlation (R^2= 0.017). When there is a low rainfall observed in Sep-2016, the NDVI area is very high, which contradicts the relationship of rainfall and vegetation cover and the year 2015/16 from Pettitt's test indicates the change year for the increment of forest or healthy plant. So, this shows other factors are contributing to vegetation cover improvement that is watershed management activities carried out in the watershed.

The NDVI area and rain are very weakly correlated with (R^2 = 0.0158), in which the rainfall is going to decreases, the NDVI area is going to increases. A higher NDVI area was observed even if in smaller rain. This also further verified with weak correlation and decreasing trend results obtained from autocorrelation between rainfall and NDVI for lag times from 0 months to 12 months (table 4.4). The autocorrelation is analyzed based on the assumption that rain occurred first and then the response had followed, that is, vegetation (NDVI change). However, the significant increase in vegetation cover in the watershed could be due to other factors: (i) impact of appropriate watershed management activities implemented to rehabilitate the degraded land; (ii) area exclosure by protecting grazing land. This agrees with early studies by Hishe *et al*. (2017) observed a significant negative correlation between pixels based mean SAVI and average annual precipitation and concluded the considerable increment in vegetation density is due to soil and water conservation activities. Whiting (2017), in his studies, also found that the improvement of vegetation cover is not expected to an increase in rainfall, but due to personal investment in restoring degraded land to productivities.

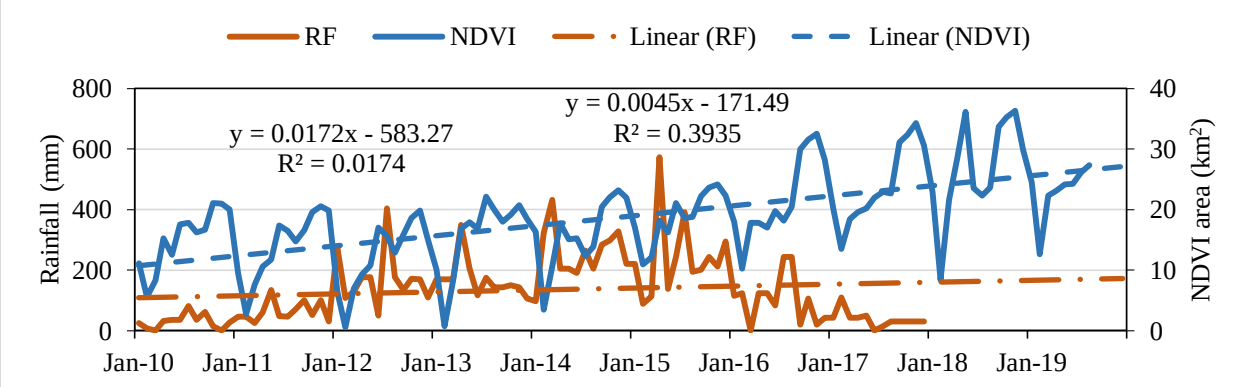

Figure 4.6: Variation of NDVI and rainfall at Areka stations

Table 4.4: Autocorrelation between rainfall and NDVI for lag times from 0 months to 12 months

Lag (Month)	Autocorrelation
0	1
1	-0.1259
2	-0.1367
3	-0.1625
4	-0.1845
5	-0.1892
6	-0.1988
7	-0.1998
8	-0.2
9	-0.2034
10	-0.2053
11	-0.2003
12	-0.1948

4.6 Verification through Citizen Science

This is also confirmed by a brief citizen science approach conducted by the authors through field observations and discussions with elders residing in the watershed, where the citizens have cited the improvement due to the impact of watershed management interventions.

The watershed management practices introduced in the study area have thus resulted in a better restoration in the natural environment of land. A few photos taken by the author are shown in annex figure 6. After biological soil and water conservation (forage grasses, terrace and trenches at hillside) by SLM, the degraded landscape started to recover its grasses and vegetation density. In most of these managed areas, the community is benefited directly or indirectly from conservation activities. For example, dry spring emerged, which is used by the community for their day-to-day uses. Ginger, banana and coffee production on farmer's land after the soil regained enough moisture content as a result of SLM intervention. In addition, during discussions made with nearby communities, it is revealed that, before the intervention, people live in the upstream of the watershed were faced with massive erosion in their farmland, which affected the crop yield and production, since the cereals grown in the farmland used to be washed away to the river by erosion. However, after SLM intervention, the crop yield increases, water is readily available for domestic purposes, and the living standards have improved.

4.7 Separate Quantification of different SWC activities in increasing vegetation density

The impact of soil and water conservation activities carried out in the watershed in increasing vegetation cover was quantified so far. However, a separate quantification is required to know the efficiency of each of the different SWC practices in increasing vegetation densities. From different physical and biological SWC practices introduced in the study area, terraces and bunds are compared because both of them are highly contributing to increasing vegetation cover. For this study, seven mini watersheds based on Boloso Bombe Woreda kebele shape are identified and their corresponding areas are extracted from Google earth pro and converted into a shape file. NDVI-08022019 map retrieved in the earlier section was used to quantifying the contribution of terraces and bunds in increasing vegetation cover. The shape of the micro watershed is overlaid on the NDVI map and values are extracted using extraction by mask and reclassified in three vegetation cover classes.

Table 4.5 shows a summary of some selected SWC activities and their corresponding area of vegetation cover classes. The code ZT, the first letter Z, implies name the micro watershed Zaba; the second letter T indicates terraces or if it is B means bunds.

Table 4.5: Summary for some selected SWC activities in increasing vegetation density

Code	Name of micro watershed	Type of SWC activities	Area treated (km^2)	%NDVI area bare	%NDVI area shrub	%NDVI area forest
ZT	Zaba	Terrace	0.09	28.57	42.86	28.57
GB	Gamo Walana	Bund	0.25	30.69	45.85	23.47
GT	Gandisa (I)	Terrace	0.02	16.67	50	33.33
MB	Morocha	Bund	0.34	46.97	40.63	12.4
UB	Udula Matala	Bund	0.68	37.7	42.33	19.97
BT	Buna Gandisa	Terrace	0.24	33.96	37.74	28.3
MB	Matala Walana	Bund	0.1	37.74	41.51	20.75

The NDVI area (%) for each vegetation cover classes is plotted with their codes to see the contribution of terrace and bunds in increasing vegetation cover (figure 4.7). Evidently, a high NDVI area for forest land, low NDVI area for bare land and relatively a high NDVI area for shrubland were observed for terraces. This implies that the increase of vegetation density for the study area was more contributed from terraces. Similar ideas are pointed out by early studies; for example, Desta et al. (2005) pointed out terraces like hillside terraces are the most commonly adopted SWC works and are suitable for tree planting and somewhat effective in controlling

runoff and erosion. The study conducted by Woldeamlak (2006) note that in Ethiopia, vast areas have been covered by terraces, and millions of trees are have been planted. Therefore, Damene et al. (2012) concluded that terracing was effective in increasing vegetation densities and effective against soil and nutrient loss. On the other hand, low NDVI areas for forest land and high NDVI area for bare land are observed for bunds. Buns are also contributing to vegetation increment but compared to terraces low.

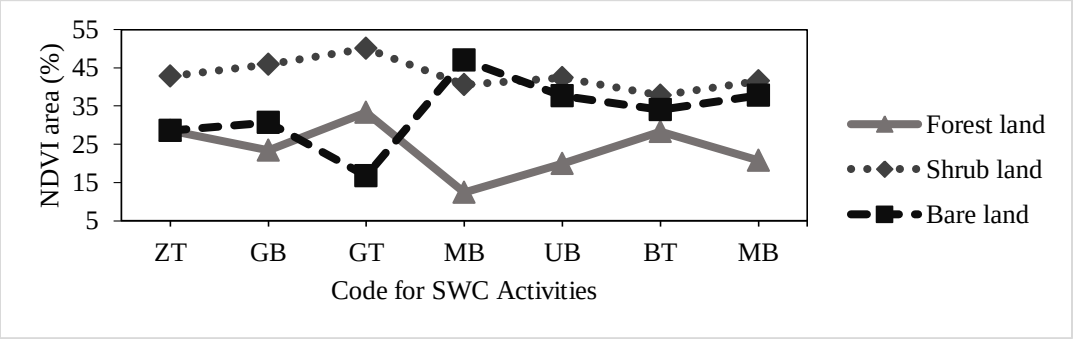

Figure 4.7: Terraces and bunds responses in vegetation cover increment. ZT: terrace in Zaba; GB: bund in Gamo Walana; GT: terrace in Gandisa; MB: bund in Morocha; UB: bund in Udula Matala; BT: terrace in Buna Gandisa; MB: bund in Matala Walana

4.8 Land use land cover classification and change detection

4.8.1 Accuracy Assesment

Before to use the prepared LULC map for change detection, the testing pixel must be validated against reference data in the form error matrix. Table 4.6 shows the error matrix for classified LULC map of 2019 with two errors, such as omission error and commission error and four accuracy assessment parameters such as producer's accuracy, user's accuracy, overall accuracy and kappa coefficient. The overall accuracy is 92.8%, with a kappa coefficient of 0.89 for the LULC map of 2019. Similarly, for the 2010 LULC map, overall accuracy is 93.4% is with a kappa coefficient of 0.91 and for the LULC map of 2014, overall accuracy is 89.7% with kappa coefficient 0.87. According to Anderson et al., (1976), an overall classification accuracy of 85% and above is recommended and According to Thomnlinson et al., (1999), no classes of less than 70% is recommended. Hence these result meets the standard recommended by earlier studies. Thus, Spot 7 Images and NDVI maps helped to improve the overall accuracy.

Table 4.6: Error matrix for LU/LC map and accuracy assessment derived from 2019

LU/LC classes	Reference data					Classified total	Producer's accuracy (%)	Omission error (%)
	Bare land	Shrub land	Grass land	Agricultural land	Forest land			
Bare land	3	0	0	0	0	3	60	40
Shrub land	1	21	1	0	0	23	87.5	12.5
Grass land	0	1	7	0	0	8	77.8	22.2
Agricultural land	1	2	1	59	1	64	96.7	3.3
Forest land	0	0	0	2	40	42	97.6	2.4
Reference Total	5	24	9	61	41	140		
User's accuracy (%)	100	91.3	87.5	92.2	95.2			
Commission error (%)	0	8.7	12.5	7.8	4.8			
Overall Accuracy		92.8%		Overall Kappa Coefficient		0.89		

4.8.2 LULC maps for three peroids

Figure 4.8 shows a classified LULC map of 2010, 2014 and 2019. As can see from the figure 4.8, there is not too much clear upper-lower classification has observed between the LULC classes because of, the land was covered by mixed land use/cover as observed in the fieldwork period. Even though not too much detail upper-lower classification was shown like for other LULC maps, the study area was accurately classified with the identified mixed land use/cover. To classify such mixed land use/cover accurately is difficult with the only medium resolution, thus why these studies applied ancillary data like NDVI map, high-resolution SPOT 7 Image, a sufficient number of collected GCPS.

The area covered under each LULC class and their percentage distribution are shown in table 4.7 and figure 4.9a. During the period 2010, the lower part (outlet) of the watershed was noticeably covered by bare land, grassland and agricultural land. The middle of the watershed was more covered by forest land, slightly with bare land and agricultural land. Shrublands more covered the upper part. In 2014 a considerable increment of shrubland was observed in the middle part of the watershed and also slightly reduction of bare land observed. By the year 2019, a significant increment of agricultural land was observed throughout the watershed and an increase of forest cover was also found in the middle and upper part of the watershed. Slightly reduction in bare land was also observed.

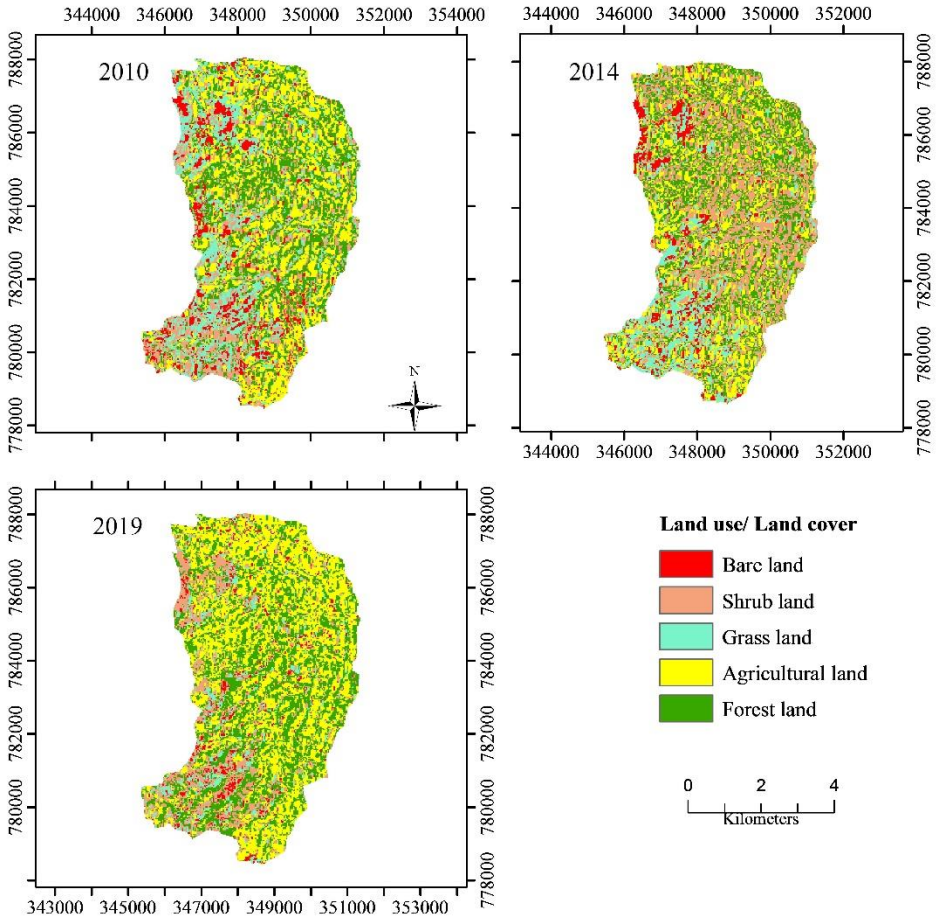

Figure 4.8: Land use land cover map of the study area (2010, 2014 and 2019)

Table 4.7: Area percentage covered by LULC classes and their corresponding area changes

LU/LC classes	Area of 2010 (km^2)	%of area occupied	Area of 2014(km^2)	%of area occupied	Area of 2019(km^2)	% of area occupied	% of change 2010-2014	% of change 2014-2019	% of change 2010-2019
Bare land	3.2	8.6	2.5	6.8	1.7	4.6	-22.9	-31.4	-47.1
Shrub land	7	18.7	10.9	30	5.4	14.5	56.4	-50.6	-22.7
Grass land	6.8	18.2	5.1	13.9	2.6	7.1	-25.7	-47.6	-61
Agricultural	10.7	28.6	8.2	22.6	15.2	40.9	-23.1	85.2	42.4
Forest land	9.8	26	9.8	26.8	12.3	33	0.1	25.7	25.8

4.9 Change detection between 2010 and 2019

By the year 2010-2014, the area occupied by shrubland showed an increase and bare, grass and agricultural land showed a decrease (figure 4.9 and table 4.7). The forest land remains the same. SWC activities were started in 2013/14. In this period, agricultural productivity was declined because of land degradation and more of the area was occupied by bare land and grassland. That

is why SLM has targeted this watershed. Forest land doesn't show any change because of, more regions are occupied by shrubland.

The period of 2014-2019 is the main focusing period for this research because intensive watershed management practices are carried out and SLM objectives start achieving in this period. Bare land, shrubland and grassland continuously decreased to 31.4%, 50.6% and 47.1%, respectively (table 4.7 and figure 4.9). Conversely agricultural land and forest land increased to 85.2% and 25.7% respectively. The highest percentage of the decline of 50.6% was found in the case of shrubland. The fall is mainly due to the conversion of shrubland into forest land. One of the objectives of SLM is to increase production and productivity of agriculture. The drastic increase observed in agricultural land was mainly due to the conversion of bare land and grassland into farmland and is the result of intensive watershed management activities carried out in the watershed.

Throughout 2010 -2019, the area occupied forest land and agricultural land showed an increase, whereas bare, shrub and grassland showed a decrease (table 4.7 and figure 4.9). The increase in forest land in the watershed by 25.8% is mainly due to the conversion of shrubland and land into forest land. These results show a positive change in landscape pattern due to proper watershed management activities. On the other hand, the agricultural land was increased by 42.4% and bare land was decreased by 47.1%. These negative changes are mainly due to the conversion of bare land into agricultural land.

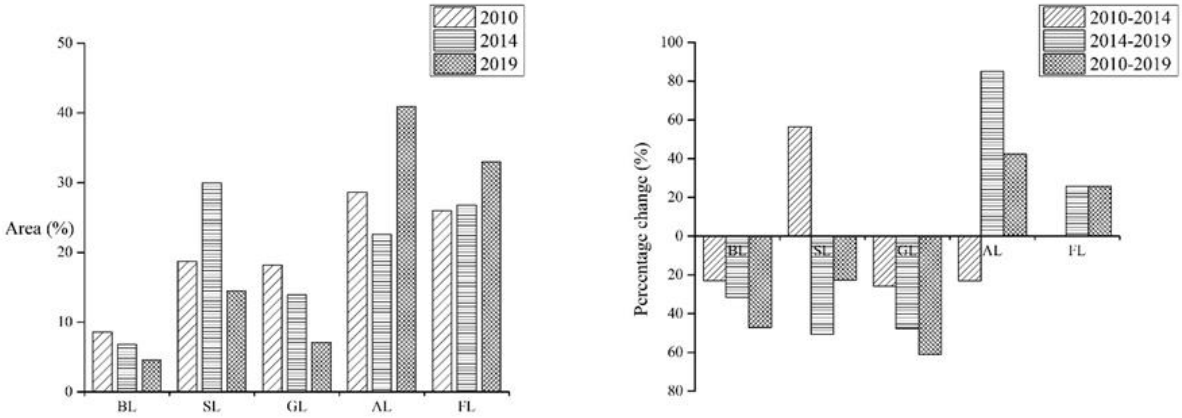

Figure 4.9: Area coverage (%) by different LULC types (left) and the corresponding percentage change (right) from 2010 to 2019. BL: bare land; SL: shrubland; GL: grassland; AL: agricultural land; FL: forest land

4.10 Soil moisture change detection as caused by SLM intervention

4.10.1 Observed soil moisture

From Feb.8, 2019 to May.31, 2019, overall 40 averaged direct and indirect methods measured soil samples. Out of 40 sample points, 34 sample points were measured both by direct and indirect methods, whereas 6 sample points were measured by the only indirect method. Soil moisture was measured directly by the gravimetric method in a laboratory, whereas, indirectly by portable sensor HH2 meter. For all sampling days, the sample was taken both by direct and indirect from the same reference point. But for sampling day May.15, 2019, the sample was only made by the indirect method.

The reason why sampling was taking both by the direct and indirect method was to calibrate the indirect measurement (portable sensor) by direct measurement. So, after calibrating the portable senor by gravimetric method, 6 sample points were re-analyzed by equation developed from the calibration of both methods and later, it was used to analyze the soil moisture of the study area. Annex figure 4 and annex table 2 shows the calibration of the HH2 sensor using lab soil moisture estimate and a correlation coefficient R^2 of 0.725 and mean absolute error (MAE) of 0.29 cm^3/cm^3 was obtained. This indicates that the two measurements are in good agreement. Less than 29% of variation has come from other factors than soil moisture; hence, the portable HH2 sensor can be used as a reference measurement for further analysis.

4.10.2 Soil texture

Soil texture is the proportion of the three sizes such as clay, sand and silt. The percentage of sand, clay and silt were estimated from the particle size distribution graph (annex figure 3) by using United State Department of Agriculture (USDA) Soil classification system. For example, for soil sample E2, Clay of (19.61%), silt (68.20%), sand (12.17) and gravel of (0%) where estimated from gradation curve of particle size and percent finer (table 4.8). Triangular classification method developed by USDA were also used to further classify the soil in to its fineness or coarseness. Using the estimated value of soil particle size and triangular classification methods, the texture for this soil sample where silt loam.

The same procedure where followed for the reset of ten sample point to analyze the sieve analysis, hydrometry analysis, particle size and textural classes. Table 4.8 summarizes the results of soil texture and soil moisture content for eleven soil samples.

Table 4.8: The results of soil texture and moisture content for eleven soil samples

Code	X	Y	Moisture content by volume (%)	Clay (%)	Silt (%)	Sand (%)	Gravel (%)	Texture using USDA triangle method
B1	346871	787916	26.99	47.46	37.8	14.54	0.2	clay
B3	346885	787900	31.59	59.57	31.1	9.33	0	clay
C1	346728	787838	17.83	36.55	48.61	14.84	0	silty clay loam
C5	346712	787849	25.48	32.76	51.24	14.84	1.15	silty clay loam
D1	346598	787271	23.96	44.97	45.55	9.48	0	silty clay
D2	346606	787253	21.39	35.38	55.34	9.28	0	silty clay loam
E1	346734	787325	20.38	25.48	62.38	12.14	0	silt loam
E2	346729	787308	22.42	19.61	68.2	12.17	0	silt loam
F1	346849	785738	33.16	25.77	63.1	11.13	0	silt loam
G1	346638	785686	19.36	32.76	51.24	14.84	1.15	silty clay loam
G3	346649	785675	17.32	24.14	59.11	16.65	0.1	silt loam

As mentioned earlier, a soil with a high percentage of silt and clay particles, which describes fine soil, has a higher water-holding capacity. As can see from table 4.8 the percentage of clay and silt particles takes more than other soil particles and their corresponding soil moisture content is high. A soil with high moisture content has a clay soil texture. For example, test pit B1 and B2 have high moisture content and corresponding soil texture is clay. From all the results averagely, high moisture has a clay type of soil texture. On the contrary, a soil with low moisture content has a texture of loam. Generally, the soil texture verified the soil moisture content, mean that soil with high moisture content has fine soil, clay or silt texture and with low moisture content has coarser soil, sand or loam texture and this is a nearly similar result with other literature.

The results of 4 textural classes were mapped in ArcGIS with their corresponding coordinate to determine the spatial distributions of soil textures of the study area. Figure 4.10 shows the soil texture of the study area and the dominant soil texture is silt clay and followed by silt loam.

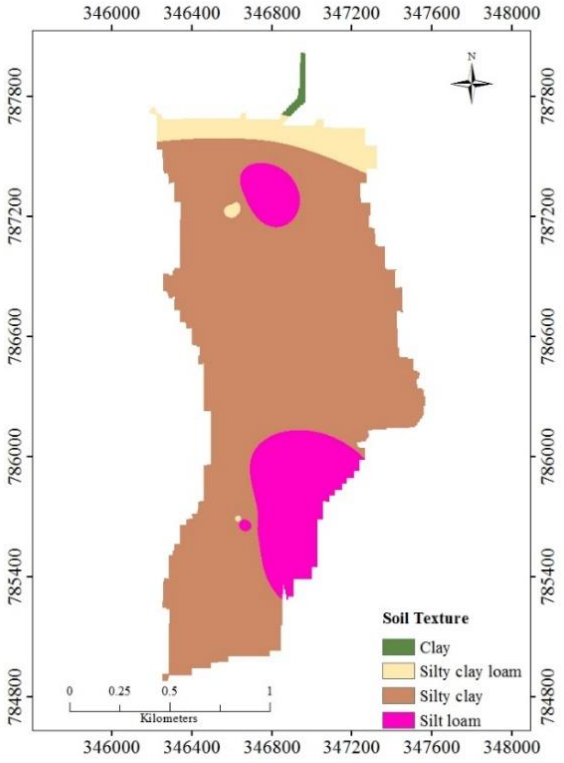

Figure 4.10: Textural classes of the study area

4.10.3 Remote sensing measurement

NDVI map is retrieved from Landsat 8 images for all the days of soil sample was taken. Figure 4.11 shows for some selected dry and wet seasons NDVI map. Wet season images were affected by cloudy but till provide good information's. There is spatially and temporally variation in NDVI in the study area. Extreme red shown for NDVI of 28/02/2019 and 31/05/2019 are not low vegetation cover but because of cloud effect.

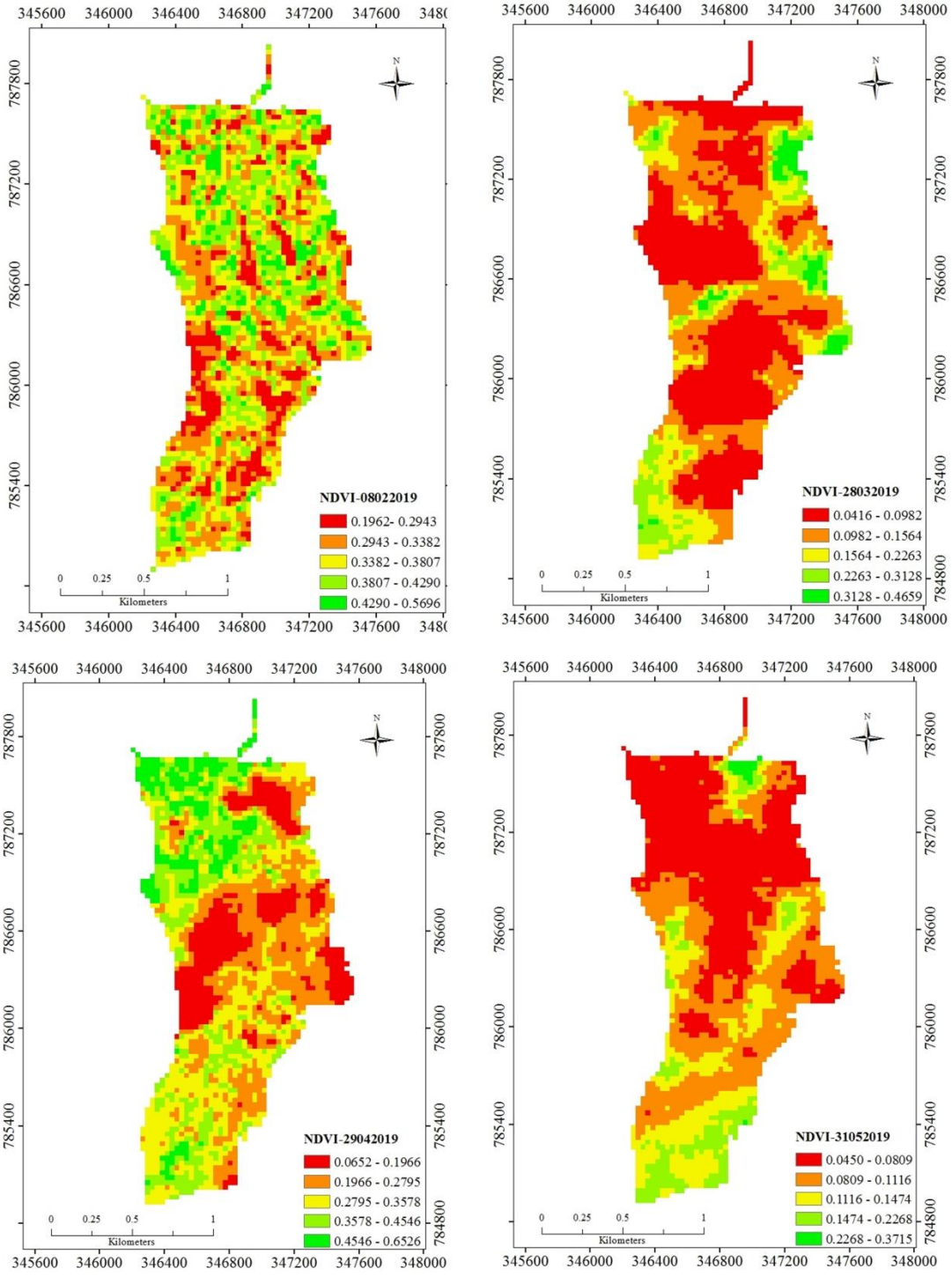

Fig 4.11: NDVI map for the study area

Land surface temperature (LST) is the radiative skin temperature of the ground which depends on albedo, vegetation cover and soil moisture of the land surface. LST is retrieved from NDVI

and thermal band. In reality, LST and NDVI are inversely related, when vegetation cover increases, land surface temperature decreases and vice versa. This relationship was observed for dry seasons because, a thermal band which is band 10 captures the reflectance temperature from the earth surface, so, in dry season information's are accurately captured, but for the rainy season because of the effect of cloud coverage and low solar radiation, little reflectance temperature was recorded. In this case, there might be a direct relationship between NDVI and LST. Figure 4.12 shows the land surface temperature in degree Celsius (^{o}C) for the study area is dry and wet seasons. High LST (32.7 ^{o}C) was observed in dry seasons for Feb.08, 2019 and low LST (11.8 ^{o}C) was observed in the rainy season for May.31, 2019. LST and NDVI are essential parameters for calculating the soil moisture index (SMI).

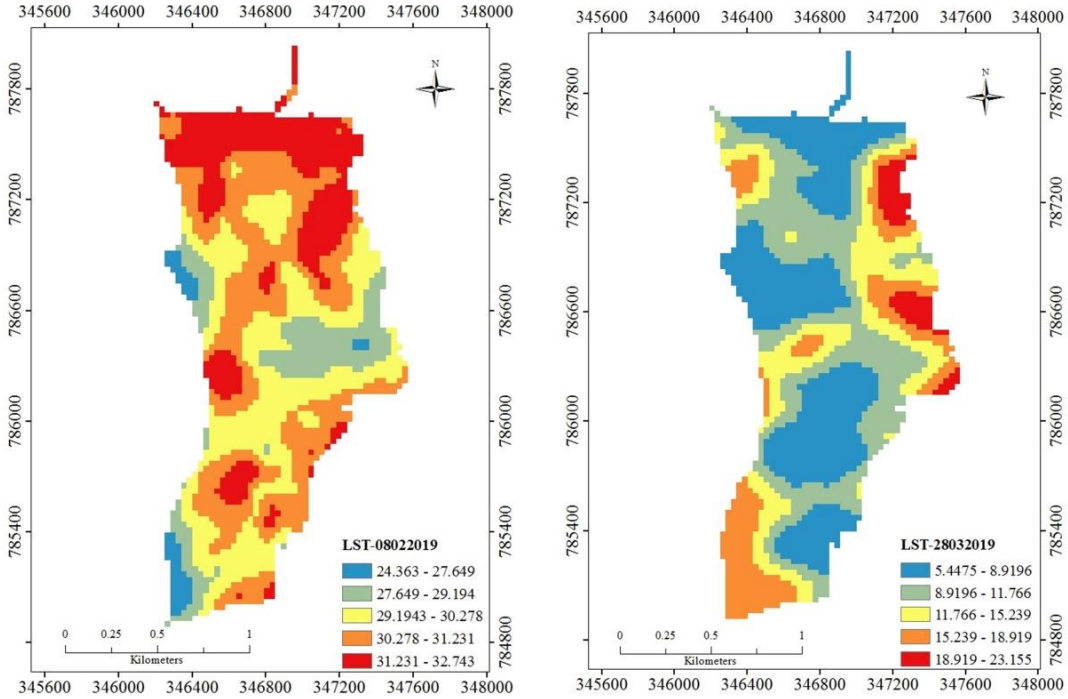

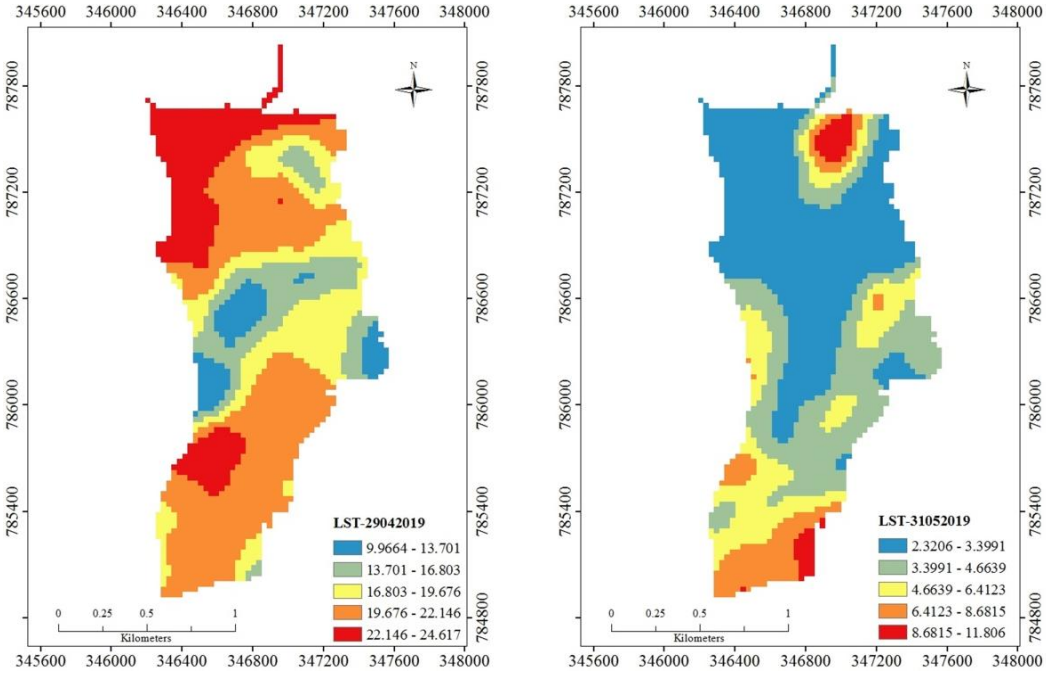

Fig 4.12: LST map of the study area

4.10.4 Scatter plot of NDVI and LST

The scatter plot for the land surface temperature versus NDVI of 08/02/2019, 24/02/2019, 28/03/2019/, 29/04/2019, 15/05/2019 and 31/05/2019 are shown in figure 4.13. The scatter plot of 08/02/2019 and 24/02/2019 shows a more precise a trapezoid shape, following the theoretical trapezoid of the SMI. Linear regression was applied to the wet edge (LSTmin) and dry edge (LSTmax). A strong positive and negative relationship was found in LSTmax and LSTmin observations, respectively. The wet edge has a positive correlation indicates that when vegetation cover increases, land surface temperature increases. The dry edge has a negative relationship suggests that when the vegetation cover increase, the land surface temperature decreases. These wet edge and dry edge were used to calculate the SMI.

The result of the scatter plot indicates that there was a strong correlation with R^2 of 0.74 to 0.81 for 08/02/2019 and R^2 of 0.69 to 0.72 for 24/02/2019, meaning that a linear equation adequately represents the wet edge and dry edges. The result is an agreement with early studies of Potic et al. (2017) and Burapapol and Nagasawa. (2016). From the figure, for 08022019, the slope (-6.17) of the dry edge tends towards the negative side as compared to the slope (12.65) of the wet edge. This difference is attributed to the vegetation cover and LST as the dry edge was determined by

observing maximum LST against an interval on NDVI values from a scatter plot. The negative slopes associated with dry edge might be the effect of evapotranspiration and bare soil surface with confining water conditions.

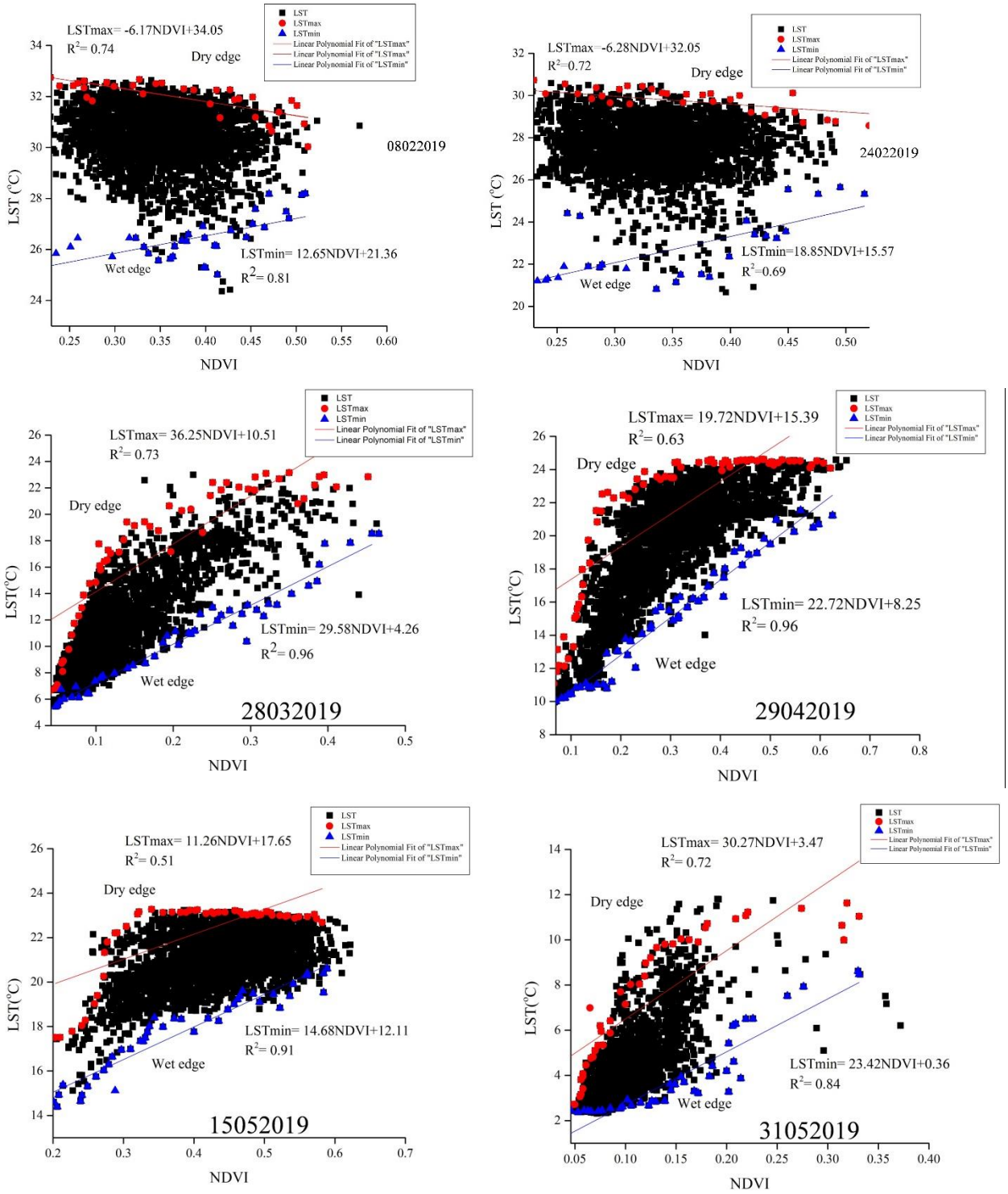

Fig 4.13: Observed relationships for NDVI-LST based on conceptual SMI model

4.10.5 Soil moisture index (SMI)

Soil moisture index is based on an empirical parameterization of the relationship between land surface temperature (LST) and normalized difference vegetation index (NDVI). Soil moisture of the study area was analyzed from SMI. The final results obtained from Eq. 3.28 was presented within the values range from 0 to 1, where value near 1 is the region with a high amount of vegetation cover and a low amount of surface temperature and presents a higher level of soil moisture. The value near 0 is the areas with a low amount of vegetation cover and high surface temperature and gives a low level of soil moisture. The distribution shows that SMI in the study area is primarily determined by vegetation cover. This result agrees with previous research work of Zhan *et al*. (2004) and Parida *et al*. (2008).

Figure 4.14 shows soil moisture index (SMI) distributions for the study area. For dry seasons of Feb.08, 2019, low SMI distribution was observed in downstream of watershed along with the outlet, this is because of agricultural land are considered as bare soil in dry seasons, but highly vegetated areas along with the upstream and middle result in high SMI. This clearly shows that SMI is highly dependent on vegetation cover. In May.31, 2019, high SMI distribution was observed along the middle and downstream of the watershed because in rainy seasons, agricultural land holds more moisture than any other land cover types. All results confirm that SMI has capable of accurately estimating the soil moisture of the study area and is highly dependent on vegetation cover. This SMI latter validated by ground observed soil moisture to map the spatial and temporal soil moisture of the study area.

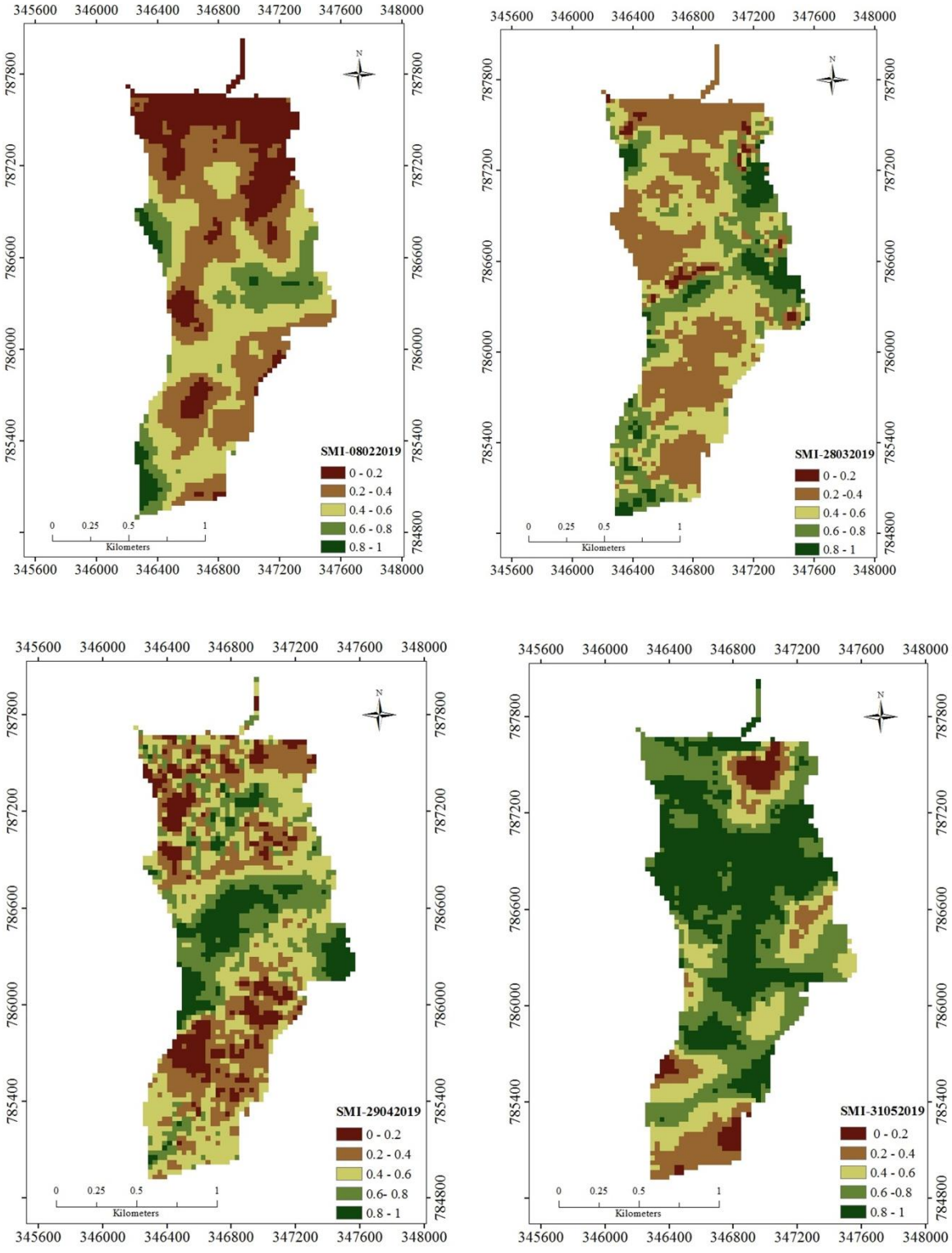

Fig 4.14: Soil moisture index (SMI) map of the study area

4.10.6 Simulated soil moisture

Linear regression models for soil moisture estimation were calculated using the SMI as dependent variables, and ground observed soil moisture as the independent variable. A total of 26 sample points were used to calibrate the model and 14 points were used for validation. The linear regression was set up using field-measured soil moisture content and SMI for all pixels matching the site of each observed sampling sites. Both calibration and validation were done to check the performance of the developed model. The model constructed has a strong response to the actual soil moisture and has a more exceptional ability to accurately estimate soil moisture based on its high R^2 (0.768) and low RMSE (0.033cm^3/cm^3) for ground soil moisture versus estimated soil moisture. Therefore, the soil moisture model fulfills the requirements with an increase in the R^2 and a reduced RMSE, which can increase the efficiency of soil moisture estimation. Annex figure 5 shows the correlation made between the actual soil moisture to the simulated soil moisture using the model.

The developed model was tested for accuracy about field-measured soil moisture and the model fulfills the statistical requirements with an R^2 of 0.519, low RMSE of 0.030 cm^3/cm^3, AAD values of 0.0243 cm^3/cm^3 and model precision of 52.64% between the actual and estimated soil moisture. The result of statistical tests demonstrates that the model developed from SMI can provide a reliable estimate of soil moisture. Based on these results, the developed model was applied to each image to estimate the spatial and temporal soil moisture of the study area. Figure 4.15 shows some selected dry and wet moisture content of the study area. The spatial mean simulated soil moisture for the study period is shown in table 4.9

Table 4.9: Average soil moisture of Wutame micro watershed derived from the model

Day	Average SM (cm^3/cm^3)
8022019	0.1949
24022019	0.1976
28032019	0.2616
29042019	0.3066
15052019	0.2889
31052019	0.3469

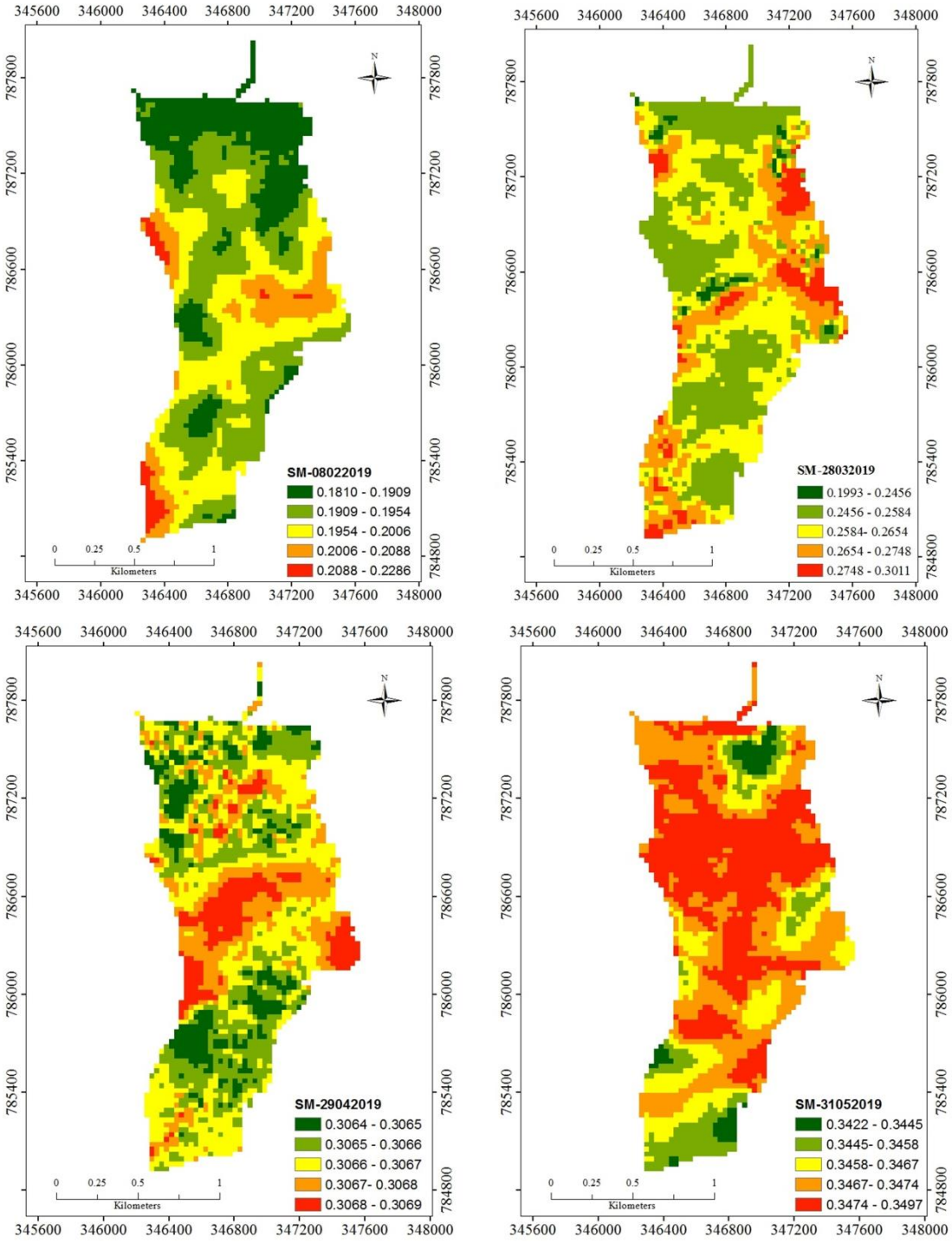

Figure 4.15: Spatial and temporal soil moisture of Wutame micro watershed derived from the model

4.10.7 Soil moisture change detection

In the earlier section, SMI confirmed that it has capable of accurately estimating the soil moisture of the study area and is highly dependent on vegetation cover. Higher vegetation cover results in low land surface temperature and high soil moisture content. Lower vegetation cover results in high land surface temperature and low soil moisture content. The detail vegetation cover of the study area was analyzed in an earlier section and the result shows that the vegetation cover was increased after intensive watershed management intervention so, these result confirms the increase of soil moisture of the study area because soil moisture (SMI) and vegetation cover (NDVI) has a direct relationship. For all soil moisture sampling dates, high moisture content was observed on the highly vegetated area and low soil moisture content was found on bare land. A drastic decrease in bare land and a dramatic increase in forest or vegetation cover was observed after SLMP intervention since 2014. These indicate that there was a significant increase in soil moisture of the study area after soil and water conservation activities.

This study further shows that sustainable land management program (SLMP) reduced soil erosion, runoff and sedimentation problem in lower part of watershed and which interns, increased also soil moisture content which could be explained by emerging dry streams, increased groundwater recharge (the abundance of shallow wells observed), increased the incomes of the farmer with increased in crop production, improved ecological balance, stabilized gullies and rehabilitation of degraded lands, increase in honey production after applying the modern beehives, as conducted by the authors through field observations and discussions with by elders residing in the watershed.

5. CONCLUSION AND RECOMMENDATION

5.1 Conclusions

This study evaluated the changes observed in vegetation cover, land cover and soil moisture using remote sensing following the implementation of watershed intervention. To evaluate vegetation cover changes, satellite images were used to retrieve NDVI. The threshold NDVI classification analysis revealed three vegetation cover classes, including "no plants", "weak plants" and "healthy plants" which were designated in an increasing order of vegetation vigor. The area under "no plants" drastically decreased whereas, the area under "healthy plants" dramatically increased after intensive watershed management interventions.

The Mann-Kendal trend test also suggested that there is an increasing positive significant trend at 5% level for healthy plants and decreasing trend for no plants and weak plants. The change detection tests showed that the year 2015 as the exact change year for increasing and decreasing the area for three vegetation cover classes which verified that the observed change was after SLM intervention since 2013/14. Further, weak and decreasing correlation was observed in between rainfall and NDVI area. This clearly shows that the significant increase in vegetation cover is not only from the rainfall influence; instead, other factors like watershed management practices applied in the area contribute significantly. It is concluded that the vegetation cover of the study area was increased following the SLM intervention.

The land cover dynamics following SLM intervention was evaluated by generating the LULC maps and analyzing its change detection. The key LULC changes observed in the watershed were increased in both agricultural and forest land and decreased in bare, shrubland as well as, in grassland. The highest decline was observed for shrubland, which accounts for about 50.6% and the decline is mainly due to the conversion of shrubland into forest land. The highest increment was shown for forest land, which accounts for about 25.8% and the increase is mainly due to the conversion of shrubland and grass land into forest land. These results indicate that watershed management implemented in the study area is successfully achieved.

The soil moisture change observed in the study area is evaluated using a soil moisture index (SMI) model, which was developed from a combination Landsat 8 OLI- driven LST and NDVI. It was observed that the SMI, which considers vegetation index and LST relationship, can be used effectively and appropriately for the estimation of soil moisture. SMI data revealed that the

value near to 0 indicates low vegetation cover and low soil moistures whereas, the value near to 1 indicates high vegetation cover high moisture content. It is concluded that the soil moisture content of the watershed was increased after SLM intervention since, the increment of vegetation cover. It is also concluded that SMI extracts soil moisture and is useful for frequently studying soil moisture over a small micro watershed.

Overall, this study proved that the remote sensing approaches have the capability of detecting, mapping, and monitoring vegetation cover, land use and soil moisture changes at the micro watershed as the result of sustainable land management (SLM). The findings of this research provided the scientific evidence that shows hydrological impacts of SLM interventions on fluxes and state variable such as vegetation cover and soil moisture that has been not /limitedly documented to date.

5.2 Recommendations

From the main limitation faced in this study, the following essential points are recommended in the future works for better results.

- NDVI results showed that vegetation cover of the study area for all images was taken in dry months was accurately quantified. However, some images which were taken even in dry months are profoundly affected by cloud cover, which in turns affected the results of NDVI so, this cloud covers are removed by developing algorithm like cloud masking algorithm which requires a vast knowledge of remote sensing, are recommended in the future works.
- Rainfall and potential evapotranspiration have a significant impact on soil moisture content. It is well known that the increment in soil moisture of the watersheds is not only from watershed management; therefore, a separate effect of rainfall and evapotranspiration evaluation is recommended to know the exact changes caused by the interventions.
- It should be noted that LSTmin (wet edge) and LSTmax (dry edge) are the main sensitive parameters for estimating soil moisture using the SMI model. The two parameters are carefully extracted from NDVI and LST to improve the soil moisture results. Obtaining these two parameters is a significant research problem till now and also for those who

studied soil moisture earlier using the SMI model. Errors are always raised in extracting the maximum and minimum land surface temperature from the corresponding pixels of NDVI because of, inversely relationship of NDVI and LST. Therefore, to minimize such errors and to improve the model result, it is highly recommended to apply additional software's like programming language software's to extract the dry and wet edges accurately.

- LULC map results showed it is challenging to classify the micro watersheds into different land cover classes accurately and to generate the accurate LULC map using coarser resolution like Landsat. In addition, without collecting of sufficient training samples (GCPs) for training and validating data, without applying of some ancillary data such as NDVI during supervised classification and without verifying the classified LULC maps using high-resolution satellite-like SPOT imageries, is also challenging to get accurate classified images. So, lack of applying these knowledge's and using of the coarser-resolution satellite during classification, it's not expected to get accurate LULC map in small size watersheds, therefore, high-resolution satellite-like Sentinel 2, collecting enough ground truth data through regular visiting of the watershed and applying the suggested knowledge before classification is highly recommended.
- It should be noted from the accuracy results of the SMI model when validating the ground observed soil moisture, limiting numbers of a soil sample point and soil sampling in the wet season can affect the performance of the model. A sufficient number of sampling points from the different land cover, which is representative of the study area, were needed for calibrating and validating the model. The main limitation of using optical satellite/ Landsat for soil moisture estimations cannot penetrate through the cloud in rainy seasons and, as a result, don't provide accurate information on land surfaces. It is better to take soil sample more in dry seasons than wet season while using optical satellite. Therefore, taking the long duration of soil sampling in both dry and wet seasons at a different place, which is representative of the study area on different land covers, is highly recommended for better results.

6. REFERENCES

A., Di Gregorio. (2005). Land cover classification system: Classification concepts and user manual: LCCS. Rome:. FAO Publishing Management Service.

A., Shimizu, Ishimura, Y., B. P., Rahimzadeh, and Omasa, K. (2011). Remote sensing of Japanese beech forest decline using an improved Temperature Vegetation Dryness Index (iTVDI). iForest-Biogeosciences and Forestry,4, 195-199. http://dx.doi.org/10.3832/ ifor0592-004.

A.M. Wu and Y.Y. Lee. (2001). Geometric Correction of High Resolution Images Using Ground Control Points. Singapore Institute of Surveyors and Valuers (SISV) ; Asian Association on Remote Sensing (AARS).

Abd EI-Kway, O.R.A., Rod, J.K., Ismail,H.A., Suliman, S., 2001. (2011). Land use land cover change detection in western Nile delta of Egypt using remote sensing data. Appl.Geogr. 31, 483-494.

Adimassu Z, Mekonnen K, Yirga C, et al. (2014). Effect of soil bunds on runoff, soil and nutrient losses, and crop yield in the central highlands of Ethiopia. Land Degradation & Development, 25(6): 554–564.

Adimassu, Z., and Langan, S. (2016). Comprehensive impact assessment of watershed management interventions in Ethiopia. Addis Ababa, Ethiopia: International Water Management Institute.

Ahmadi H, and Nusrath A. (2012). " Vegetation change detection of Neka river in Iran by using remote sensing and GIS". Journal of geography and Geology, 2 (1)., pp. 58-67.

Al-Doski, J., Mansor, S. B., & Shafri, H. Z. M. (2013). NDVI differencing and post-classification to detect vegetation changes in Halabja City, Iraq. IOSR Journal of Applied Geology and Geophysics (IOSR-JAGG), 1(2), 01-10.

Alemayehu, F., Taha, N., Nyssen,J., Girma,A., Zenebe, A., Behailu,M.,Deckers, S., Poesen,J.,. (2009). The impacts of the watershed managment on land use and land cover dynamics in eastern Tigray(Ethiopia) . Resour.Conserv. Recy. 53(4), 192-198.

Ali, A. M. S. (2007). September 2004 flood event in southwestern Bangladesh: a study of its nature, causes, and human perception and adjustments to a new hazard. Natural Hazards, 40(1), 89-111.

and rural settlements in Su-Xi-Chang region: implications for building a new countryside in coastal China. Land Use Policy 26 (2), 322–333.

Aplin, P. & Atkinson, P.M. . (2004). Predicting missing field boundaries to increase per-field classification accuracy . Photogrammetric Engineering and Remote Sensing, Vol. 70, no. 1, 141-149.

Atasoy, M., Biyik, C., Ayaz, H., Karsli, F., Demir, O., Baskent, E. Z. (2006). Monitoring land use changes and determinating the suitability of land for different uses with digital Photogrammetry. Cairo, Egypt.: Remote Sensing and Photogrammetry.

B, Barrett, Dwyer, E, Whelan,P. (2009). Soil moisture retrieval from active space borne microwave observations: An evaluation of current techniques. Remot Sens. 1, 210-242.

B. Yoganand, and Gebremedhin. Tesfa. (2006). Participaratory Watershed Management for Sustainable Rural Livelihoods in India Research Paper.

Babiker, M.E.A. and S.K.Y. Akhadir. (2016). The effect of Densification and Distribution of Control points in the Accuracy of Geometric Correction.

Baboo, S.S. and M.R. Devi. (2011). Geometric correction in recent high resolution satellite imagery: a case study in Coimbatore, Tamil Nadu. International Journal of Computer Applications 14(1): , p.32-37.

Baboo, S.S. and Thirunavukkarasu. (2014). Geometric Correction in High Resolution Resolution Satellite Imagery using Mathematical Methods: A Case Study in Kiliyar Sub Basin. Global Journal of Computer Science and Technology, 14 (1-F):, p. 35.

Bai, Z. G., Dent, D. L., Olsson, L., & Schaepman, M. E. (2008). Global assessment of land degradation and improvement: 1. identification by remote sensing (No. 5). ISRIC-World Soil Information.

Bakr, N., Weindorf, D.C., Bahnassy, M.H., Marei,S.M., EI-Badawi,M.M.,. (2010). Monitoring land use changes in newly reclaimed area of Egypt using Multi-temporal Landsat data. Appl.Georg. 30, 592-605.

Barrett, K. (1999). Ecological enginerring in water resources: The benefits of collaborating with nature . Water International, Jounal of the International Water Resources Association. , V 24,p182-188.

Berihun, M.L, Tsunekawa,A., Haregeweyn, N., Meshesha, D.T, Adgo, E, Masunaga, T., Fenta, A.A, Sultan, D. Yibeltal. M, Ebabu.K., (2019). Hydrological responses to land use/land cover

change and climate variability in contrasting agro-ecological environments of the Upper BlueNile basin, Ethiopia. Science of the Total Environment

Bhandari, A. K., Kumar, A., & Singh, G. K. (2012). Feature extraction using Normalized Difference Vegetation Index (NDVI): A case study of Jabalpur city. Procedia technology, 6, 612-621

Bhandari.A.A and Karaburun . K. (2010). " Estimation of C factor for soil erosion modelling using NDVI in Buyukcekmece watersehd ozean. Journal of applied sciences 3, 77-85.

Bierman, PM, and Rosen CJ. (2005). Nutrient cycling and maintaining soil fertility in fruit and vegetable crop systems. University of Minnesota.

Bishop, Yvonne M.M., Stephen E. Feinberg, Holland. (1975). Discrete Multivariate Analysis. MIT Press, 396.

Biswas, S. (2002). Remote sensing and geographic information system based approach for watershed conservation. J. Surv. Eng., 128,108-124.

Boori, M.S., Voz ent lek, V., Choudary, K. (2015). Land use/cover disturbance due to tourism in Jeseni ky Mountain, Czech Republic: a remote sensing and Gis based approach. Egypt. J. Remote Sens Space Sci. 18 (1), 17-26, http: //dx.doi. org/10.1016/ j.ejrs. 2014.12. 002.

Buckwell, A. (2009). "Rise task force on public goods from private land.Rise rural investment support for Europe" . Retrieved Aug. 5, 2011, from , http://www.agriculture.gov.ie/media/migration/agri-foodindustry/foodharvest2020/.

Buishand TA (1982). Some Methods for Testing the Homogeneity of Rainfall Records." journal of Hydrology, 58, 1127.

Burapapol, K., & Nagasawa, R. (2016). Mapping Soil Moisture as an Indicator of Wildfire Risk Using Landsat 8 Images in Sri Lanna National Park, Northern Thailand. *J. Agric. Sci*, *8*, 107.

Campbell,James ,B. (1987). Introduction to Remote Sensing . The Guilford Press, New York, 1987, p. 340.

Carlson, T. N. (2007). An overview of the triangle method for estimating surface evapotranspiration and soil moisture from satellite imagery. Sensors, 7, , 1612-1629. http://dx. doi.org/ 10.3390/ s7081612.

Cerna, L. & Chytry, M. . (2005). Supervised classification of plant communities with artificial neural networks. Journal of Vegetation Science, Vol. 16. 4, pp.407-414.

Chen, S., Wen, Z., Jiang, H., Zhang, X., & Chen, Y. . (2015). Temperature vegetation dryness index estimation of soil moisture under tree species. Sustainability, 7, 11401-11417. http:// dx.doi.org/ 10.3390/ su70911401.

Chouhan R, and Rao N, . (2012). " Vegetation detection in Multi spectral remote sensing images: protective Role-analysis of coastal vegetaion in 2004 Indian Ocean Tsunami. Geo-Information for Disaster Management Procedia Technology 6, pp. 612-621.

Chowdary, V.M.,Paul,S.,Srinivas Kumar T., Sudhakar, S.,. (2001). Remote Sensing and GIS approach for watershed monitoring and evaluation. In Proceedings of the 22nd Asian Conference on Remote Sensing. Singapore.

Conacher, A. J., & Sala, M. (1998). Land degradation in Mediterranean environments of the world: nature and extent, causes and solutions. John Wiley and Sons Ltd.

Congalton, Russel G. (1991). A review of Assessing the Accuracy of Classifications of Remotley Sensed Data. Remote Sensing of Environment vol 37, pp.35-46.

Csaplovics, E. (1998). High resolution imagery for regional environment monitoring status quo and future trends. Int. Arch. Photogramm. Remote Sens. 32(7), 211-216.

D.A. Robinson, C.S. Campbell, J.W. Hopmans, B.K. Hornbuckle, S.B. Jones, R. Knight, F. Ogaden,J.Selker, O. Wendroth. (2008). Soil misture measurement for ecological and hydrological watershed observatories: . A review Vadose Zone J. 7(1), 358-389.

Damene S, Tamene L, Vlek P. . (2012). Performance of Farmland Terraces in Maintaining Soil Fertility: A Case of Lake Maybar Watershed in Wello, Northern Highlands of Ethiopia. J Life Sci, 6: 1251-1261.

De Troch, F.P., Troch, P.A, Su Z., Lin, D.S. (1996). Application of Remote Sensing for Hydrological Modelling. In: Abbott M B, Refsgaard J C, eds. Distributed Hydrological Modelling. Dordrecht: Kluwer Academic Publishers, Chapter 9:.

Demisachew Tadele and Mihret Dananto. (August 2018). Quantifying the the Impact of Integrated Watershed Management on Groundwater availability in Gerduba Watershed, Yabello District, Ethiopia . International Journal of Water Resources and Environmental Engineering , Vol. 10(7), PP. 90-99.

Desta, G., Nyssen, J., Poesen, J., Deckers, J., Mitiku, H., Govers, G., Moeyersons, J. (2005). Effectiveness of stone bunds in controlling soil erosion on cropland in the Tigray Highlands, northern Ethiopia. Soil Use and management, 21, 287-297.

Dowmann I., and Dolloff, J. (2000). An evaluation of rational function for Photogrammetric restitution . International Archives of Photogrammetry and Remote Sensing, Amsterdam, The Netherlands, July 16-23, (Amsterdam, The Netherlands: GITC) Vol. 33 (B3), pp. 254-266.

Dutta, D.,Narasimhan,Sharman J.R., Adiga, S. (2003). Remote sensing based rapid watershed health appraisal-a case study of NWDPRA watershed of Rajasthan,Water resources. Map india Conference.

Dwivedi, R.S., Ramana, K.V., Wani, S.P., Phatak, P., . (2001). Use of satellite data for watershed managemnt and impact assesment. In: Proceedings of the AD13-ICRISTAT-IWMI project review and planning meeting , (pp. December10-14). Hanoi, Vietnam .

Eastman JR. (2003). Guide to GIS to GIS and image processing 14. Clark University manual, USA, 239-247.

El-Gammal .M.I, R. R. Ali and R. M. Abou Samra (2014). NDVI Threshold Classification for Detecting Vegetation Cover in Damietta Governorate, Egypt

El- Manadili, Y., and Novak, K. (2009). Precision Rectification of Spot Imagery using the direct linear .

Eltohamy, F. and E. Hamza. . (2009). Effect of ground control points location and distribution on geometric correction accuracy of remote sensing satellite images. In 13th International Conference on Aerospace Sciences & Aviation Technology , 13.

Engman, E. T. (1991). Application of microwave remote sensing of soil moisture for water resources and agriculture . Remote Sensing of Environment 35:, 213-226.

ERDAS Field Guide Fifth Edition, R. a. (2013).

Erdas Imagine 8.5 Field Guide. (2002).

FAO, I. (2015). Status of the World's Soil Resources (SWSR)–technical summary. Food and Agriculture Organization of the United Nations and Intergovernmental Technical Panel on Soils, Rome, Italy.

FAO. (1986). "Highlands reclamation study: Ethiopia", Final Repot. pp.166-169.

Ferance J, Hazeru G, Chistensen S. (2007). Corine land cover change detection in Europe (case studies of the Netherlands and SI ovakia). Land Use Policy, 24 (1), p.234-247.

Foody, G. (2002). Status of land covers classification accuracy assessment. Remote Sens.Environ.80, 185-201.

G/ mariam Yaebiyo, Yayneshet Tesfay, Dereje Assefa. (2015). Scio-Economic Impact Assessment of Integrated Watershed Management in Sheka Watershed, Ethiopia. Journal of Economics and Sustainable Development vol.6 No.9 , ISSN 2222-1700 (Paper) ISSN 2222-2855 (online).

Gao, B. (1996). NDWI-normalized difference water index for remote sensing of vegetation liquid water from space. Remote Sens. Environ. 58(3), 257-266.

Gibson P.J., Power C.H. (2000). Introductory Remote Sensing: Digital Image Processing and Application. Routledge, London.

Goetz, S. J. (1997). Multi sensor analysis of NDVI, surface temperature and biophysical variables at a mixed grassland site. International Journal of Remote Sensing, 18 (1), , 71-94. http: // dx. doi. org/ 10.1080/ 014311697219286.

Gong P. and P.J. Howarth. (1990). An assessment of some factors influencing multispectral land-cover classification. Photogrammetric Engineering and Remote Sensing, 56 (5):, 597-603.

Gross, D. (2005). Monitoring Agricultural Biomass Using NDVI Time Series, Food and Agriculture Organization of the United Nations (FAO), Rome, Italy.

Hafez Abbas Afity . (2002). Planimetric Accuracy of Rectified DSpot Imagery Lecturer, Dpt of Transportation Engineering, Faculty of Engineering, Tata University, Tanta, Egypt.

Haregeweyn N, Tsunekawa A, Poesen J, et al. 2017. Comprehensive assessment of soil erosion risk for better land use planning in river basins: Case study of the Upper Blue Nile River. Science of the Total Environment, 574: 95–108.

Haregeweyn, N., Berhe, A., Tsunekawa, A., Tsubo, M., & Meshesha, D. T. (2012). Integrated watershed management as an effective approach to curb land degradation: a case study of the enabered watershed in Northern Ethiopia. *Environmental management*, *50*(6), 1219-1233.

Hendrickx, J.M.H., J.Harrison, J.B., Borchers, B. and Rodriguez-Marin, G. (2010). High-Resolution Soil Moisture Mapping Using Operational Optical Satellite Imagery.

Hirsch RM, Slack JR, Smith RA. 1982. Techniques of trend analysis for monthly water quality data. Water Resources Research 18: 107–121.

Hishe. S, Lyimo. J, Bewket. B. (2017). Soil and water conservation effects on soil properties in the Middle Silluh Vally, Northern, Ethiopia . International soil and water conservation research 5 , 231-240.

Honja, T., Geta, E., & Mitiku (2016) A. Mango Value Chain Analysis: The Case of Boloso Bombe Woreda, Wolaita Zone, Southern Ethiopia.

Hord, R. Michael, and Willian Brooner. (1976). Land Use Map Accuracy Criteria . Photogrammetric Engineering and Remote Sensing, vol 42, No. 5. , pp.671-677.

I.E, Mladenova, Jackson, T.J., Njoku, E., Bindlish, R., Chan, S., Cosh, M.H., Holmes., T.R.H., Dejeu, R.A.M.,Jones, L., Kimball, J., Paloscia, S. (2014). Remote monitoring of soil moisture using passive microwave-based techniques-theoretical basis and over view of selected algorithms for AMSRE-E. Remote Sens. Environ 144, 197-213.

Igbokwe, K.N., and Adede, J. (2001). Integrated watershed management in Eastern Tigray-Ethiopia. Mid term impact evaluation report. Nairobi, Kenya, 72 p.

ILWIS, I. L. (2007). International Institute for Geo-Information science and Earth Observation. ITC Enschede.

J., Peng, and A., Loew. (2017). Recent advances in soil moisture estimation from remote sensing. water 9 (7), 530-534.

J.Li, and S. Islam. (1999). On the estimation of soil moisture profile and surface fluxes partitioning from sequential assimilation of surface layer soil moisture. Journal of Hydrology 220:, 86-103.

J.S. Famiglietti, D.R. Ryu, A.A. Berg, M. Rodell, T.J. Jackson. (2008). Field observations of soil moisture variability across scales. . Water Resour. Res. 44(1), W01423, 1-16.

Jansen, J. (2005). Introductory Digital Image Processing: A Remote Sensing Perspective, third ed. Pearson Prentice Hall, Upper Saddle River.

Johannes van der kwas. (2009). Thesis entitled " Quantification of top soil moisture patterns".

John Richards and Xiuping Jia. (1999). "Remote Sensing Digital Image Analysis -An Introduction " . Springer 3rd edition .

Kendall MG. 1975. Rank Correlation Measures. Charles Griffin: London.

Kerr, J., & Chung, K. (2002). Evaluating watershed management projects. *Water Policy, 3*(6), 537-554.

Kirubel Mekonen and Gebreyesus Birhane Tesfahunegn. (2011). Impact assessment of soil and water conservation measure at Medego Watershed in Tigray, Northern Ethiopia. Maejo Int. J. Sci. Technol, 5 (03), 312-330.

Kumar CP. (2003). Estimation of groundwater recharges using soil moisture balance approach. Journal of soil and Water conservation 2 (1-2), 53-58.

Kumar, G., Sena, D.R.,Kurothe, R.S., Pande, V.C., Rao, B.K, Vishwakarma, A.K., Bagdi, G.L., Mishra, P.K. (2014). Watershed impact evaluation using remote sensing. Current Science, Vol. 106, No. 10, pp. 1369-1378.

L., Chen, and Wang, L. (2018). Recent advance in earth observation big data for hydrology. Big Earh Data, 1-22.

Lacombe G, Cappelaere B, Leduc C. (2008). Hydrological impact of water and soil conservation works in the Merguellil catchment of central Tunisia. *Journal of Hydrology* **359**: 210-224..

Lambin E.F., & Geist, H.J. (2002). Proximate Causes and Underlying Driving Forces of Tropical Deforestation. Bio Science 52(2).

Lanfredi, M., Coppola, R., Simoniello, T., Coluzzi, R., D'Emilio, M., Imbrenda, V., & Macchiato, M. (2015). Early identification of land degradation hotspots in complex bio-geographic regions. Remote Sensing, 7(6), 8154-8179.

Langley, S.K., Cheshire, H.M., Humes, K.S. . (2001). A comparison of single date and multi temporal satellite image classifications in a semi-arid grassland. Journal of Arid Environments, Vol. 49, no. 2 , pp. 401-411.

Legesse. A, Bogale. M, Likisa. D . (2108). Impacts of Community Based Watershed Management on Land Use/ Cover Change at Elemo Micro-Watershed, Southern Ethiopia. American Journal of Environmental Protection vol 6 No. 3, 59-67.

Lievens N.E.C, H., Wagner, W., Alvarez-Mozos J., Moran, M.S., and Mattia F. (2008). On the soil roughness parameterization problem in soil moisture retrieval of bare surfaces from synthetic aperture radar". Sens. J...8, , 4213-4248.

Lillesand, T.M. & Keifer, R.W. (1994). Remote Sensing and Image Interpretation.

Long, H., Liu, Y., Wu, X., Dong, G., (2009). Spatio-temporal dynamic patterns of farmland

Lu, D., Mausel, P., Brondi zio, E., Moran, E. (2004). Change detection techniques . Int.J. Remote Sens. 25, 2365-2407.

Lu, D., Weng, Q. (2007). A survey of image classification methods and techniques for improving classification performance. Int. J. Remote Sens. 28(5),, 823-870.

Lunetta, R.S., Johnson, D.M. Lyon, J.G., Crotwell, J. (2004). Impact of imagery temporal frequency on land cover change detection monitoring . Remte Sen. Envirnon, 444-454.

Lwin, K. (2010). Estimation of Landsat TM Surface Temperature Using ERDAS Imagine Spatial Modeler. SIS Tutorial Series, Division of Spatial Information Science.

Mann HB. 1945. Non-parametric tests against trend. Econometrica 13245–259.

McCormick PG, Kamara AB, Girma T, editors. (2-4 December 2002). Integrated water and land management research and capacity building priorities for Ethiopia. Proceedings MoWR/EARO/IWMI/ILRI international workshop at ILRI. Addis Ababa, Ethiopia: IWMI (International Water Management Institute), Colombo, Sri Lanka, and ILRI (International Livestock Research Institute), Nairobi,Kenya: 2003.

Mekonen, K., & Tesfahunegn, G. B. (2011). Impact assessment of soil and water conservation measures at Medego watershed in Tigray, northern Ethiopia. *Maejo International Journal of Science and Technology*, *5*(3), 312.

Mekuriaw, A. (2017). Assessing the effectiveness of land resource management practices on erosion and vegetative cover using GIS and remote sensing techniques in Melka watershed, Ethiopia. Environment System Research.

Mengistu D.A and Waktola, K.D . (2016). Monitoring land use/cover change impacts on soils in data scare environments, A case of south-centeral Ethipia. J. land use sci,11, 98-112.

Merkineh Mesene Mena, Aklilu Bajigo Madalcho, Efrem Gulfo and Gismu. (2018). Community Adoption of Watershed Management Practices at Kindo Didaye District, Southern Ethiopia. International Journal of Environmental Science & Natural Resources ISSN: 2572-1119..

MoRAD (Ministry of Agricuture and Rural Development). (2005). Guide line for integrated watershed management. Addis Ababa, Ethiopia.

Morteza Sadeghi, Ebrahim Babaeian, Markus Tuller, Scott B. Jones. (2017). The Optical trapezoid model: A novel approach to remote sensing of soil moisture applied to Sentinel-2 and Landsat-8 observations. Remote Sensing of Environment.

Naiman, Rober I. (1994). Watershed Management: Balancing Sustainablity and Envirnmental Change. Berlin: Springer Verlag.

Naseer, A., & Pandey, P. (2018). Assessment and monitoring of land degradation using geospatial technology in Bathinda district, Punjab, India. Solid Earth, 9(1), 75.

Nigussie Haregeweyn, Ademnur Berhe, Atsushi Tsunekawan, Mitsuru Tsubo, Dereje Tsegaye Meshesha. (2012). Integrated Watershed Management as an Effective Approach to Curb Land Degradation: A case Study of the Enabered Watershed in Northern Ethiopia. Environmental Management, 50:, 1219-1233.

Njoku, E.G., and Kong, J.A. (1977). Theory for passive microwave remote sensing of near-surface soil moisture. Geophys Res, 82(20):, 3108-3118.

Nunes, J. S., Araújo, A. S. F. D., Nunes, L. A. P. L., Lima, L. M., Carneiro, R. F. V., Salviano, A. A. C., & Tsai, S. M. (2012). Impact of land degradation on soil microbial biomass and activity in Northeast Brazil. *Pedosphere*, *22*(1), 88-95

Nyssen J, Clymans W, Descheemaeker K, PoesenJ, Vandecasteele I, Vanmaercke M, Zenebe A, Van Camp M, Haile M, Haregaweyn N, Moeyersons J . (2010). Impact of soil and water conservation measures on catchment hydrological response a case in north Ethiopia . Hydrological Processes 24 (13), 1880-1895.

O' Neill, P.E., A. Joseph, G. De Lannoy, R. Lang, C. Utku, E. Kim, P. Houser and T. Gish. (2003). Soil moisture Retrieval Through Changing Corn Using Active/Passive Microwave Remote Sensing . Proc. IEEE, , pp. 407-409.

OrthoEngine, G. (2017). Geomatica Training Guide . Markham, Ontario L3R6H3, CANADA: PCI Geomatics Enterprises, Inc. 90 Allstate Parkway, Suite 501.

Ozesmi, S.L, and Bauer, M.E., . (2002). Satellite remote sensing of wetlands. Wetlands Ecol. Manage. 10, 381-402.

Parida B. R., Collado W.B., Borah R., Hazarika M.K., and Samarakoon L. (2008). Detecting Drought Prone Areas of Rice Agriculture Using a MODIS-Derived Soil Moisture Index. GIS Science and Remote Sensing, 45, No. 1, 109-129.

Parida, B. R., Collado, W. B., Borah, R., Hazarika, M. K., & Samarakoon, L. (2008). Detecting drought-prone areas of rice agriculture using a MODIS-derived soil moisture index. *GIScience & Remote Sensing*, *45*(1), 109-129.

Pettitt A. 1979. A nonparametric approach to the change-point problem. Applied Statistics 28: 126–135.

Potic, I., Bugarski, M., Matic-Vrenica, J. (2017). Soil Moisture Determination Using Remote Sensing Data For The Property Protection And Increase of Agriculture Production. Wshington DC: The World Bank .

Rawat, J.S., and Kumar, M. (2015). Monitoring land use/ cover change using remote sensing and Gis techniques: a case study of Hawalbah block,district Almora,Uttarakhand, India. Egypt. J. Remote Sens Sci. 18 (1), 77-78, <http:// dx.doi.org/10.1016/ j.ejrs.2015.02.002>.

Rawat, J.S., Biswas, V., Kumar, M. (2013). Change in land use/cover using geospatial techniques: a case study of Ramnagar town area, distict Nainital, Uttarakhad, India. Egypt. J. Remote Sens. Space Sci. 16, 111-117.

Richards, J.A & Jia, X. . (2006). Remote sensing digital image analysis: . an introduction, Springer Verlag.

Rocchini D., Di Rita A. (2005). Relief effects on aerial photos geometric correction. Applied Geography doi: http:// dx.doi.org/10.1016/j.apgeog.2005.03.002, 159-168.

Rouse J. W., Schell J. A. and Deering D. W. (1974). Monitoring Vegetation systems in the Great Plains with ERTS. Third ERTS-1 Symposium (pp. PP.309-317). Washingtondc, NASA: NASA SP -351.

S.,Ward, Darghouth, C., Gambarelli, G., Styger, E. and Roux, J. (2008). Watershed Managemnt Approaches, Polices and Operations : Lessons for Scaling Up. Washington, DC: Water Sector Board Discussion Paper Series Paper No 11. The World Bank.

S.J. Scherr and S.N. Yadav . (1996). "Land degradation in the developing world: Implications for food, agricuture, and the environment to 2020". Food, Agricuture and Environment Discussion Paper 14. Washington, D.C., U.S.A: International Food Policy Research Institute .

Santosh Baboo, S., and Renuka Devi, M. (2011). Geometric correction in recent high resolution satellite imagery: a case study in Coimbatore. Tamil Nadu. . Int. J. Comput. Appl. 14 (1), , 32-37.

Senseman, G.M., Bagley, C.F, and Tweddale, S.A. (1994). Accuracy Assessment of the Discrete Classification of Remotely-Sensed Digital Data for Land cover Mapping. USACERL Technical Report EN-95/04.

Shalaby, A., Tateishi, R., . (2007). Remote sensing and GIS for mapping and monitoring land cover and land use changes in the north western coastal zone of Egypt. APP Geogr., 28-41.

Shanwad, U.K., Patil, V.C., Honne Gowda, H., Dasog, G.S., . (2008). Application of remote sensing technology for impact assessment of watershed management programme. J.Indian Soc.Remote sens. 36,, 375-386.

Singh R, Garg KK, Wani Sp, Tewari RK, Dhyani SK. (2014). Impact ofwater management interventions on hydrology and ecosystem services in Garhkundar-Dabor Watershed of Boundelkhand region Centeral India. Journal of Hydrology 509, 32-149.

Skidmore, A. (1989). Unsupervised training area selection in forests using a nonparametric distance measured and spatial information. Remote Sensing, Vol. 10, no.1, 133-146.

Smyth, A.J. and Dumanski, J. (1993). FESLM: An international framework for evaluating sustainable land management. A discussion paper World Soil Resources Report 73 (p. 74 pp). Rome, Italy: Food & Agriculture Organization .

T.E. Ochsner, Cosh, M.H., Cuenca, R.H., Dorigo, W.A., Draper, C.S., Hagimoto, Y. (2013). State of the art in large-scale soil moisture monitoring. Soil Sci. Soc.Am.J.77 (6), , 1888-1919.

Tabatabaeenejad, A., Burgin, M., Duan, X., Moghaddam, M.,. (2015). P-band radar retrieval of subsurface soil moisture profile as a second-order polynomial: first AirMOSS results.IEEE Trans. Geosci. Remote Sens. 53(2), 645-658.

Taddese, G.(2001). Land degradation: a challenge to Ethiopia. Environmental management, 27(6), 815-824.

Tadele Demisachew and Dananto Mihret.(2018). Quantifying the Impact of Integrated Watershed Management on Groundwater availability in Gerduba Watershed, Yabello District, Ethiopia . *International Journal of Water Resources and Environmental Engineering* , Vol. 10(7), PP. 90-99.

Teferi, E, Bewket W, Unlenbrook, S, Wenninger, J. (2013). Understanding recent land use and land cover dynamics in the sources region of the upper Blue Nile, Ethiopia: Spatially explicit statistical modelling of systematic transitions. Agric. Ecosyst. Environ. 165, 98-117.

Teressa Dejene and Guteta Etefa. (2018). The Effects of Community Based Watershed Management on Livelihood Resources for Climate Change Adaptation the Case in Gemechis District, Oromiya. *International Journal of Environmental Science & Natural Resources ISSN: 2572-1119*

Thakkar, A.K., Desai, V.R., Patel, A., Potdar, M.B. (2017). Impact assessment of watershed management programmes on land use/ land cover dynamics using remote sensing and GIS. Remote Sensing Applications: Society and Environment 5, 1-15.

Thanh. (2015). Optical Ground Control Points for Geometric Correction Using Genetic Algorithm with Global Accuracy.

Thomas M. Lillesand and Ralph W. Kiefer. (2000). Remote Sensing and Image Interpretion 4th edition, Joh Wiley & Sons.

Tou, J.T. & Gonzalez, R.C. . (1974). Pattern recognition principles . Image Rochester NY, vol. 7.

Tsegaye, D.A; Moe, S.R; Vedeld, P; Aynekulu, E. . (2010). Land use/cover dynamics in Northern Afar rangelands Ethiopia. Agric. Ecosyst. Environ, 139, 174-180.

Tucker, C. J. . (1979). Red and photograohic infrared linear combinations for monitoring vegetation . Remote Sensing of Environment, 8,, 127-150. Retrived from http:// ntrs.nasa.gov/ 19780024582. pdf.

U. Bosshart. (1997). Catchment discharge and suspended sediment transport as indicators of physical soiland water conservation in the Minchet catchment, Anjemi research unit: A case study in the northwestern highlands of Eritrea", Research Report 39, Soil Conservation Research Project, Centre for Development and Environment, University of Bern, p.137.

UNCCD. (1994). Elaboration of an International Convention to Combat Desertification in Countries Experiencing Serious Drought and/or Desertification, Particularly In Africa; Final Textoftheconvention.Retrievedfrom https://observatoriop10.cepal.org/sites/default/files/documents/treaties.

Van Genderen, J.L., and B.F. Lock . (1976). Testing Land -Use Map Accuracy . Photogrammetric Engineering and Remote Sensing, vol 43, No.9, pp. 1135-1137.

W.T., Berg, Crow, Cosh, M.H., Loew, A., Mohanty, B.P., Panciera, R., Rosnay, P., Ryu, D., Walker, J.P. (2012). Upscaling sparse ground-based soil moisture observations for the v. Rev.Geophys. 50.

W.Xu, Zeng, C., Huang, J., Wu, J., Tuller, M. (2016). Predicting near-surface soil moisture content of saline soils from NIR reflectance spectra with a Modified Gaussian model. Soil Sci.Soc. Am.J., http: //dx.doi. org/10.2136/sssaj2016.06.0188.

Weng Q., Lu D. and Schubring J. (2004). Estimation of land surface temperature-vegetation abundance relashinship for urban heat island studies. Remote Sensing of Envirnoment (pp. 467-483). New York NY 10159 USA, 89: Elsevier Science Inc., Box 882.

Whiting A (2017) Ethiopia's Tigray Region bags gold award for greening its drylands. https://www.reuters.com/article/us-land-farming/ethiopias-tigray-region-bags-gold-award-for-greening-its-drylands-idUSKCN1B21CT. Accessed 25 Nov 2017

Woody Biomass Inventory and Strategic Planning Project (WBISPP). (2005). A National Strategic Plan for the Biomass Energy Sector:.

WZFEDD. (2014). (Wolaita Zone Finance and Economic Development Department). Wolaita Zone socio-economic information.

Y.Y., Liu, Dorigo, W.A, Parinussa, R.A.M , Wangar, W, McCabe, M.F, Evans, J.P, vn Dijk, A.I.J.M. (2012). Trend-preserving blending of passive and active microwave soil moisture retrievals . Remote Sens. Environ123, 280-297.

Yisehak Ossa Jokka (2019) Determinants Households: of Food insecurity: The Case of Boloso Bombe Woreda, Wolaita Zone, Southern Region, Ethiopia

Zenebe Adimassu, and SimonLangan. (2016). Comprehensive impact assessment of watershed management interventions in Ethioipa. https:// wle.cgiar.org/project/comprehensiv-impact-assessment-watershed-management-interventions-ethiopia, Doi: 10.13140/RG2.1.17122167.

Zeng Y., Feng Z. and Xiang N. . (2004). Assessment of soil moisture using Landsat ETM+ temperature /vegetation index in semiarid environment . Geoscience and Remote Sensing Symposium, IGARSS 04 Proceeding (pp. 4306-4309). IEEE International Volume; 6.

Zhan X., Miller, S., Chauhan, N, Di L, Ardanuy P, Running S. (2002). Soil Moisture Visible/ Infrared Imager/ Radiometric Suite Algorithm Theoretical Basis Document . Version 5.

Zhan Z., Qin Q. and Wang X. (2004). The application of LST/NDVI Index for Monitoring Land Surface Moisture in Semiarid Area. Proceedings 2004 IEEE International (pp. 1551-1555). Geoscience and Remote Sensing, IGARSS 04.

Zribi, M., Baghdadi, N., & Nolin, M. (2011). Remote sensing of soil. Applied and Environmental Soil Science, 2011.

ANNEXS

Annex table 1: Geographic location of soil sampling site, field (Kit) and labaratory result

ID	X	Y	%SM-lab (mass)	%SM-sensor (vol)	dbd (g/cm^3)	%SM-lab (vol)	Land cover
P1	346955	788014	17.79	7.4	1.06	18.86	Bare land
P2	346951	788010	17.32	8	0.912	15.8	Bare land
P3	346960	788009	16.84	4.7	0.999	16.82	Bare land
P4	346961	788014	17.58	9.2	0.927	16.81	Bare land
P5	346952	788020	18.27	12.7	1.004	18.34	Bare land
Q1	347112	787368	15.36	8.7	0.875	13.44	Vegetation
Q2	347113	787364	18.86	13.6	0.892	16.82	Vegetation
Q3	347118	787371	22.43	9.8	1.035	23.22	Vegetation
Q4	347112	787376	21.16	9.5	0.998	21.12	Vegetation
Q5	347105	787369	21.57	9.9	1.039	22.42	Vegetation
R1	347292	786500	16.48	12.8	1.33	21.92	Vegetation
R2	347298	786497	13.07	5.3	1.045	13.66	Vegetation
R3	347296	786508	13.75	10	1.053	14.48	Vegetation
R4	347287	786504	15	8.9	0.999	14.99	Vegetation
R5	347287	786495	17.7	11	1.238	21.92	Vegetation
T1	346888	786218	15.08	11.2	1.134	17.1	Bare land
T2	346893	786216	20.56	16.3	1.264	25.98	Bare land
T3	346889	786225	16.79	13.8	1.067	17.91	Bare land
T4	346882	786220	15.13	10.4	0.976	14.77	Bare land
T5	346887	786212	21.04	13.8	1.234	25.96	Bare land
S1	346505	787537	20.87	20.7	1.05	21.91	Bare land
S2	346504	787533	20.71	19.9	1.02	21.12	Bare land
S3	346512	787537	22.48	15.8	1.067	23.99	Bare land
S4	346509	787543	23.81	21	1.07	25.48	Bare land
S5	346501	787540	14.74	15.4	0.897	13.22	Bare land
U1	346395	787094	11.89	7.9	1.157	13.75	Vegetation
U2	346399	787088	8.85	0.54	0.877	7.76	Vegetation
U3	346400	787098	13.84	10.2	1.097	15.18	Vegetation
U4	346393	787101	14.58	6.9	1.123	16.37	Vegetation
U5	346390	787093	13.24	0.9	1.154	15.28	Vegetation

Annex table 2: Mean absolute percentage error of soil moisture sensor

Code	X	Y	SM-lab (cm^3/cm^3)	SM-sensor (cm^3/cm^3)	Error	Mean Abs error (cm^3/cm^3)	Percentage (%)
P1	346955	788014	0.173	0.084	0.089	0.515	51.51
Q1	347112	787368	0.194	0.103	0.091	0.469	46.91
R1	347292	786500	0.174	0.096	0.078	0.448	44.8
T1	346888	786218	0.203	0.131	0.072	0.356	35.61
S1	346505	787537	0.211	0.186	0.026	0.122	12.22
U1	346395	787094	0.137	0.053	0.084	0.613	61.32
v1	346678	785382	0.13	0.094	0.037	0.281	28.06
w1	346540	785442	0.154	0.083	0.071	0.461	46.07
x1	346919	785426	0.173	0.075	0.098	0.567	56.69
y1	346912	786599	0.153	0.101	0.052	0.338	33.85
z1	346966	787271	0.172	0.114	0.058	0.336	33.64

A1	346419	787546	0.153	0.115	0.038	0.246	24.64
B1	346875	787562	0.292	0.099	0.193	0.661	66.06
C1	346454	787546	0.224	0.109	0.115	0.514	51.39
D1	346598	787271	0.244	0.103	0.141	0.578	57.85
E1	346734	787325	0.216	0.094	0.122	0.566	56.63
F1	346849	785738	0.348	0.12	0.228	0.655	65.52
G1	346638	785686	0.193	0.106	0.087	0.452	45.19
A1	346873	787510	0.221	0.224	-0.003	0.012	1.24
B1	346734	787323	0.274	0.22	0.054	0.196	19.57
C1	346846	785742	0.331	0.265	0.065	0.198	19.79
D1	346682	785379	0.31	0.264	0.046	0.148	14.8
E1	346324	787569	0.322	0.266	0.055	0.172	17.18
F1	346599	787272	0.296	0.278	0.017	0.058	5.79
G1	346665	785704	0.251	0.211	0.04	0.159	15.89
H1	346558	785456	0.253	0.233	0.02	0.079	7.9
5A	346679	785387	0.327	0.314	0.013	0.041	4.1
2W	346560	785448	0.353	0.32	0.034	0.095	9.48
4f	346894	785427	0.377	0.379	-0.003	0.007	0.74
1c	346900	786594	0.354	0.344	0.01	0.028	2.79
1a	346734	787325	0.338	0.35	-0.012	0.034	3.42
1A-	346598	787271	0.354	0.329	0.025	0.071	7.14
1i	346394	785115	0.296	0.208	0.088	0.298	29.78
5e+	346786	785123	0.347	0.378	-0.031	0.089	8.88
			N=34		MAPE	0.29 (cm^3/cm^3)	29%

Annex figure 1: Soil sampling schems at different land cover within Wutame watershed

Annex figure 2: Soil hydrometry analysis in laboratory recording reading (a), shaking for 10min (b), soil sieve analysis (c), and soil moisture content analysis in laboratory (d)

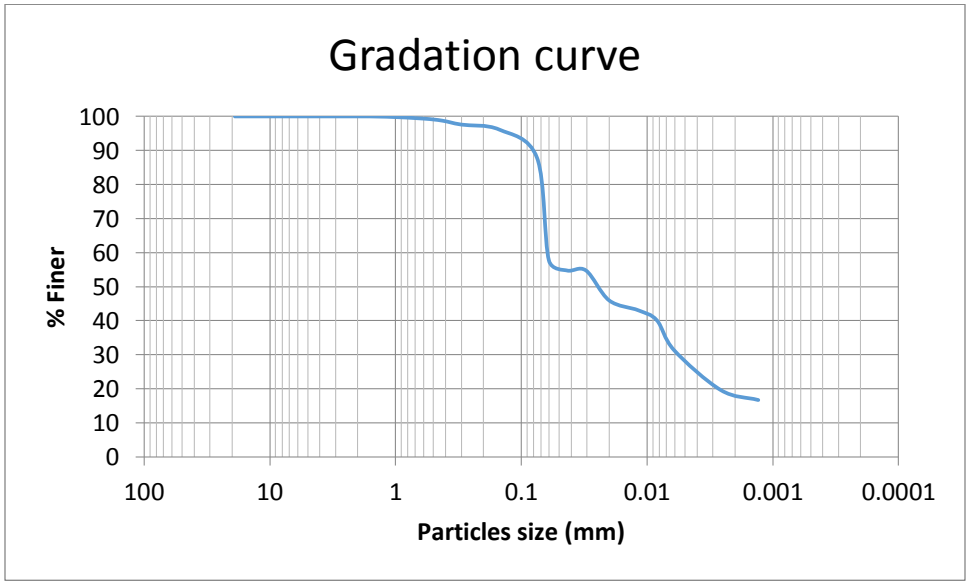

Annex figure 3: particles size distribution for 1m depth soil sample

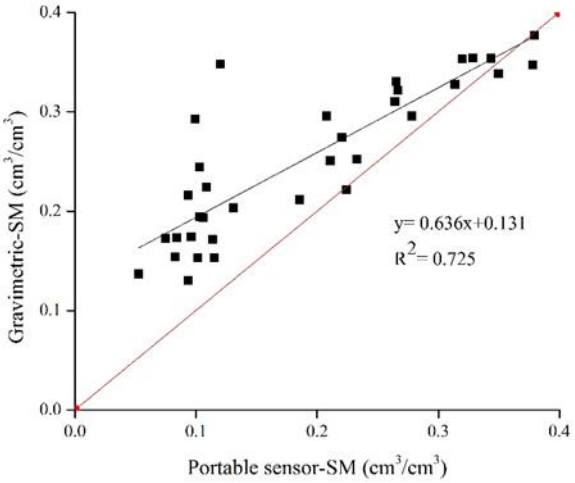

Annex figure 4: Calibration of HH2 sensor using laboratory soil moisture estimate

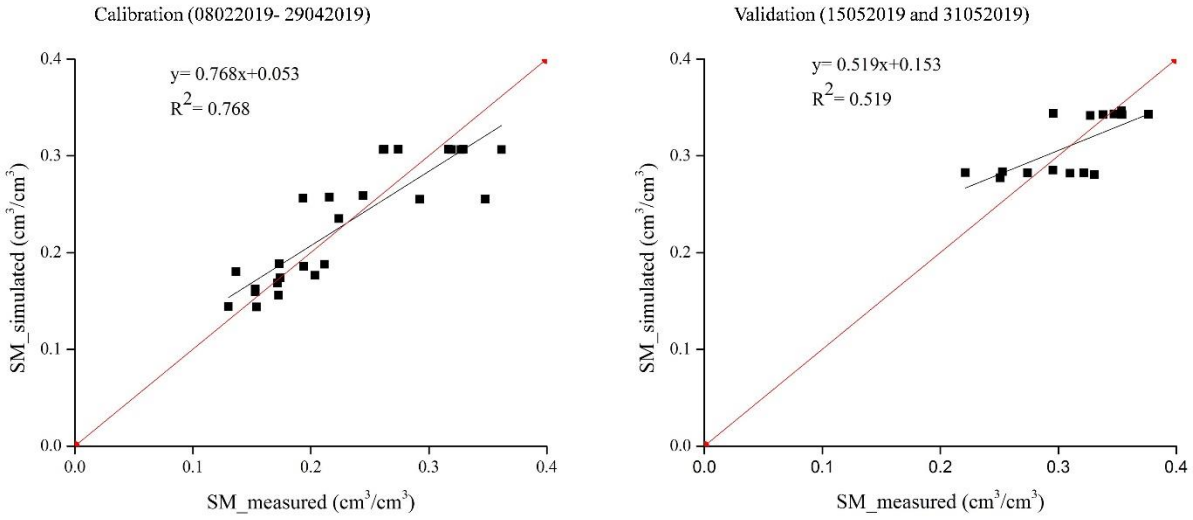

Annex figure 5: Correlation of actual and simulated soil moisture using the model

Annex figure 6: Restoration of degraded land and its benefit to local community

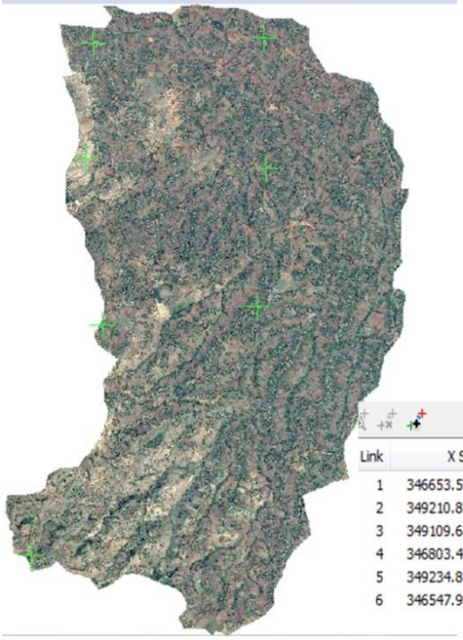

Total RMS Error: Forward:0.504806

Link	X Source	Y Source	X Map	Y Map	Residual_x	Residual_y	Residual
1	346653.575376	787463.554153	346654.000000	787464.000000	0.0710985	0.282339	0.291153
2	349210.818973	787538.494134	349210.000000	787538.000000	-0.0310019	0.0213472	0.0376406
3	349109.613960	783452.985465	349108.000000	783453.000000	0.450478	-0.340106	0.564449
4	346803.459312	783158.485149	346802.000000	783160.000000	-0.35083	0.501019	0.611639
5	349234.810558	785550.866805	349233.000000	785551.000000	-0.368195	0.244356	0.441902
6	346547.944623	785688.151331	346548.000000	785688.000000	0.22845	-0.708956	0.744854

(a) Georeferenced Spot 7 Images with GCPs

(b) RMSE for Georeferenced Spot 7 Images

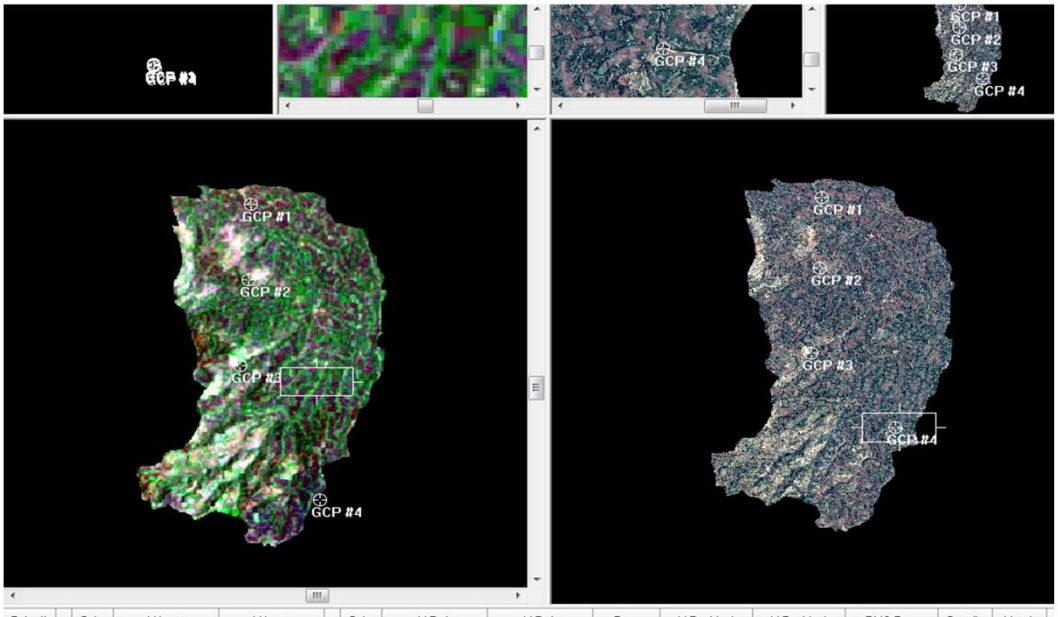

Point #	Color	X Input	Y Input	Color	X Ref.	Y Ref.	Type	X Residual	Y Residual	RMS Error	Contrib.	Match
1		348087.388	787524.629		348098.978	787520.222	Control	1.322	1.088	1.712	0.926	
2		348058.703	785521.173		348059.667	785586.987	Control	-2.348	-1.933	3.041	1.645	
3		347849.250	783240.691		347830.742	783270.115	Control	0.938	0.772	1.215	0.657	
4		349770.000	779670.000		349911.702	781255.757	Control	0.088	0.072	0.114	0.062	0.000
5							Control					

(c) Image to image registration of Landsat 8-2019 images with already Georeferenced Spot 7 images

Annex figure 7: Georeferenced Spot 7 images with GCPs and image to image registration